

Annual Report  
on  
ELECTROMAGNETIC INTERFERENCE (EMI) DESIGN CRITERION FOR  
POWER ELECTRONICS BUILDING BLOCK (PEBB)

Principal Investigator

Professor Raj Ramchandani, Ph.D, P.E.

Associate Investigators

Pablo Narvaez, Graduate Student

Serge Outaman, Senior Student

George Tlaxca, Senior Student

Bishara Albella, Senior student

Choo Binh Ong, Senior Student

California State University at Los Angeles

Per Grant No: N00014-95-1-1126

For

Mr. Terry Ericson, Program Manager,  
Office of Naval Research, Arlington VA.

June 1996 - May 1997

## A B S T R A C T

The PEBB EMI simulation demands and the doubling of student participation in the PEBB simulations necessitated the purchase of an additional SUN workstation. The EMI lab now has a local network of four SUN workstations. The commercial software packages are fulfilling the expectation of being the workhorse for the PEBB EMI simulations.

Frequency Domain Crosstalk EMI simulations were initiated. Six PEBB relevant geometries with different levels of complexities were selected for these simulations. Theoretical models were also developed for these geometries. Fifty seven frequency domain crosstalk simulations were done for the six geometries. The simulations were directed to investigate the impact of trace separation, trace orientation, trace geometry and trace discontinuities on the crosstalk. Five crosstalk EMI design criteria were obtained from these simulations.

Radiated EMI simulations were also initiated. A second set of six PEBB relevant geometries with different levels of complexities were selected for Radiated EMI simulations. Theoretical models were also developed for these six geometries. Thirty four Radiated EMI simulations were done for the six geometries. The Radiated EMI simulations are memory and time intensive. A few simulations took as much as 120 hours. The simulations were directed to investigate the impact of trace length, trace discontinuities and loop sizes on the Radiated EMI. Frequency Sweeps for the six geometries were also done. A by-product of these simulations was the development of a technique to cross-check the partial reliability of the near field obtained by these simulations. The near fields obtained from all these simulations were indeed reliable. Three Radiated EMI design criteria were derived from these simulations.

Induced EMI simulations were also initiated. A third set of six PEBB relevant geometries with different levels of complexities were selected for Induced EMI simulations. The Induced EMI models are currently in the investigative stage.

The goals for the next year are a) consolidate Radiated EMI simulations, b) consummate Induced EMI simulations and c) initiate Common Mode EMI simulations. A major goal for the next year is to modify the Radiated and Induced EMI models to predict the susceptibility of PEBB to Radiated and Induced EMIs.

## TABLE OF CONTENTS

|     |  |    |
|-----|--|----|
| I   | INTRODUCTION .....                                   | 5  |
|     | A. OBJECTIVE .....                                   | 5  |
|     | B. BACKGROUND .....                                  | 5  |
|     | C. SPECIFIC GOALS FOR THE SECOND YEAR .....          | 6  |
| II  | COMPUTER NETWORK STATUS .....                        | 7  |
| III | CROSSTALK EMI SIMULATIONS .....                      | 10 |
|     | A. SIMULATION GEOMETRIES .....                       | 11 |
|     | B. THEORETICAL MODELS OF THE SIX GEOMETRIES .....    | 14 |
|     | C. COMPUTER SIMULATIONS .....                        | 25 |
|     | D. COMPUTER SIMULATION RESULTS .....                 | 27 |
|     | E. DISCUSSION AND CONCLUSIONS OF THE RESULTS .....   | 30 |
| IV  | RADIATED EMI SIMULATIONS .....                       | 79 |
|     | A. SIMULATION GEOMETRIES .....                       | 79 |
|     | B. THEORETICAL MODELS OF THE SIX GEOMETRIES .....    | 83 |
|     | C. COMPUTER SIMULATIONS .....                        | 92 |
|     | D. THEORETICAL AND COMPUTER SIMULATION RESULTS ..... | 94 |
|     | E. DISCUSSION AND CONCLUSIONS OF THE RESULTS .....   | 96 |

|      |  |     |
|------|--|-----|
| V    | INDUCED EMI SIMULATIONS .....          | 125 |
|      | A. SIMULATION GEOMETRIES .....         | 126 |
| VI   | FUTURE PLANS FOR EMI SIMULATIONS ..... | 129 |
| VII  | REFERENCES .....                       | 131 |
| VIII | APPENDIX .....                         | 134 |

## I. INTRODUCTION

### A. OBJECTIVE

The Objective of this Research Grant is to develop Electromagnetic Interference (EMI) Design Criterion for the Power Electronics Building Block (PEBB). To this end, EMI models of the PEBB will be developed by using commercially available computer software.

### B. BACKGROUND

The PEBB is being developed, under ONR sponsorship, to produce 1 Megawatt with currents of the order of 1000 Amps. All PEBB hardware will be housed in a cubical box of the order of 6 inches. Switching frequencies in the PEBB will be as high as 70 KHz. High currents being turned on and off at 70 KHz will produce high EMI. EMI will be localized in the compact PEBB housing. This EMI could ultimately deteriorate the quality of power and the overall performance of the PEBB. Another problem that may result due to the EMI from the PEBB is the triggering of false alarms in the sensors of adjacent equipment. This could result in undesirable shutdowns of normally operating sensitive equipment. The EMI models of the PEBB will quantize the EMI levels produced by various components. These models can be used to determine the anticipated EMI environment of the PEBB during its life cycle and thus predict the overall PEBB performance and operation effectiveness. In effect, the predictions of the EMI models will become an engineering tool in the development of the PEBB during its various R&D stages.

This five year study was initiated in June 1995 to address some of these EMI issues pertaining to the PEBB. The approach of this study is to develop EMI models by using commercially available software packages. To this end, during its first year, twelve commercially available packages were studied for PEBB relevancy by Ramchandani et al (1996). From these twelve packages three were identified as PEBB relevant.

Also, during the first year of this study, three SUN workstations were purchased. At the outset of this study, EMI Lab was set by the University to house these computers and other experimental equipment specifically for PEBB EMI issues. All three workstations are connected to each other and to the printer to form a local network. The local network of the Computers with the software packages at the end of the first year of this study is shown in Figure 1.1. Navy 1 is the general server of the network since it has the largest capacity and the highest speed. Consequently, Navy 1 is the main workstation. Navy 2 is portable and provides mobility. Navy 3 is a relatively slower workstation as compared to Navy 1. The network was designed to make three independent PEBB simulations simultaneously using any of the combination of three commercial packages All three workstations can have their outputs printed on HP 4M.

The EMI Lab was set up with the capability to upgrade and conform to the prevailing "state of the art" technology. The hardware of each workstation can be upgraded. The workstation clocks, graphics and memory capabilities can be upgraded according to need. If needed, additional

workstations can be added to the EMI Lab network. The software packages are being constantly upgraded. The upgrades are incorporated as they come along. The operating systems of the individual workstations can also be upgraded to conform to the needs of the software packages. For the foreseeable future, the EMI Lab has the capability to preserve its "state of the art" status with routine hardware and software upgrades. Also, during the first year of this study three elementary PEBB relevant models were simulated to acquire expertise in the usage of the software packages. Simulations were done for Crosstalk in a dual trace card and radiated EMI from a single trace card. These simulations were verified theoretically and experimentally. The EMI Lab has limited experimental capability, but adequate equipment, to do some basic and elementary measurements to build confidence in the software packages.

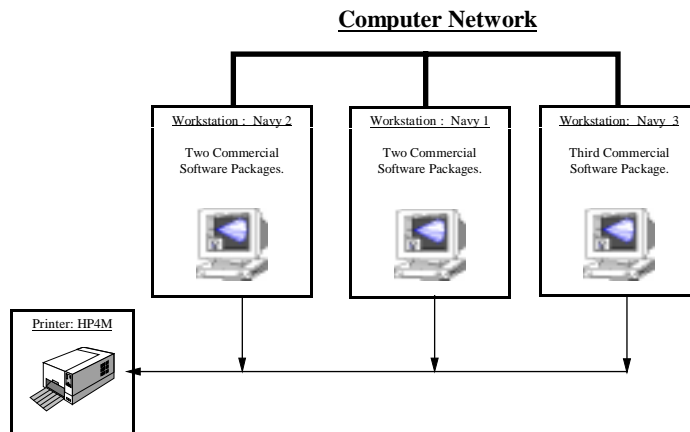


Figure 1.1 Computer Network During the First Year.

Thus, at the end of the first year of this study three PEBB EMI relevant software packages were identified. A computer local network of three SUN workstations was set up in the EMI Lab. The three packages were installed. EMI Lab was set up with a capability to perform three independent PEBB simulations simultaneously, using any combination of the three packages. Basic software expertise was acquired and elementary PEBB relevant models were simulated and verified, both theoretically and experimentally, by Ramchandani et al (1996).

### C. SPECIFIC GOALS FOR THE SECOND YEAR

The goals for the second year as stated in the first year's report were:

1. Acquire confidence and usage expertise for all three software packages.
2. Initiate the development of EMI Design Criterion for Intra-Card Layouts.
3. Initiate the development of EMI Design Criterion for Multiple Cards.
4. Initiate the development of Design Criterion for Inter-System Compatibility.

To accomplish these goals the following EMIs were initiated and investigated in depth:

1. Crosstalk EMI. This EMI would be a major contributor to the Intra-Card EMI. It would have a significant impact on the Design Criterion for Intra-Card Layouts.
2. Radiated EMI. This EMI is a major contributor for Inter-Card and Inter-System EMIs. Consequently, the Radiated EMI would have a significant impact on the Design Criterion for Multiple Cards and Inter-System Compatibility.
3. Induced EMI. This EMI will also be a significant factor for Inter-Card and Inter-System EMIs. Therefore, the Induced EMI would have a significant impact on the Design Criterion for Multiple Cards and Inter-System Compatibility.
4. Initiating and investigating the Crosstalk, Radiated and Induced EMIs would automatically accomplish the goal of acquiring software usage expertise.

Thus, the Specific Goals for the second year were:

1. Initiate and investigate in depth the Crosstalk EMI.
2. Initiate and investigate in depth the Radiated EMI.
3. Initiate and investigate in depth the Induced EMI.

## II. COMPUTER NETWORK STATUS

A Radiated EMI simulation requires an extremely large number of numerical computations. This in turn requires more computational time and more memory capacity of the workstation. To get reasonably accurate radiation results requires a non-stop simulation time of the order of 50 hours. This imposed numerous constraints on the availability time of the workstations for any other EMI simulation. Another factor putting a demand on the workstations was the increase in student participation in the EMI simulations. The student participation has doubled from four in the previous year to eight during the second year. These two factors culminated in purchasing a fourth workstation during the second year. The hardware description of the fourth workstation, Navy 4, is the following:

Sun SPARC station 20, Model 51 with:

- a) 50 MHz Super SPARC Processor.
- b) 64 MByte RAM.
- c) 1.05 GByte Internal Fast SCSI-2 Hard Drive.
- d) 1.44 MByte Internal Floppy Drive.
- e) 17 inch Color Monitor with TurboGX 8-bit Accelerated Graphics.
- f) External CD-ROM Drive with SCSI Interface.
- g) Solaris 2.3 Operating System.

Navy 4 was added to the existing Computer Network and the resulting configuration is shown in Fig 1.2. The radiation simulations are not only time intensive but also memory intensive. In addition, the results obtained from a radiation simulation are also memory intensive. These two factors put a demand on both, the ram memory and the hard disk storage memory. A stage has been

reached in which the storage of prior radiated simulations is tying up a significant portion of the memory capacity of the workstations. Consequently, less memory is available for new simulations. This in turn makes the simulation more time consuming or unable to proceed to the desired level of accuracy. The need to upgrade the memory capacity of the existing Computer Network of Figure 1.2 is becoming more acute. This will have to be addressed in the third year.

## Computer Network

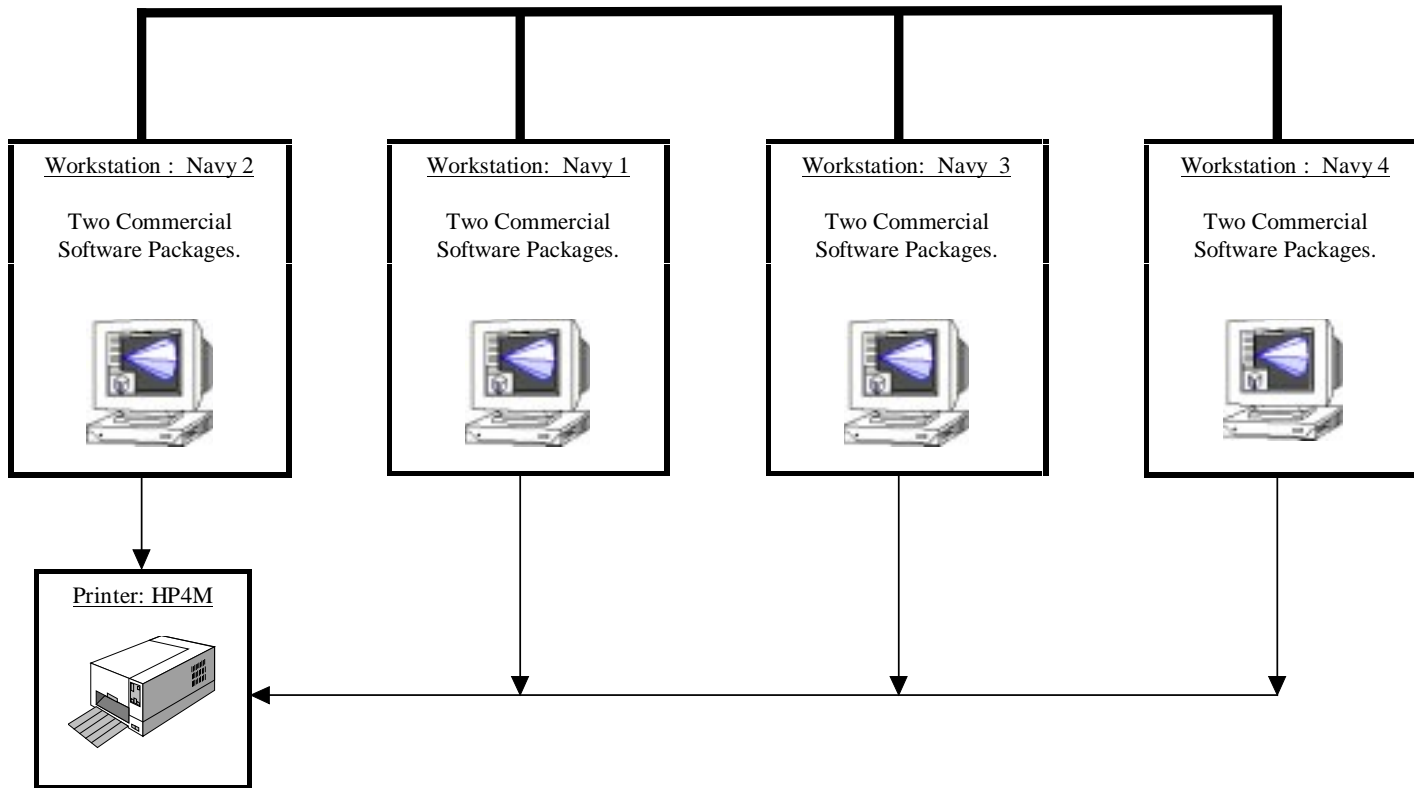


Figure 1.2 Computer Network During the Second Year.

### III. CROSSTALK EMI SIMULATIONS

The phenomenon of Crosstalk in a dual trace card was investigated by Ramchandani et al (1996). Consider a printed circuit board consisting of two traces and a ground plane as shown in Figure 3.1. One trace will act as a generator of the crosstalk. The generator trace is sometimes called the Culprit Trace. The other trace will be the receptor of the Crosstalk EMI. The receptor trace is

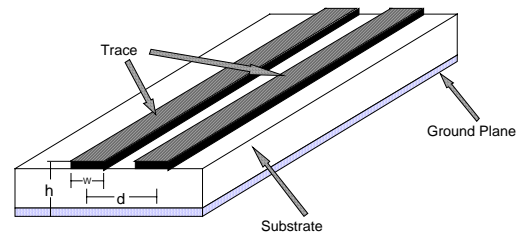


Figure 3.1. Geometry of a Dual Trace Card for Crosstalk EMI.

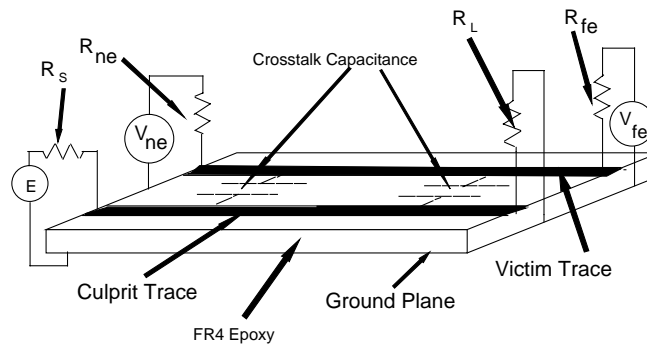


Figure 3.2. Near End and Far End Crosstalk.

sometimes called the Victim Trace. The ground plane will act as the reference conductor. The crosstalk circuitry associated with a dual trace card is shown in Figure 3.2. The current in the culprit trace circuit will produce electromagnetic fields that will interact with the victim trace circuit. This interaction will induce currents in the victim trace circuit. The induced currents in the victim trace will produce voltages  $V_{ne}$  and  $V_{fe}$  as shown in Figure 3.2. The subscripts "ne" and "fe" refer to "near end" and "far end" as shown in the Figure 3.2. Study of crosstalk involves Time Domain and Frequency Domain analysis of the near and far end voltages of the victim trace. Time-domain analysis is the determination of the time form of the victim trace voltages. Frequency-domain Crosstalk analysis is the determination of the magnitude and phase of the  $V_{ne}$  and  $V_{fe}$  for a steady state sinusoidal input to the culprit trace.

## A. SIMULATION GEOMETRIES

Six geometries with different levels of complexities were selected for Crosstalk EMI simulations. The first objective in the selection of these six geometries was to develop confidence and usage expertise with the commercial software packages. The second objective was to select geometries whose Crosstalk EMI could be theoretically modeled with relative ease. The third objective in the selection of these six geometries was their PEBB relevance. All six geometries are an extension of the geometry used in crosstalk in a dual trace card by Ramchandani et al (1996). The w/h ratio of Figure 3.1 was kept at unity for all simulations. In addition, the trace separation distance (d) values were kept at 2mm, 5mm, 11mm, 23mm and 44mms. The six geometries are shown in Figure 3.3.

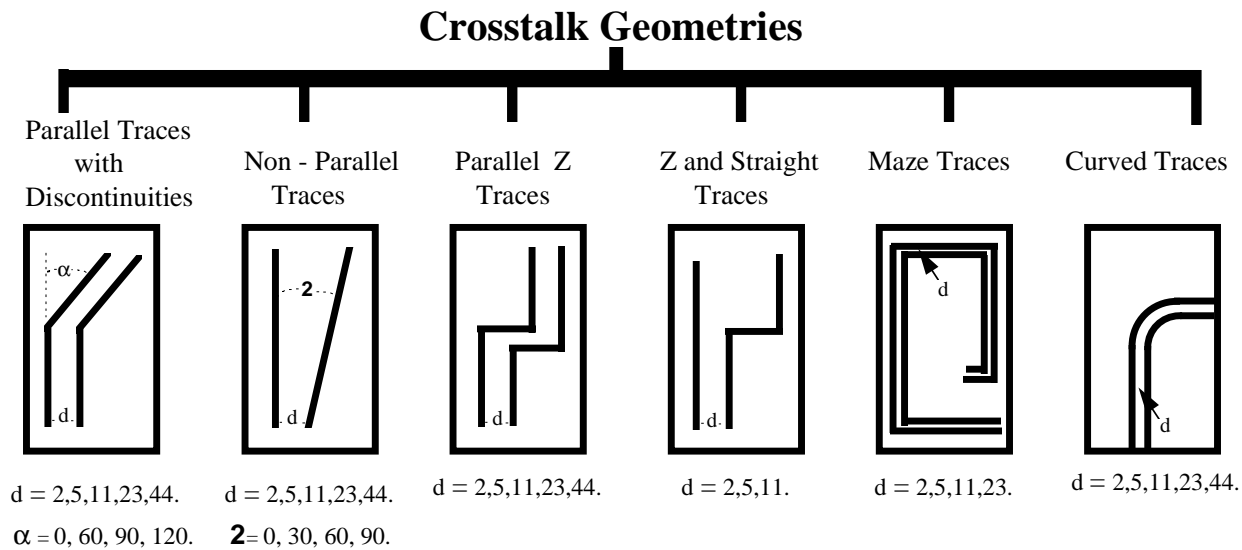


Figure 3.3. The Six Geometries for Crosstalk EMI Simulations.

## 1. Parallel Traces with Discontinuities

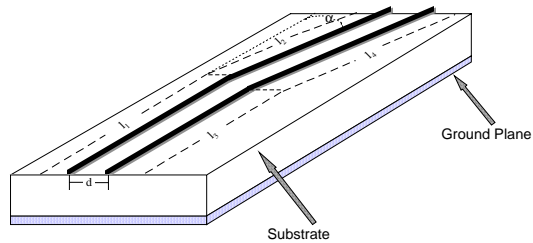


Figure 3.4. Printed Circuit Board Geometry for a Trace with Discontinuity.

This geometry comprises of two parallel traces, each with an angular discontinuity. The PEBB is going to have numerous trace discontinuities. Thus, this type of geometry would be PEBB relevant. Another reason for selecting this type of discontinuity was to study the correlation between trace separation ( $d$ ) and angular variation ( $\alpha$ ) on the Crosstalk EMI. The Printed Circuit Board Geometry of the Parallel Traces with Discontinuities is shown in Figure 3.4. The lengths  $l_1$ ,  $l_2$ ,  $l_3$  and  $l_4$  of the traces in Figure 3.4 were approx. 7 cms, 8 cms, 6.6 cms, and 8.4 cms respectively.

## 2. Non Parallel Traces

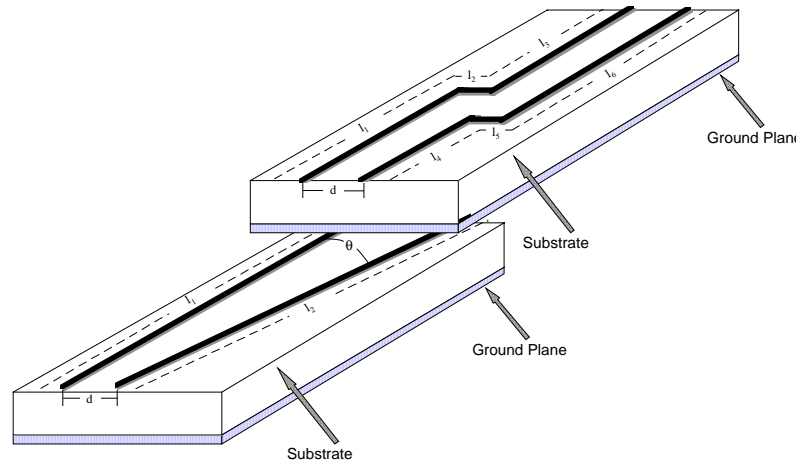


Figure 3.5. Printed Circuit Board Geometry for Non Parallel Traces.

This geometry comprises of two traces oriented at an angle of  $\theta$  relative to each other. The PEBB is going to have numerous such traces. Thus, this type of geometry would be PEBB relevant. One other reason for selecting this type of geometry was to study the impact the trace orientation ( $\theta$ ) would have on the reduction of crosstalk. The Printed Circuit Board Geometry of the Non Parallel Traces is shown in Figure 3.5. The lengths  $l_1$ , and  $l_2$  of the traces in Figure 3.5 were approx. 14 cms and 16 cms respectively.

### 3. Parallel Z Traces

Figure 3.6. Printed Circuit Board Geometry for Parallel Z Traces.

This geometry comprises of two abrupt 90 degree discontinuities in each trace. The PEBB is going to have numerous such abrupt discontinuities. One other reason for selecting this geometry was to compare the crosstalk from parallel Z traces with that from two straight parallel traces. The Printed Circuit Board Geometry of the Parallel Z Traces is shown in Figure 3.6. The lengths  $l_1$ ,  $l_2$ ,  $l_3$ ,  $l_4$ ,  $l_5$ , and  $l_6$  of the traces in Figure 3.6 were approx. 7 cms, 1 cms, 7 cms, 6.5 cms, 1 cms and 7.5 cms respectively.

### 4. Z and Straight Traces

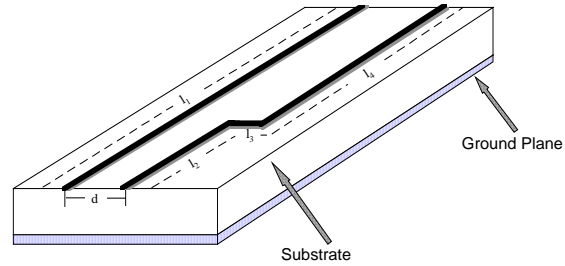


Figure 3.7. Printed Circuit Board Geometry for Z and Straight Traces.

This geometry comprises of one straight trace and the other with two abrupt 90 degree discontinuities. The PEBB is going to have traces which could be approximated to this situation. Another reason for selecting this geometry was to compare the crosstalk from this geometry with the crosstalk from parallel Z traces. The Printed Circuit Board Geometry of the Z and Straight Traces is shown in Figure 3.7. The lengths  $l_1$ ,  $l_2$ ,  $l_3$ , and  $l_4$  of the traces in Figure 3.7 were approx. 14 cms, 7 cms, 1 cms and 7 cms respectively.

## 5. Maze Traces

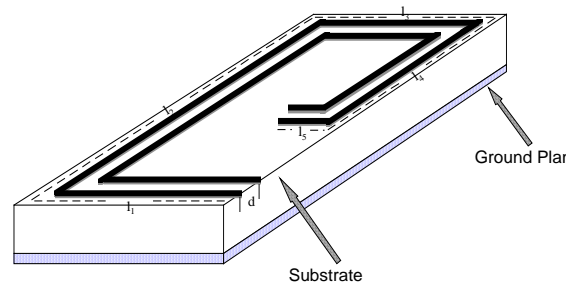


Figure 3.8. Printed Circuit Board Geometry for Maze Traces.

This geometry comprises of two parallel traces with four abrupt 90 degrees discontinuities in each trace. A major consideration for selecting this geometry was to incorporate manageable complexities in the simulation models. The Printed Circuit Board Geometry of the Maze Traces is shown in Figure 3.8. The lengths  $l_1$ ,  $l_2$ ,  $l_3$ ,  $l_4$ , and  $l_5$  of the traces in Figure 3.8 were approx. 10.8 cms, 13.6 cms, 10.6 cms, 8 cms, 1 cm and 5.3 cms respectively.

## 6. Curved Traces

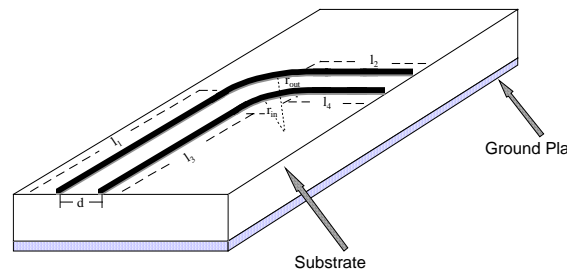


Figure 3.9. Printed Circuit Board Geometry for Curved Traces.

This geometry comprises of two parallel traces each with a quarter circle and two straight traces. A major consideration in selecting this geometry was to incorporate curvature in a trace. The PEBB is going to have traces which could be approximated to this situation. The Printed Circuit Board Geometry of the Curved Traces is shown in Figure 3.9. The lengths  $l_1$ ,  $l_2$ ,  $l_3$ , and  $l_4$  of the traces in Figure 3.9 were approx. 6.2 cms, 3.2 cms, 6.2 cms and 3.2 cms respectively. The radius of the outer and inner quarter circle were 9 cms and 6.5 cms respectively.

## B. THEORETICAL MODELS OF THE SIX GEOMETRIES

Following Paul (1996), the frequency domain near and far end crosstalks for a dual trace card with a ground plane as shown in Figure 3.2 are given by:

$$\frac{V_{ne}}{V_S} = j\omega [ \text{IND}_{ne} + \text{CAP}_{ne} ]$$

$$\frac{V_{fe}}{V_S} = j\omega [ \text{IND}_{fe} + \text{CAP}_{fe} ]$$

where  $R_{ne}$ ,  $R_{fe}$ ,  $R_S$  and  $R_L$  are as shown in Figure 3.2 and

$$\text{IND}_{ne} = \left( \frac{R_{ne}}{R_{ne} + R_{fe}} \right) \left( \frac{L_m}{R_S + R_L} \right)$$

$$\text{CAP}_{ne} = \left( \frac{R_{ne} R_{fe}}{R_{ne} + R_{fe}} \right) \left( \frac{R_L C_m}{R_S + R_L} \right)$$

$$\text{IND}_{fe} = \left( \frac{R_{fe}}{R_{ne} + R_{fe}} \right) \left( \frac{L_m}{R_S + R_L} \right)$$

$$\text{CAP}_{fe} = \left( \frac{R_{ne} R_{fe}}{R_{ne} + R_{fe}} \right) \left( \frac{R_L C_m}{R_S + R_L} \right)$$

where

$\omega = 2 \pi f =$  Angular velocity in radians per second.

$f =$  Frequency in Hertz.

$L_m = l_m l =$  Total mutual inductance between culprit and victim traces in Henries.

$C_m = c_m l =$  Total mutual capacitance between culprit and victim traces in Farads.

$l_m =$  Per unit length mutual inductance between culprit and victim traces in Henries per meter.

$c_m =$  Per unit length mutual capacitance between culprit and victim traces in Farads per meter.

$l =$  Trace length in meters.

.....(3.1)

## 1. Parallel Traces with Discontinuities

From the Printed Circuit Board Geometry of Figure 3.4 it can be seen that there are two parallel traces each with an angular discontinuity ( $\alpha$ ). A trace with an angular discontinuity can be considered to be made up of two traces oriented an angle  $\alpha$ . Chadha et al (1981) and Walker (1990) have shown that there exists mutual inductance and capacitance between two traces on a printed circuit board. Ramchandani et al (1996) used this method to determine the mutual inductance and capacitance between two parallel traces. Parallel traces with discontinuities is an extension of the work done earlier by Ramchandani et al (1996). For determining the mutual

inductances and capacitances of this geometry there are essentially four traces. Inductive and Capacitive coupling mechanisms for these four traces are shown in Figures 3.10 and 3.11 respectively. Following Walker (1990), the mutual Inductances and Capacitances are given by:

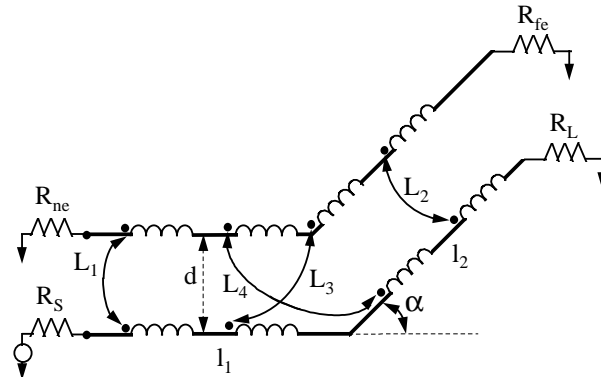


Figure 3.10. Mutual Inductances for Parallel Traces with Discontinuities.

$$L_1 = \frac{\mu l_1}{4\pi} \ln\{1 + (2h/d)^2\} \quad \text{Henries}$$

$$L_2 = \frac{\mu l_2}{4\pi} \ln\{1 + (2h/d)^2\} \quad \text{Henries}$$

$$L_3 = \mu \Delta l_i \quad 2h$$

$$L_3 = \sum_{i=1} \frac{1}{4\pi} \ln \left[ 1 + \left\{ \frac{2h}{(m l_i + d)} \right\}^2 \right] \text{ Henries}$$

$$L_4 = \sum_{i=1}^N \frac{\mu \Delta l_i}{4\pi} \ln \left[ 1 + \left\{ \frac{2h}{(m l_i + d)} \right\}^2 \right] \text{ Henries}$$

$$L_m = L_1 + L_2 + L_3 + L_4 \quad \text{Henries}$$

where

$\mu = \mu_r \mu_o =$  Permeability of the substrate in Henries per meter.

$\mu_o =$  Permeability of free space.  $= 4\pi 10^{-7}$  Henries per meter.

$\mu_r =$  Relative permeability of the substrate.

$l_1 =$  Length of the horizontal trace in meters.

$l_2 =$  Length of the inclined trace in meters.

$\Delta l_i =$  Differential segment of the respective trace.

$m = \tan(\alpha) =$  Slope of the trace.

$w =$  Width of the trace in meters.

$h =$  Height of the trace in meters.

$d =$  Separation distance between the traces in meters.

.....(3.2)

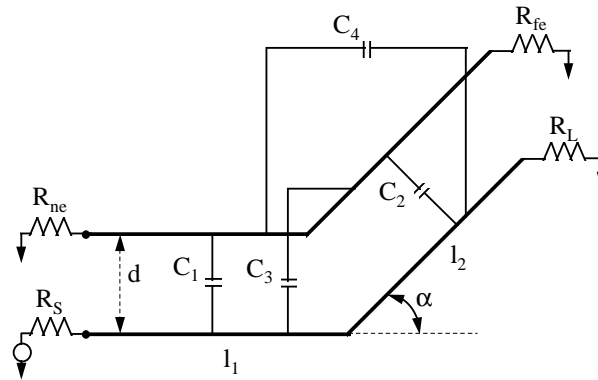


Figure 3.11. Mutual Capacitances for Parallel Traces with Discontinuities.

$$C_1 = \frac{\epsilon l_1}{\pi} K_c K_L \left\{ \frac{w}{d} \right\}^2 \quad \text{Farads}$$

$$C_2 = \frac{\epsilon l_2}{\pi} K_c K_L \left\{ \frac{w}{d} \right\}^2 \quad \text{Farads}$$

$$C_3 = \sum_{i=1}^N \frac{\epsilon \Delta l_i}{\pi} K_c K_L \left\{ \frac{w}{(m l_i + d)} \right\}^2 \quad \text{Farads}$$

$$C_4 = \sum_{i=1}^N \frac{\epsilon \Delta l_2}{\pi} K_c K_L \left\{ \frac{w}{(m l_i + d)} \right\}^2 \quad \text{Farads}$$

$$C_m = C_1 + C_2 + C_3 + C_4 \quad \text{Farads}$$

where

$$\epsilon = \epsilon_0 \epsilon_r = \text{Permittivity of the substrate in Farads per meter.}$$

- $\epsilon_0$  = Permittivity of free space. =  $(1/36\pi) 10^{-9}$  Farads per meter.
- $\epsilon_r$  = Relative permittivity of the substrate.
- $K_c$  = Fringing factor for capacitance.
- $K_L$  = Fringing factor for inductance.
- $l_1$  = Length of the horizontal trace in meters.
- $l_2$  = Length of the inclined trace in meters.
- $\Delta l_i$  = Differential segment of the respective trace.
- $m$  =  $\tan(\alpha)$  = Slope of the trace.
- $w$  = Width of the trace in meters.
- $h$  = Height of the trace in meters.
- $d$  = Separation distance between the traces in meters.

.....(3.3)

## 2. Non Parallel Traces

From the Printed Circuit Board Geometry of Figure 3.5 it can be seen there are two non parallel traces oriented at an angle of  $\theta$  relative to each other. Inductive and Capacitive coupling mechanisms for these two traces are shown in Figure 3.12. Following Walker (1990), the mutual Inductances and Capacitances are given by:

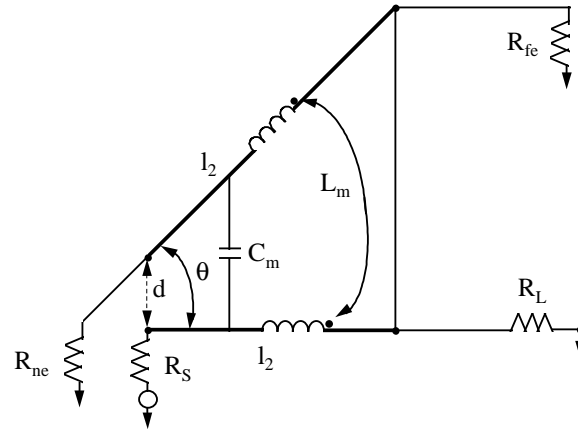


Figure 3.12. Mutual Inductances and Capacitances for Non Parallel Traces.

$$L_m = \sum_{i=1}^i \frac{\mu \Delta l_i}{4\pi} \ln \left[ 1 + \left\{ \frac{2h}{(m l_i + d)} \right\}^2 \right] \text{ Henries}$$

$$C_m = \sum_{i=1}^i \frac{\epsilon \Delta l_i}{\pi} K_c K_L \left\{ \frac{w}{(m l_i + d)} \right\}^2 \text{ Farads}$$

where

$\mu = \mu_r \mu_o =$  Permeability of the substrate in Henries per meter.

$\mu_o =$  Permeability of free space.  $= 4\pi 10^{-7}$  Henries per meter.

$\mu_r =$  Relative permeability of the substrate.

$\epsilon = \epsilon_o \epsilon_r =$  Permittivity of the substrate in Farads per meter.

$\epsilon_0$  = Permittivity of free space. =  $(1/36\pi) 10^{-9}$  Farads per meter.

$\epsilon_r$  = Relative permittivity of the substrate.

$K_L$  = Fringing factor for inductance.

$K_c$  = Fringing factor for capacitance.

$m$  =  $\tan(\theta)$  = Slope of the traces relative to each other.

$\Delta l_i$  = Differential segment of the trace in meters.

$w$  = Width of the trace in meters.

$h$  = Height of the trace in meters.

$d$  = Separation distance between the traces in meters.

.....(3.4)

### 3. Parallel Z Traces

From the Printed Circuit Board Geometry of Figure 3.6 it can be seen that there are two abrupt 90 degree discontinuities in each trace. Inductive and Capacitive coupling mechanisms for these two traces are shown in Figure 3.13. Following Walker (1990) the mutual Inductances and Capacitances are given by:

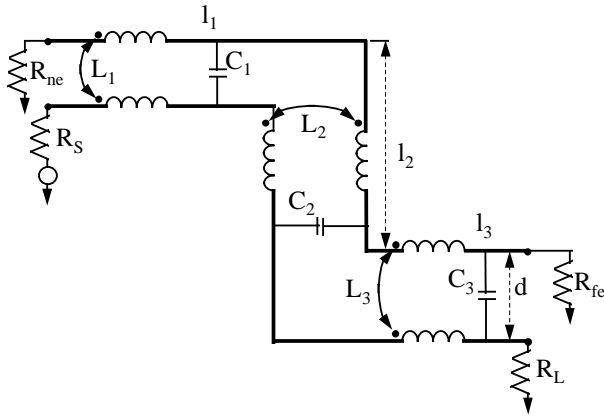


Figure 3.13. Mutual Inductances and Capacitances for Parallel Z Traces.

$$L_m = \sum_{i=1}^3 \frac{\mu l_i}{4\pi} \ln \{ 1 + (2h/d_i)^2 \} \quad \text{Henries}$$

$$C_m = \sum_{i=1}^3 \frac{\epsilon l_i}{\pi} K_c K_L \{ w/d_i \}^2 \quad \text{Farads}$$

where

$$\mu = \mu_r \mu_o = \text{Permeability of the substrate in Henries per meter.}$$

$$\mu_o = \text{Permeability of free space.} = 4\pi 10^{-7} \text{ Henries per meter.}$$

$$\mu_r = \text{Relative permeability of the substrate.}$$

$$\epsilon = \epsilon_o \epsilon_r = \text{Permittivity of the substrate in Farads per meter.}$$

$\epsilon_0$  = Permittivity of free space. =  $(1/36\pi) 10^{-9}$  Farads per meter.

$\epsilon_r$  = Relative permittivity of the substrate.

$K_L$  = Fringing factor for inductance.

$K_c$  = Fringing factor for capacitance.

$l_i$  = Length of the  $i$ th trace in meters.

$w$  = Width of the trace in meters.

$h$  = Height of the trace in meters.

$d_i$  = Separation distance between the traces in meters.

.....(3.5)

#### 4. Z and Straight Traces

From the Printed Circuit Board Geometry of Figure 3.7 it can be seen that there is one straight trace and the other with two abrupt 90 degree discontinuities. Inductive and Capacitive coupling mechanisms for these two traces are shown in Figure 3.14. Following Walker (1990), the mutual Inductances and Capacitances are given by:

$$L_m = \sum_{i=1}^2 \frac{\mu l_i}{4\pi} \ln \left\{ 1 + (2h/d_i)^2 \right\} \quad \text{Henries}$$

$$C_m = \sum_{i=1}^2 \frac{\epsilon l_i}{\pi} K_c K_L \left\{ w/d_i \right\}^2 \quad \text{Farads}$$

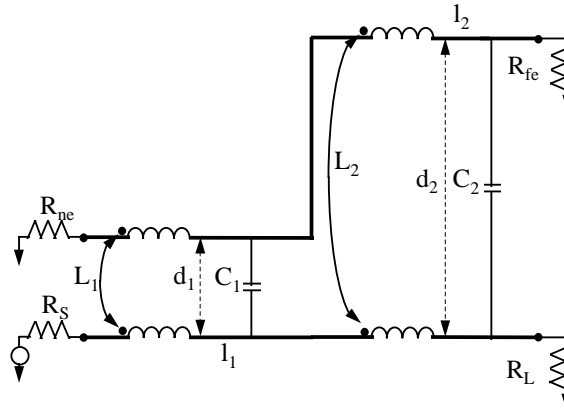


Figure 3.14. Mutual Inductances and Capacitances for Z and Straight Traces.

where

$\mu = \mu_r \mu_0 =$  Permeability of the substrate in Henries per meter.

$\mu_0 =$  Permeability of free space.  $= 4\pi 10^{-7}$  Henries per meter.

$\mu_r =$  Relative permeability of the substrate.

$\epsilon = \epsilon_0 \epsilon_r =$  Permittivity of the substrate in Farads per meter.

$\epsilon_0 =$  Permittivity of free space.  $= (1/36\pi) 10^{-9}$  Farads per meter.

$\epsilon_r =$  Relative permittivity of the substrate.

$K_L =$  Fringing factor for inductance.

$K_c =$  Fringing factor for capacitance.

- $l_i$  = Length of the trace in meters.
- $w$  = Width of the trace in meters.
- $h$  = Height of the trace in meters.
- $d_i$  = Separation distance between the traces in meters.

.....(3.6)

### 5. Maze Traces

From the Printed Circuit Board Geometry of Figure 3.8 it can be seen that there are two parallel traces with four abrupt 90 degree discontinuities. Inductive and Capacitive coupling mechanisms for these two traces are shown in Figures 3.15 and 3.16 respectively. In order to keep these two figures manageable, only major inductive and capacitive couplings are shown. Following Walker (1990), the mutual Inductances and Capacitances are given by:

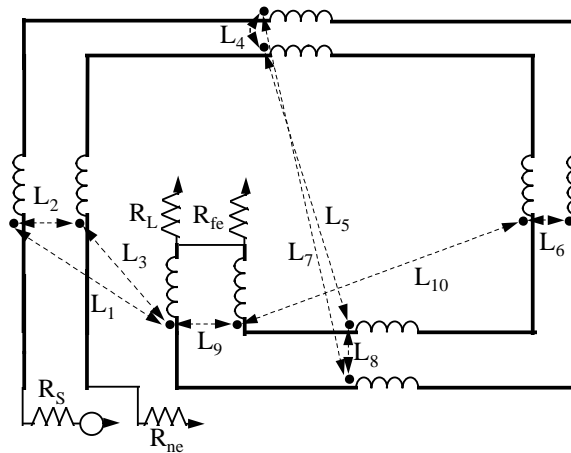


Figure 3.15. Mutual Inductances for Maze Traces.

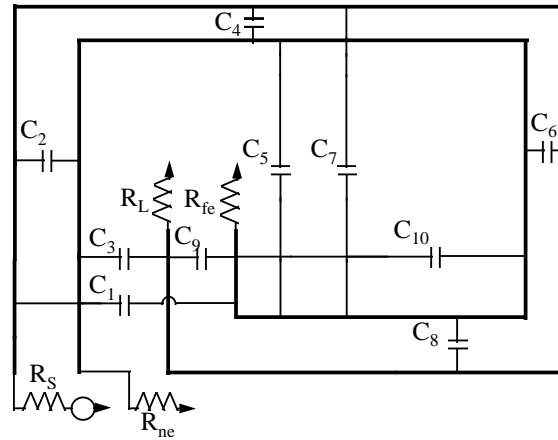


Figure 3.16. Mutual Capacitances for Maze Traces.

$$L_m = \sum_{i=1}^i \frac{\mu l_i}{4\pi} \ln \{ 1 + (2h/d_i)^2 \} \quad \text{Henries}$$

$$C_m = \sum_{i=1}^i \frac{\epsilon l_i}{\pi} K_c K_L \{ w/d_i \}^2 \quad \text{Farads}$$

where

- $\mu$  =  $\mu_r \mu_o$  = Permeability of the substrate in Henries per meter.
  - $\mu_o$  = Permeability of free space. =  $4\pi 10^{-7}$  Henries per meter.
  - $\mu_r$  = Relative permeability of the substrate.
  - $\epsilon$  =  $\epsilon_o \epsilon_r$  = Permittivity of the substrate in Farads per meter.
  - $\epsilon_o$  = Permittivity of free space. =  $(1/36\pi) 10^{-9}$  Farads per meter.
  - $\epsilon_r$  = Relative permittivity of the substrate.
  - $K_L$  = Fringing factor for inductance.
  - $K_c$  = Fringing factor for capacitance.
  - $l_i$  = Length of the trace in meters.
  - $w$  = Width of the trace in meters.
  - $h$  = Height of the trace in meters.
  - $d_i$  = Separation distance between the traces in meters.
  - $i$  = Number of major couplings.
- .....(3.7)

## 6. Curved Traces

From the Printed Circuit Board Geometry of Figure 3.8 it can be seen that there are two parallel traces each with a quarter circle and two straight traces. Inductive and Capacitive coupling mechanisms for these two traces are shown in Figure 3.17. Following Walker (1990), the mutual Inductances and Capacitances are given by:

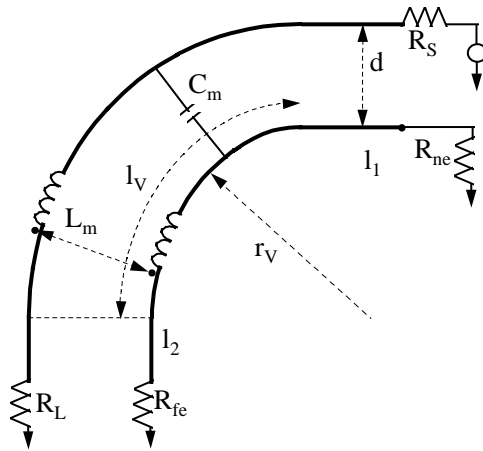


Figure 3.17. Mutual Inductances and Capacitances for Curved Traces.

$$L_m = \frac{\mu (l_1 + l_2 + .5\pi r_v)}{4\pi} \ln \{ 1 + (2h/d_i)^2 \} \quad \text{Henries}$$

$$C_m = \frac{\epsilon (l_1 + l_2 + .5\pi r_v)}{\pi} K_c K_L \{ w/d_i \}^2 \quad \text{Farads}$$

where

$$\mu = \mu_r \mu_o = \text{Permeability of the substrate in Henries per meter.}$$

$$\mu_o = \text{Permeability of free space.} = 4\pi 10^{-7} \text{ Henries per meter.}$$

- $\mu_r$  = Relative permeability of the substrate.
  - $\epsilon$  =  $\epsilon_0\epsilon_r$  = Permittivity of the substrate in Farads per meter.
  - $\epsilon_0$  = Permittivity of free space. =  $(1/36\pi) 10^{-9}$  Farads per meter.
  - $\epsilon_r$  = Relative permittivity of the substrate.
  - $K_L$  = Fringing factor for inductance.
  - $K_c$  = Fringing factor for capacitance.
  - $l_i$  = Length of the trace in meters.
  - $w$  = Width of the trace in meters.
  - $h$  = Height of the trace in meters.
  - $d_i$  = Separation distance between the traces in meters.
  - $i$  = Number of major couplings.
- .....(3.8)

## C. COMPUTER SIMULATIONS

Computer simulation of an object using the commercial software packages require several basic steps which have to be followed in a structured format. The basic steps are: 1) Identifying the circuit parameters to solve, 2) Drawing the geometric model of the simulation object, 3) Assigning material properties to each component of the simulation object, 4) Defining conductors and sources, 5) Setting up solution criteria of the simulation, 6) Solving for capacitance, inductance and resistance matrices, 7) Post Processing to view and analyze the results and export them to a circuit analysis package like Pspice.

### 1) Identifying circuit parameters.

In this step the parameters to be computed (inductance, capacitance and resistance) are identified.

### 2) Drawing the geometric model.

This step allows the creation of a 3 D geometric model of the simulation object. In this step there

are software commands to create just about any type of a 3D object. After the model is created, it can be viewed from different positions.

### 3) Assigning material properties.

In this step all components of the simulation object are assigned their respective electromagnetic material properties. Properties such as conductivity, permittivity have to be assigned to each component of the simulation object. The software packages have a database of the attributes of commonly used materials. However, the databases can be expanded to incorporate new materials.

### 4) Defining conductors and sources.

In this step the objects which are electrical sources and objects which are conductors are identified. For capacitance computations voltage sources have to be defined. For inductance and resistance computations current sources have to be defined.

### 5) Setting up solution criteria.

In this step the starting mesh and the stopping criteria are assigned. The starting mesh could be either adaptive or specified by the user. The adaptive mesh is an optimal starting mesh generated by the package for the simulation object.

6) Solving for capacitance, inductance and resistance matrices.

This step initiates the solution of the circuit parameters of the simulation object. The solution continues until the stopping criteria specified in the earlier step are fulfilled. One of the stopping criterion is the number of passes that are made on the mesh of the object. Usually, the more passes are specified the more accurate the solution tends to be. However, more passes mean more numerical computations. This in turn requires more computational time and more memory capacity of the computer. Typically, three passes produce a reasonably accurate solution. These simulations are time efficient and take an average of an hour.

7) Post Processing to view and analyze the results and export them to a circuit analysis package.

This step displays the manner in which the solution converged. The solution convergence indicates the accuracy of the results of the simulation. In addition, this step processes the solution results to display the matrices of the requested parameters. The circuit parameters are then exported to Pspice, or its derivative, where the circuit analysis is performed.

The following, Near End and Far End Frequency Domain Crosstalk, simulations were done for the six geometries:

1. Traces with Discontinuities:  $d = 2, 5, 11, 23, \text{ and } 44$  mms.  $\alpha = 0, 60, 90, 120$  degrees.
2. Non Parallel Traces:  $d = 2, 5, 11, 23, \text{ and } 44$  mms.  $\theta = 0, 30, 60$  and  $90$  degrees.
3. Parallel Z Traces:  $d = 2, 5, 11$  and  $23$  mms.
4. Z and Straight Traces:  $d = 2, 5, 11$  mms.
5. Maze Traces:  $d = 2, 5, 11$  and  $23$  mms.
6. Curved Traces.  $d = 2, 5, 11, 23, \text{ and } 44$  mms.

The dimensions of all the geometries of the above simulations are shown in the Appendix.

#### D. COMPUTER SIMULATION RESULTS

All computer simulations of Near End and Far End Frequency Domain Crosstalks were done with  $R_{ne} = R_{fe} = R_S = R_L = 50$  ohms.

##### 1. Results for Non Parallel $\theta = 0$ , Parallel Z, Z and Straight, Maze and Curved Traces.

One set of Near End and Far End Frequency Domain Crosstalks for the five types of traces is shown in Figures 3.18 through 3.27. In each of these simulations the separation distance was varied and the two frequency domain crosstalks were determined for the five types of traces. Table 3.1 summarizes the different results with their corresponding figures for the five types of traces.

| Type of Trace             | Near End Crosstalk | Far End Crosstalk |
|---------------------------|--------------------|-------------------|
| Non Parallel $\theta = 0$ | Figure 3.18        | Figure 3.19       |
| Parallel Z                | Figure 3.20        | Figure 3.21       |
| Z and Straight            | Figure 3.22        | Figure 3.23       |
| Maze                      | Figure 3.24        | Figure 3.25       |
| Curved                    | Figure 3.26        | Figure 3.27       |

Table 3.1. Simulated Crosstalk Results for Non Parallel  $\theta = 0$ , Parallel Z, Z and Straight, Maze and Curved Traces.

The other set of Near End and Far End Frequency Domain Crosstalks for the five types of traces is shown in Figures 3.28 through 3.37. In each of these simulations the separation distance was kept constant and the two frequency domain crosstalks were determined for all five types of traces.

Table 3.2 summarizes the different results with their corresponding figures for the five types of traces.

| Separation Distance | Near End Crosstalk | Far End Crosstalk |
|---------------------|--------------------|-------------------|
| d = 2 mms           | Figure 3.28        | Figure 3.29       |
| d = 5 mms           | Figure 3.30        | Figure 3.31       |
| d = 11 mms          | Figure 3.32        | Figure 3.33       |
| d = 23 mms          | Figure 3.34        | Figure 3.35       |
| d = 44 mms          | Figure 3.36        | Figure 3.37       |

Table 3.2. Simulated Crosstalk Results for Non Parallel  $\theta = 0$ , Parallel Z, Z and Straight, Maze and Curved Traces for five separation distances.

## 2. Results for Non Parallel Traces.

One set of Near End and Far End Frequency Domain Crosstalks for Non Parallel Traces is shown in Figures 3.38 through 3.47. In each of these simulations the separation distance was kept constant and the two frequency domain crosstalks were determined for different angles of orientations ( $\theta$ ). Table 3.3 summarizes the different results with their corresponding figures for the five separation distances.

| Separation Distance | Near End Crosstalk | Far End Crosstalk |
|---------------------|--------------------|-------------------|
| d = 2 mms           | Figure 3.38        | Figure 3.39       |
| d = 5 mms           | Figure 3.40        | Figure 3.41       |

| Separation Distance | Near End Crosstalk | Far End Crosstalk |
|---------------------|--------------------|-------------------|
| d = 11 mms          | Figure 3.42        | Figure 3.43       |
| d = 23 mms          | Figure 3.44        | Figure 3.45       |
| d = 44 mms          | Figure 3.46        | Figure 3.47       |

Table 3.3. Simulated Crosstalk Results for Non Parallel Traces for five separation distances.

The other set of Near End and Far End Frequency Domain Crosstalks for Non Parallel of Traces is shown in Figures 3.48 through 3.51. In each of these simulations the angle ( $\theta$ ) of orientation was kept constant but the separation distance was varied. The two frequency domain crosstalks were determined for different separation distances. Table 3.4 summarizes the different results with their corresponding figures for the two  $\theta$ s.

| Angle of orientation $\theta$ | Near End Crosstalk | Far End Crosstalk |
|-------------------------------|--------------------|-------------------|
| 0 Degrees                     | Figure 3.48        | Figure 3.49       |
| 90 Degrees                    | Figure 3.50        | Figure 3.51       |

Table 3.4. Simulated Crosstalk Results for Non Parallel Traces for two  $\theta$ s.

### 3. Results for Parallel Traces with Discontinuities.

One set of Near End and Far End Frequency Domain Crosstalks for Parallel Traces with Discontinuities is shown in Figures 3.52 through 3.59. In each of these simulations the angle ( $\alpha$ ) of discontinuity was kept constant but the separation distance was varied. The two

frequency domain crosstalks were determined for different separation distances. Table 3.5 summarizes the different results with their corresponding figures for the four  $\alpha$ s.

| Angle of Discontinuity $\alpha$ | Near End Crosstalk | Far End Crosstalk |
|---------------------------------|--------------------|-------------------|
| 0 Degrees                       | Figure 3.52        | Figure 3.53       |
| 60 Degrees                      | Figure 3.54        | Figure 3.55       |
| 90 Degrees                      | Figure 3.56        | Figure 3.57       |
| 120 Degrees                     | Figure 3.58        | Figure 3.59       |

Table 3.5. Simulated Crosstalk Results for Parallel Traces with Discontinuities for four  $\alpha$ s.

The other set of Near End and Far End Frequency Domain Crosstalks for Parallel Traces with Discontinuities is shown in Figures 3.60 through 3.63. In each of these simulations the separation distance was kept constant and the two frequency domain crosstalks were determined for different angles of discontinuity ( $\alpha$ ). Table 3.6 summarizes the different results with their corresponding figures for the five separation distances.

| Separation Distance | Near End Crosstalk | Far End Crosstalk |
|---------------------|--------------------|-------------------|
| d = 2 mms           | Figure 3.60        | Figure 3.61       |
| d = 5 mms           | Figure 3.62        | Figure 3.63       |

Table 3.6. Simulated Crosstalk Results for Parallel Traces with Discontinuities for two separation distances.

## E. DISCUSSION AND CONCLUSIONS OF THE RESULTS

### 1. Direct dependence (20 dB per decade) of frequency domain Crosstalk on the culprit trace frequency.

For Straight Parallel, Parallel Z, Z and Straight, Maze and Curved Traces:

i) From Figures 3.18 through 3.27 it can be seen that the crosstalk is directly proportional to the culprit trace frequency for every separation distance (d). ii) From Figures 3.28 through 3.37 it can be seen that for a given trace separation distance (d), the crosstalk is directly proportional to the culprit trace frequency for all five types of traces.

For Non Parallel Traces:

i) From Figures 3.38 through 3.47 it can be seen that for a given trace separation distance (d), the crosstalk is directly proportional to the culprit trace frequency for all four angles of trace orientation ( $\theta$ ). ii) From Figures 3.48 through 3.51 it can be seen that for both angles of orientation ( $\theta = 0$  and  $90$ ), the crosstalk is directly proportional to the culprit trace frequency for every separation distance (d) between the traces.

For Parallel Traces with Discontinuities:

i) From Figures 3.52 through 3.59 it can be seen that for all four angles of discontinuity ( $\alpha = 0, 60, 90$  and  $120$ ), the crosstalk is directly proportional to the culprit trace frequency for every separation distance (d) between the traces. ii) From Figures 3.60 through 3.63 it can be seen that for a given trace separation distance (d), the crosstalk is directly proportional to the culprit trace frequency for all four angles of discontinuity ( $\alpha$ ).

The conclusion is that for any trace geometry, the Crosstalk is a direct function (20 dB per decade) of the culprit trace frequency. Thus, to minimize the crosstalk, the culprit trace frequencies should be kept as low as possible. This conclusion is reinforced by recognizing that crosstalk is the direct result of the inductive and capacitive couplings between the culprit and the victim traces. In any circuit, the inductive and capacitive contributions are direct functions of the source (culprit) frequency.

### 2. Dependence of Crosstalk on separation distance (d) between culprit and victim traces.

For Straight Parallel, Parallel Z, Z and Straight, Maze and Curved Traces:

From Figures 3.18 through 3.27 it can be seen that for all five types of traces the crosstalk is lower as the separation distance (d) increases between the Culprit and Victim traces.

For Non Parallel Traces:

From Figures 3.48 through 3.51, it can be seen that for both angles of orientation ( $\theta = 0$  and  $90$ ), the crosstalk is lower as the separation distance (d) increases between the culprit and victim traces.

For Parallel Traces with Discontinuities:

From Figures 3.52 through 3.59 it can be seen that for all four angles of discontinuity ( $\alpha = 0, 60, 90$  and  $120$ ), the crosstalk is lower as the separation distance (d) increases between the culprit and victim traces.

The conclusion is that the Crosstalk is lower as the separation distance (d) increases between the culprit and victim traces. For lower crosstalk, a critical component should be separated as much as possible from a potential culprit. This conclusion is reinforced by recognizing that as the separation distance (d) increases the inductive and capacitive crosstalk couplings between the culprit and victim traces weaken.

### 3. Dependence of Crosstalk on the orientation angle ( $\theta$ ) between culprit and victim traces.

From Figures 3.38 through 3.47, for Non Parallel Traces, it can be seen that for a given separation distance (d) the crosstalk is highest when the angle of orientation ( $\theta$ ) is zero between the traces. The crosstalk reduces as  $\theta$  increases from zero to thirty degrees. The crosstalk reduces further as  $\theta$  increases from thirty to sixty degrees. However, the dramatic reduction in crosstalk occurs when  $\theta$  is ninety degrees. At ninety degrees the crosstalk is practically non-existent. This is more poignantly shown in Figures 3.50 and 3.51.

The conclusion is that the Crosstalk reduces as the angle of orientation increases between the culprit and victim traces. Thus, for lower crosstalk, the location of a critical component should be such that it is oriented at ninety degrees from a potential culprit trace. This conclusion is reinforced by recognizing that as the angle of orientation ( $\theta$ ) increases the inductive and capacitive crosstalk couplings between the culprit and victim traces weaken. The ideal crosstalk isolation of a critical component can be achieved by incorporating both a large separation distance (d) and a ninety degree orientation from a potential culprit trace.

### 4. Dependence of Crosstalk on the geometry of the culprit and victim traces.

Straight Parallel, Parallel Z, Z and Straight, Maze and Curved Traces.

From Figures 3.28 through 3.37 it can be seen that for a given separation distance (d) the crosstalk is: highest for Maze Traces, followed by Curved Traces, Straight Parallel Traces, Parallel Z Traces and the least for Z & Straight Traces.

The Maze Traces are made up of a number of conductors in close proximity. Thus, more numerous and stronger inductive and capacitive couplings between the culprit trace and the victim trace are created. These numerous and stronger crosstalk couplings result in higher crosstalk. The Z and Straight Traces are made up of fewer conductors inherently separated by large distances. Thus, fewer and weaker inductive and capacitive couplings between the culprit trace and the victim trace are created. These fewer and weaker crosstalk couplings result in lower crosstalk for the Z and Straight Traces. The conclusion is that the Crosstalk is lower when the trace geometry possesses fewer and weaker inductive and capacitive crosstalk couplings.

#### 5. Crosstalk from Parallel Traces with Discontinuities ( $\alpha$ ).

From Figures 3.60 through 3.63 it can be seen that for a given separation distance (d) the crosstalk remains essentially the same for all four angles ( $\alpha = 0, 60, 90$  and  $120$  degrees) of discontinuity. To conclude from these figures that trace discontinuity has little or no impact on the crosstalk would be an erroneous conclusion. For these simulations the separation distance was 2 and 5 mms. For these two separation distances the inductive and capacitive couplings between the culprit trace and the victim trace are relatively strong. Furthermore, for  $\alpha$  ranging between 0 and 120 degrees, the crosstalk couplings resulting from the trace discontinuity are relatively weak. This is what Figures 3.60 through 3.63 are conveying. It is very likely that an increase in  $\alpha$  and in the separation distance (d) will result in stronger crosstalk couplings due to trace discontinuity. This issue will be revisited next year. This year there were simulation problems which prevented extending  $\alpha$  beyond 120 degrees.

Figure 3.18. Simulated Frequency Domain Near End Crosstalk for Non-Parallel Traces  $\theta = 0$  Degrees.

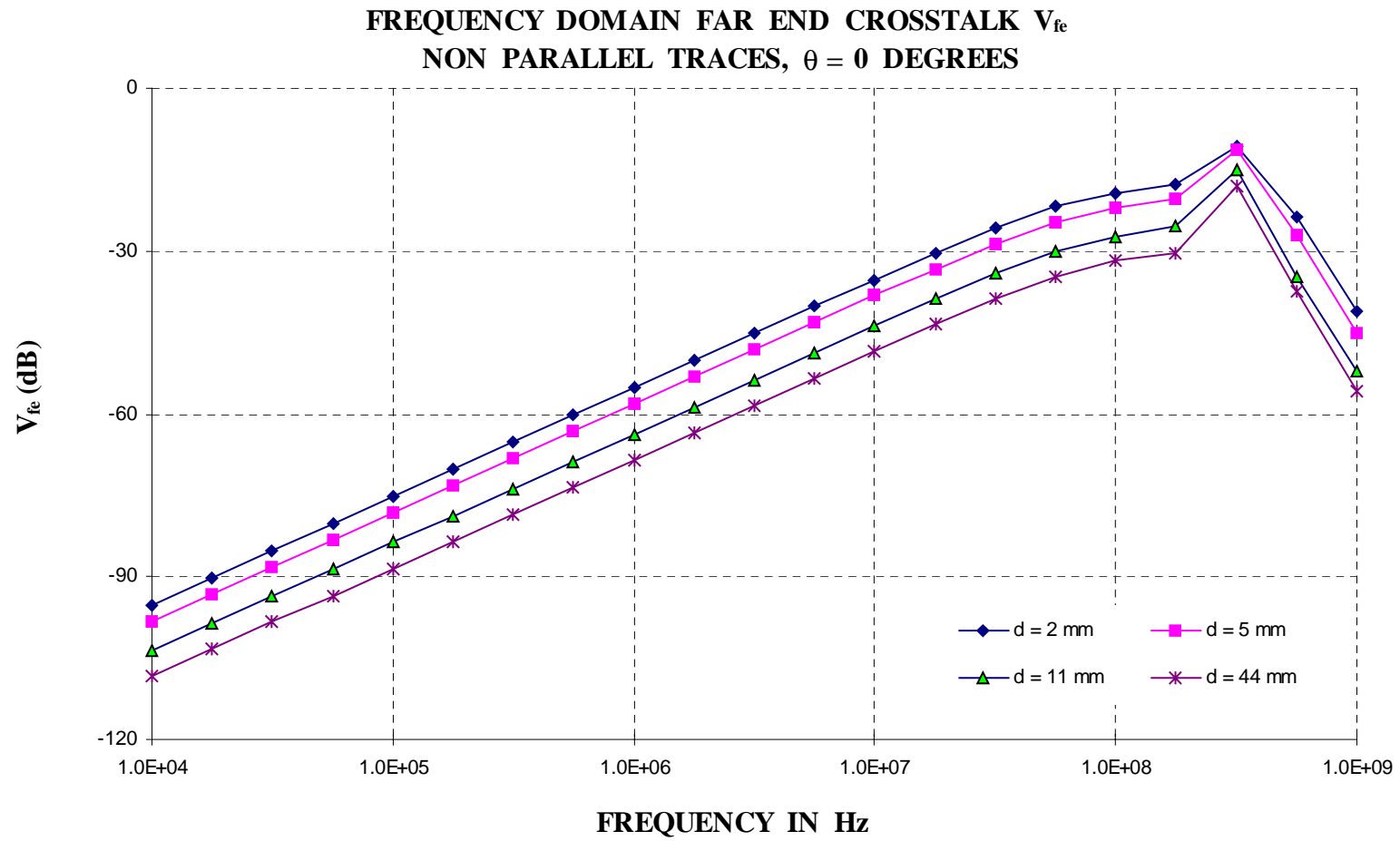


Figure 3.19. Simulated Frequency Domain Far End Crosstalk for Non-Parallel Traces  $\theta = 0$  Degrees.

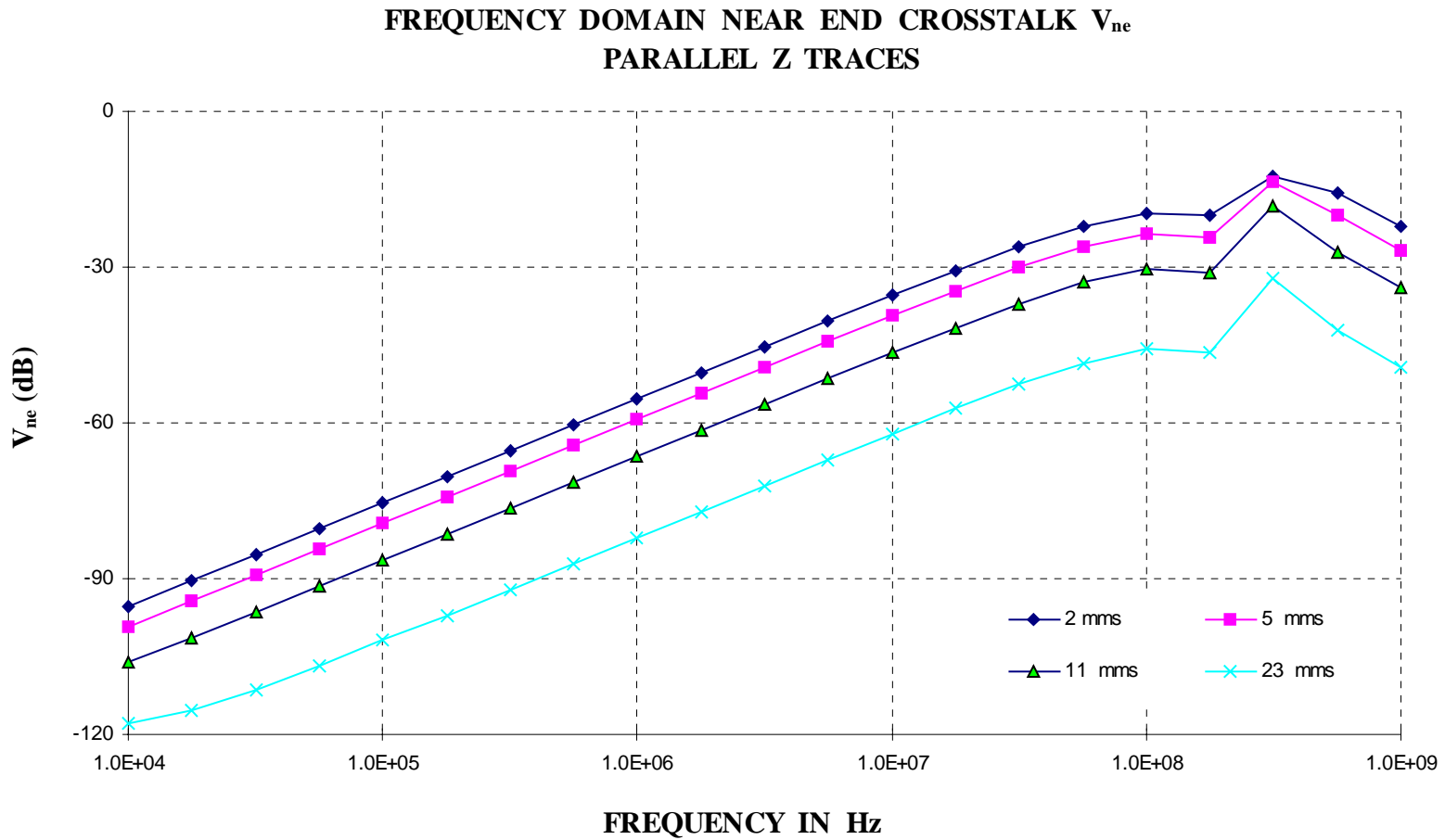


Figure 3.20. Simulated Frequency Domain Near End Crosstalk for Parallel Z Traces.

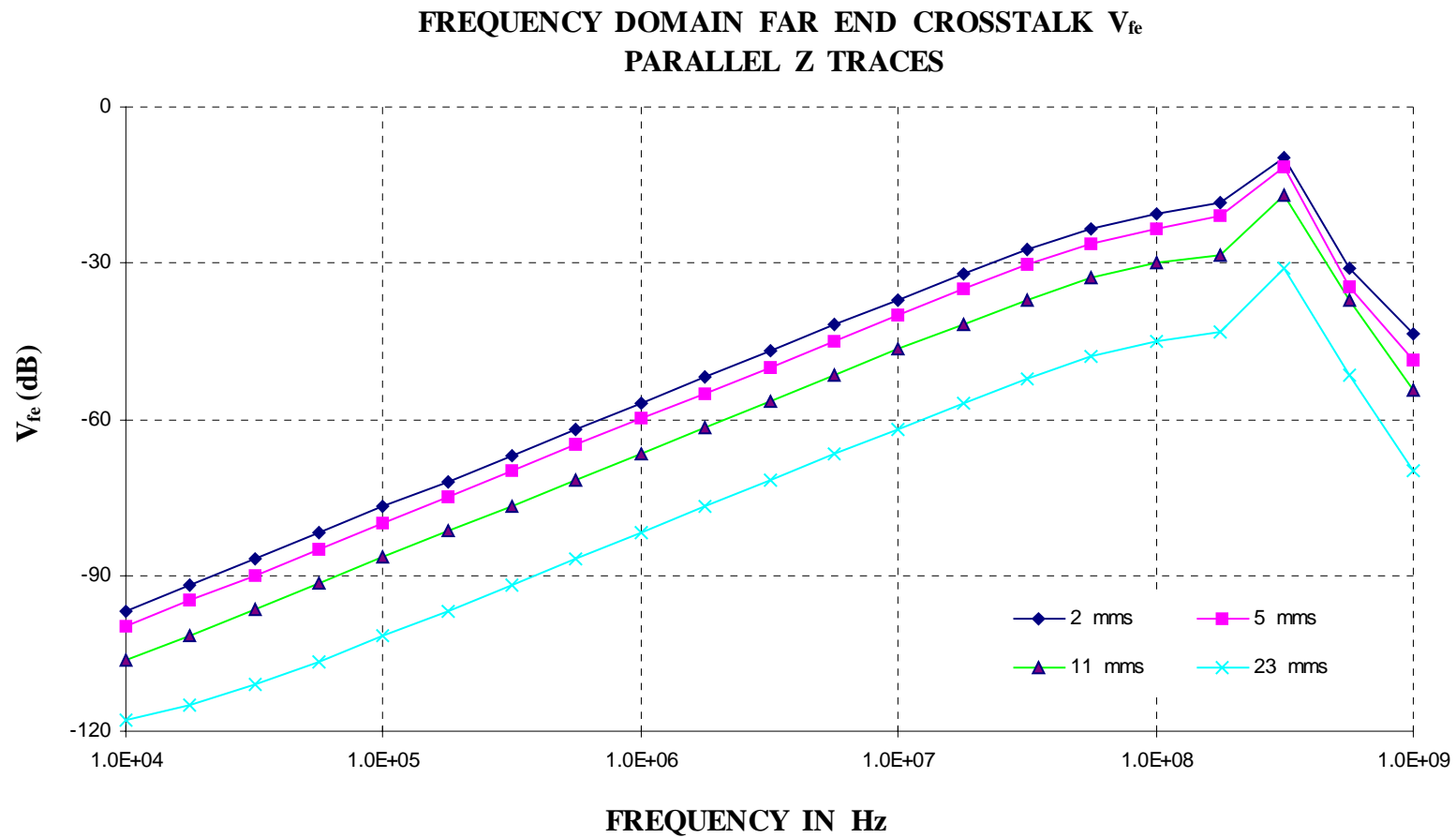


Figure 3.21. Simulated Frequency Domain Far End Crosstalk for Parallel Z Traces.

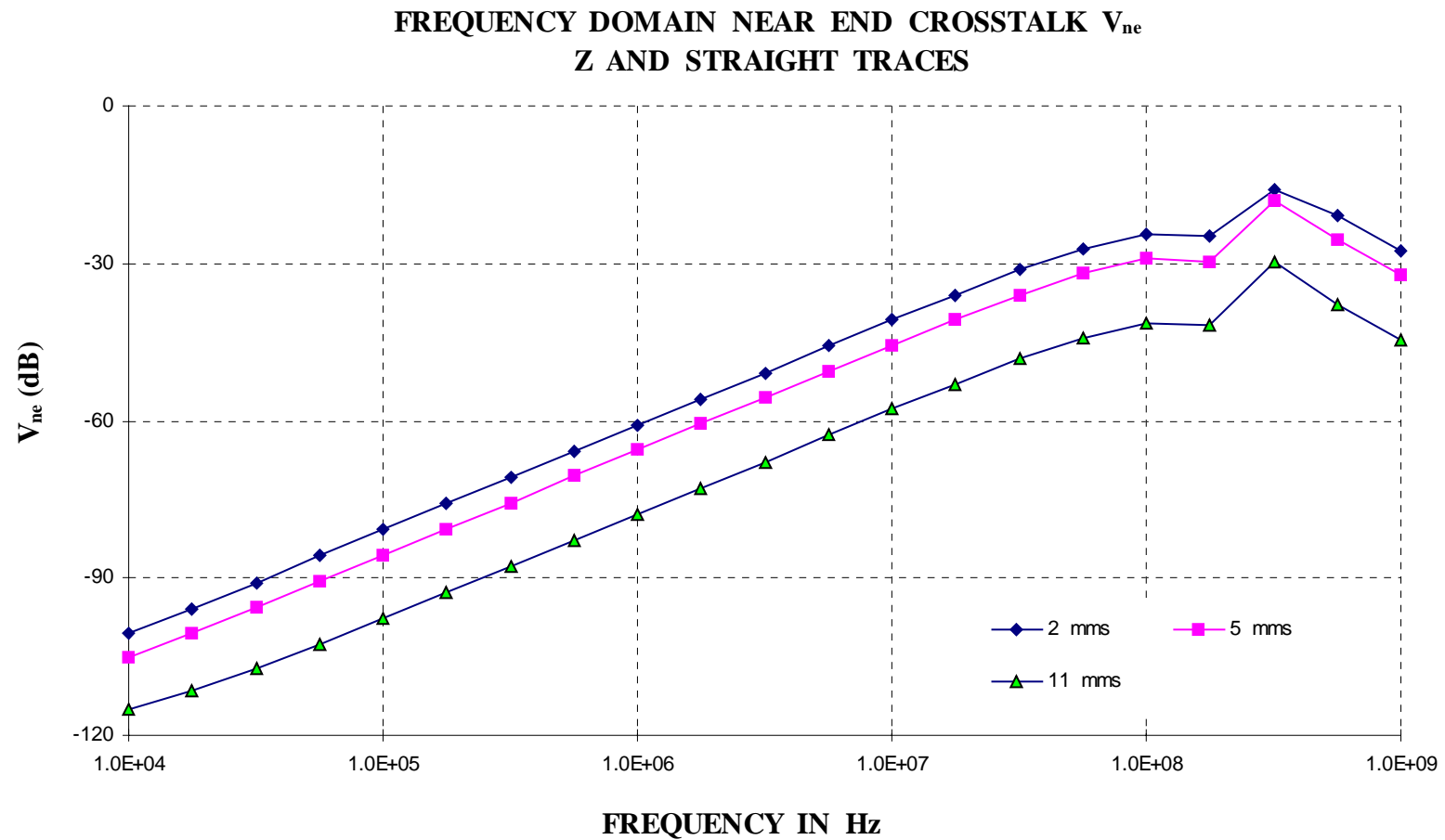


Figure 3.22. Simulated Frequency Domain Near End Crosstalk for Z and Straight Traces.

**FREQUENCY DOMAIN FAR END CROSSTALK  $V_{fe}$   
Z AND STRAIGHT TRACES**

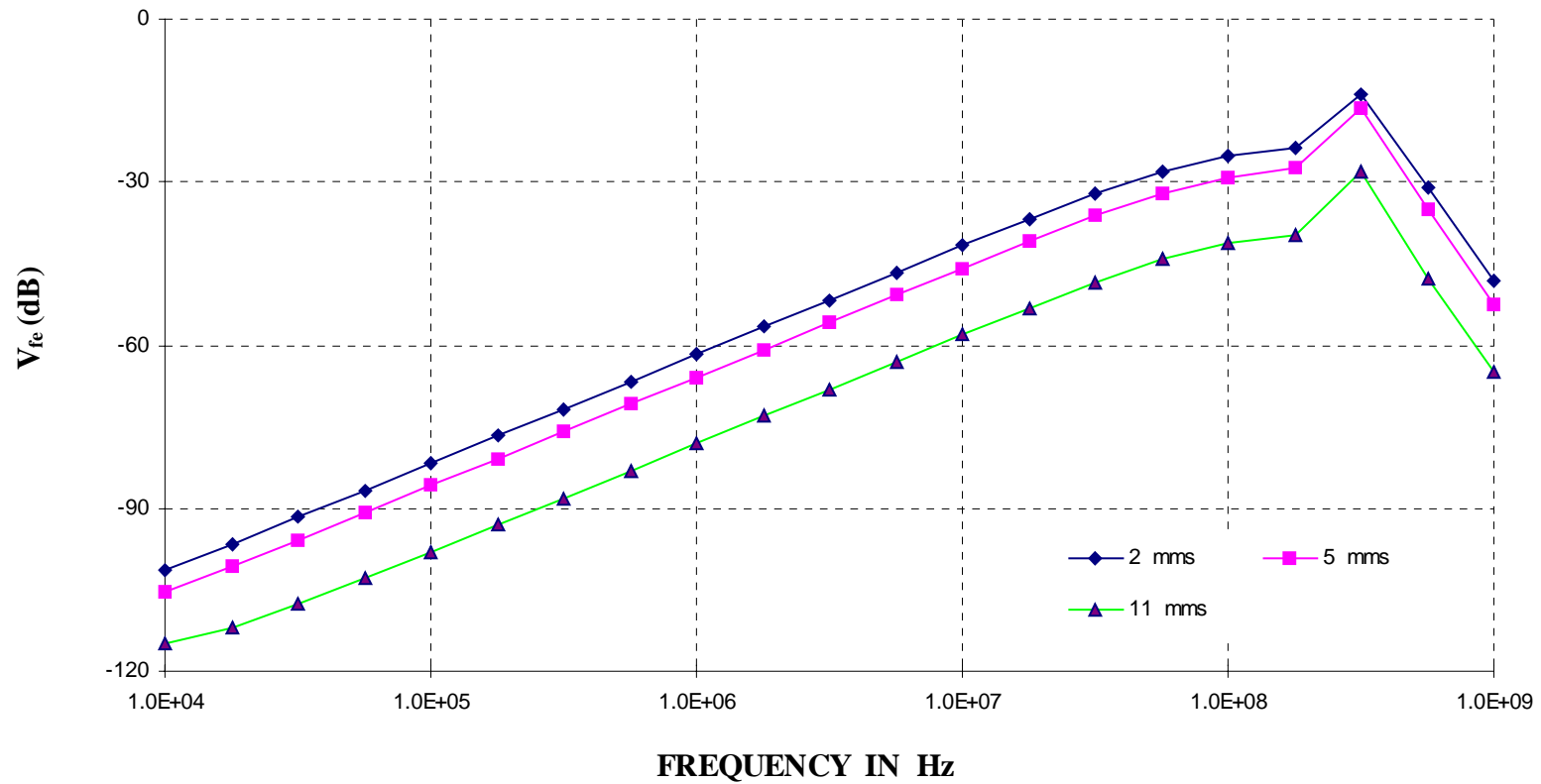


Figure 3.23. Simulated Frequency Domain Far End Crosstalk for Z and Straight Traces.

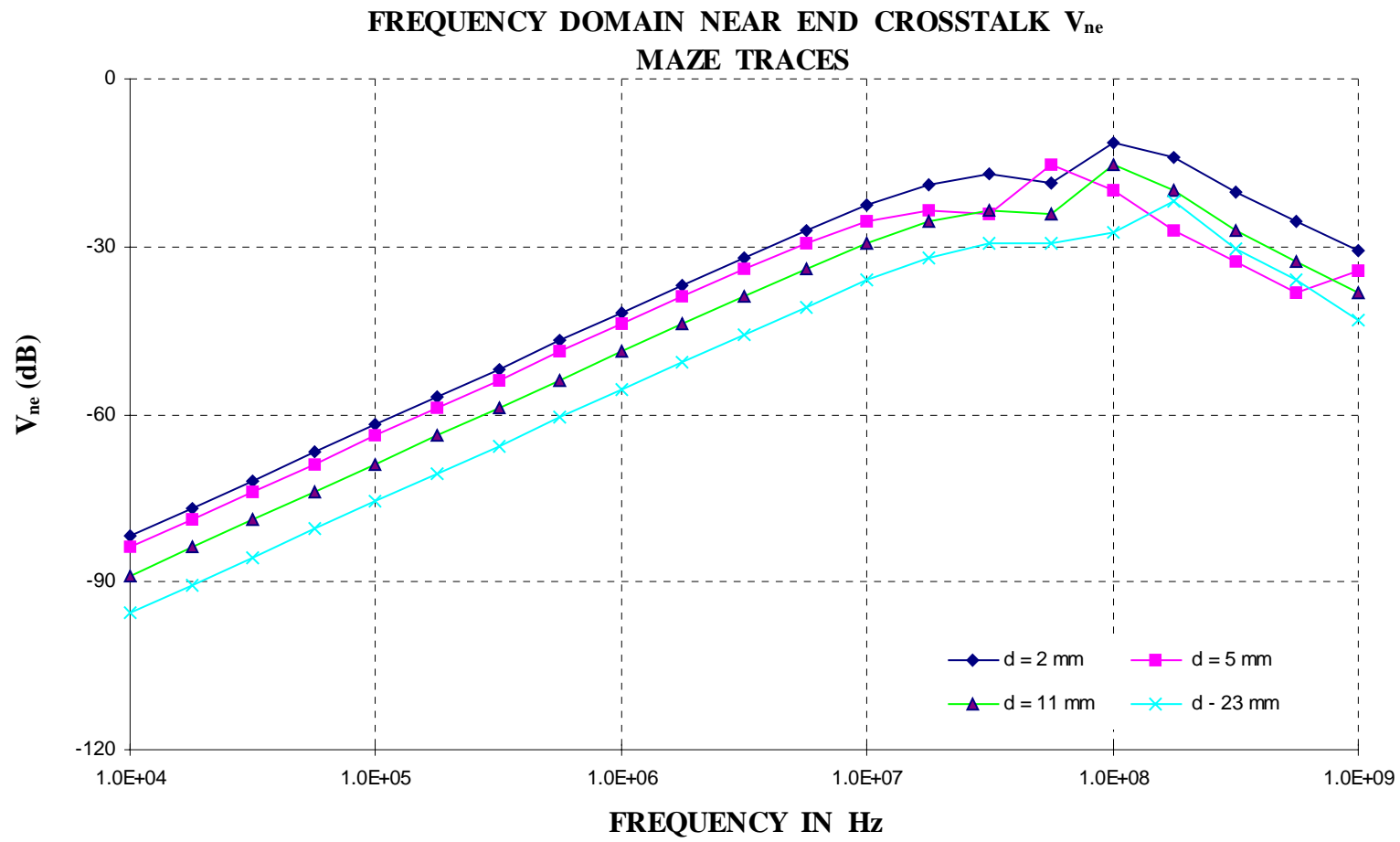


Figure 3.24. Simulated Frequency Domain Near End Crosstalk for Maze Traces.

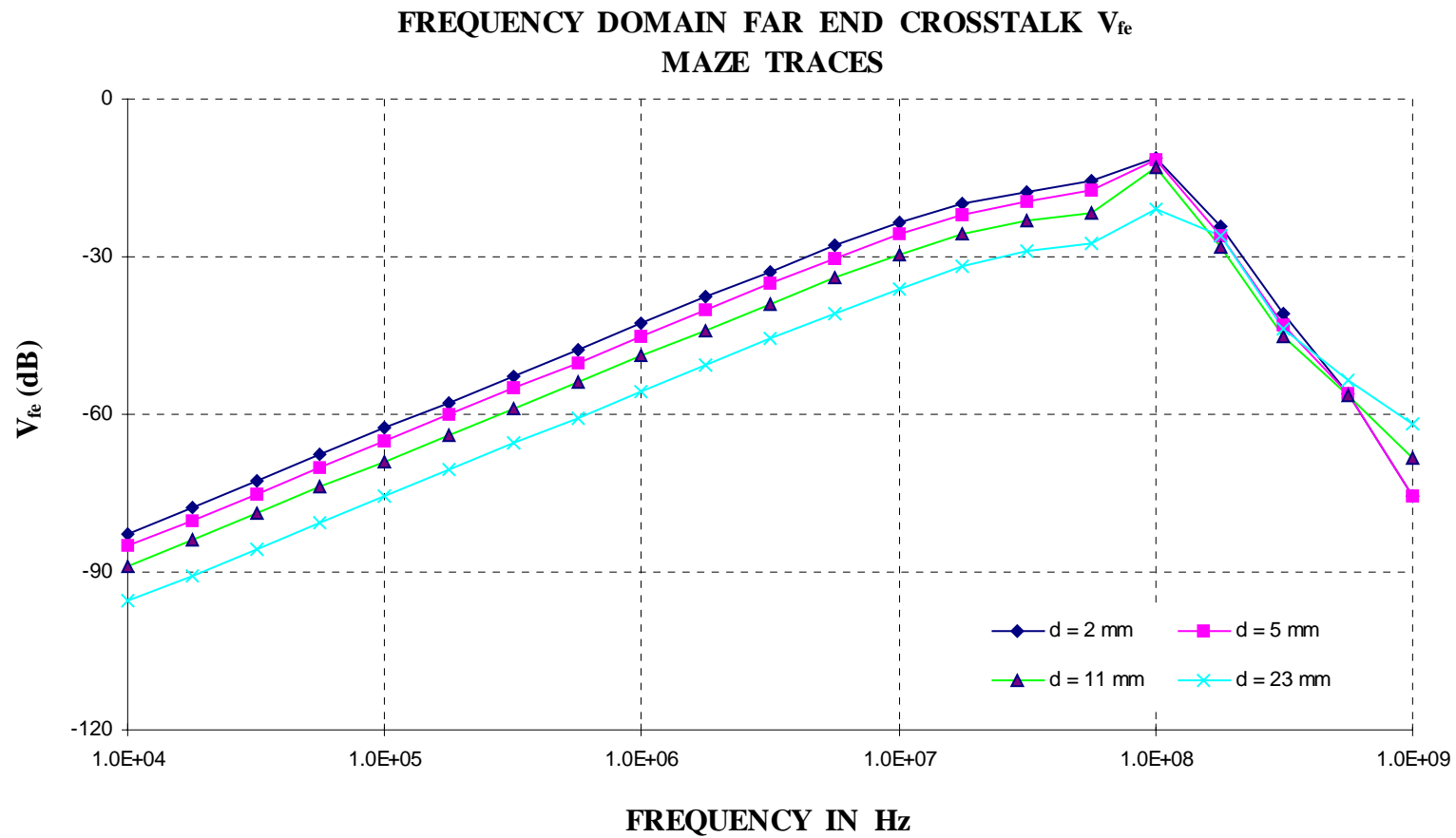


Figure 3.25. Simulated Frequency Domain Far End Crosstalk for Maze Traces.

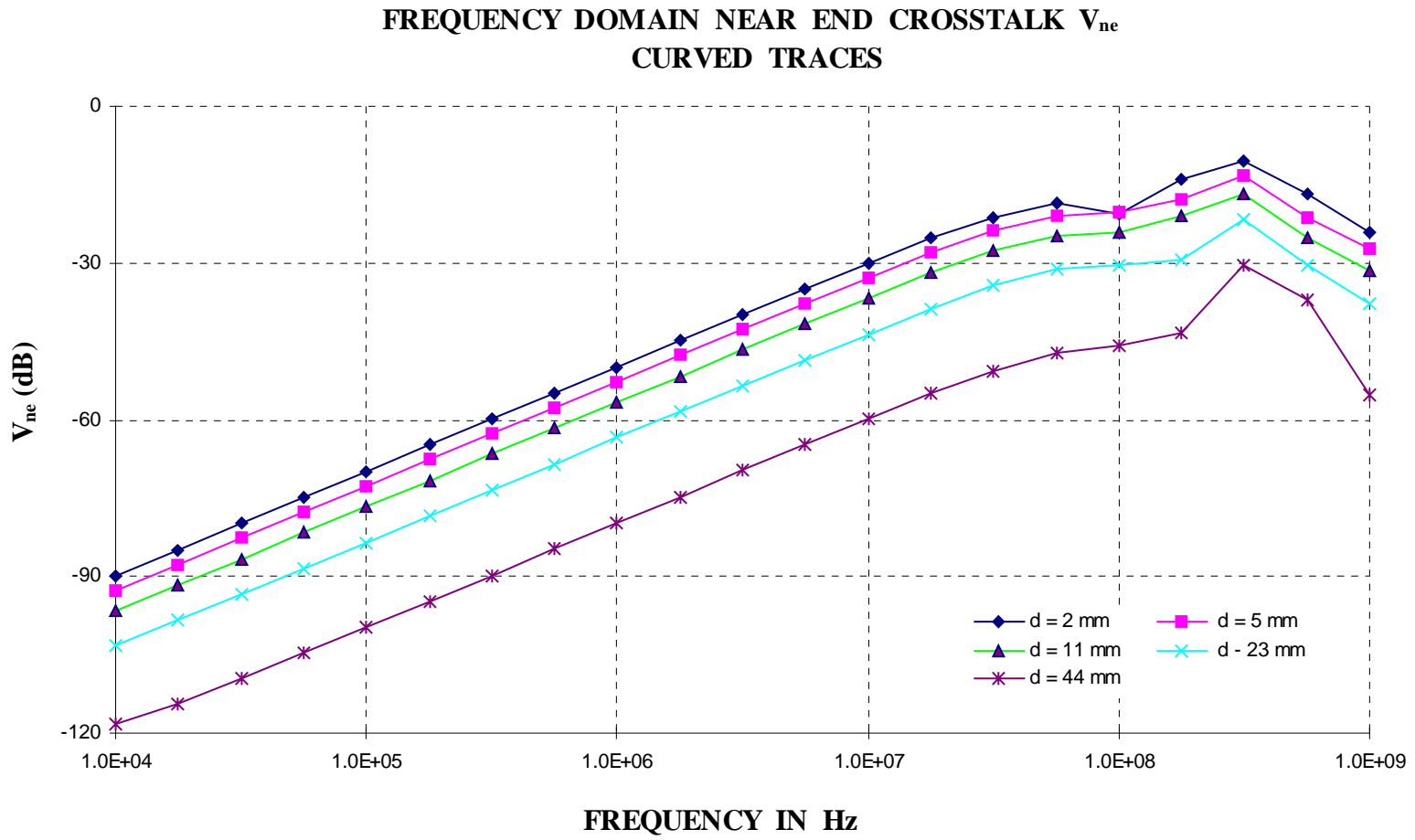


Figure 3.26 Simulated Frequency Domain Near End Crosstalk for Curved Traces.

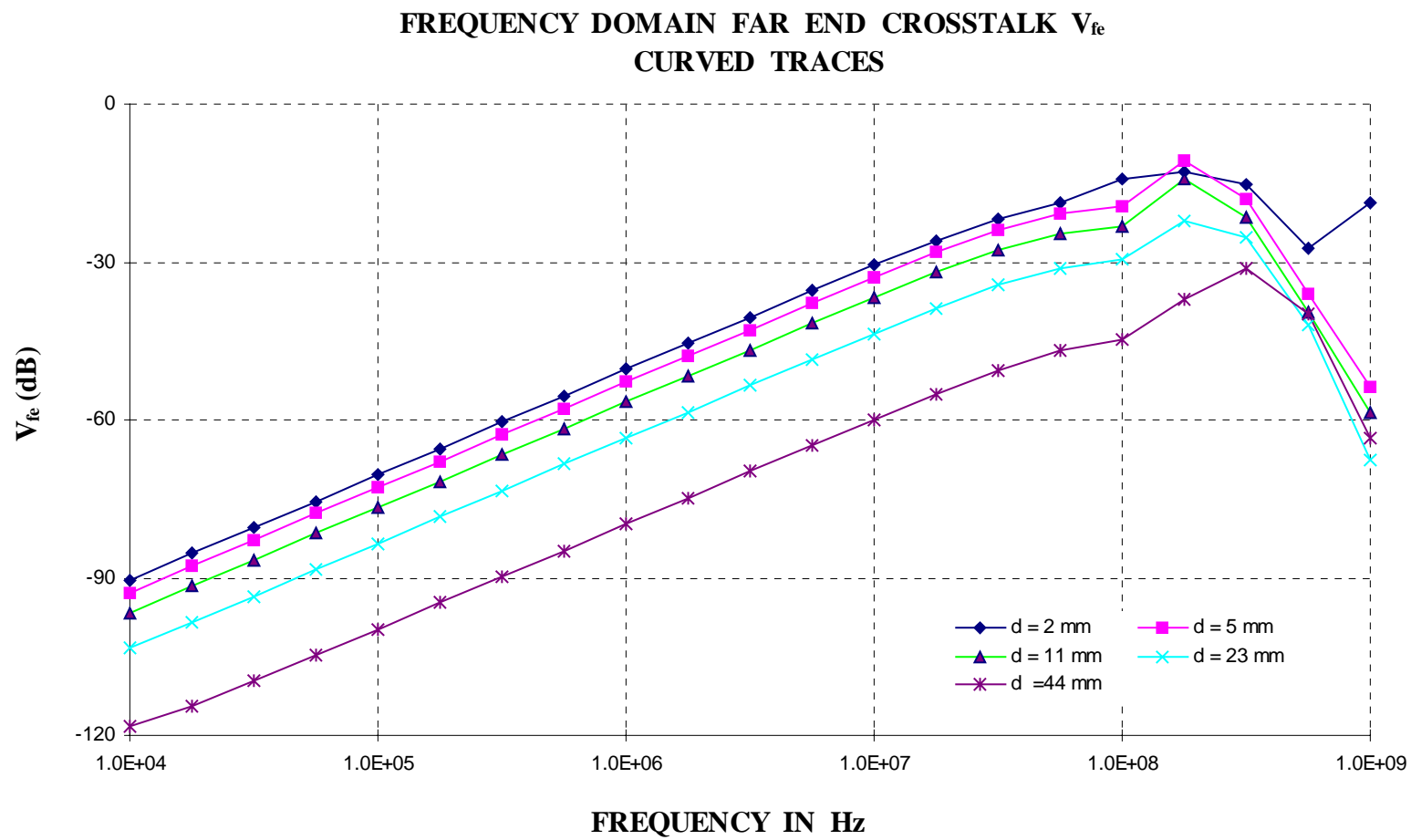


Figure 3.27. Simulated Frequency Domain Far End Crosstalk for Curved Traces.

**FREQUENCY DOMAIN NEAR END CROSSTALK  $V_{ne}$**   
**FIVE TYPES OF TRACES,  $d = 2$  mms**

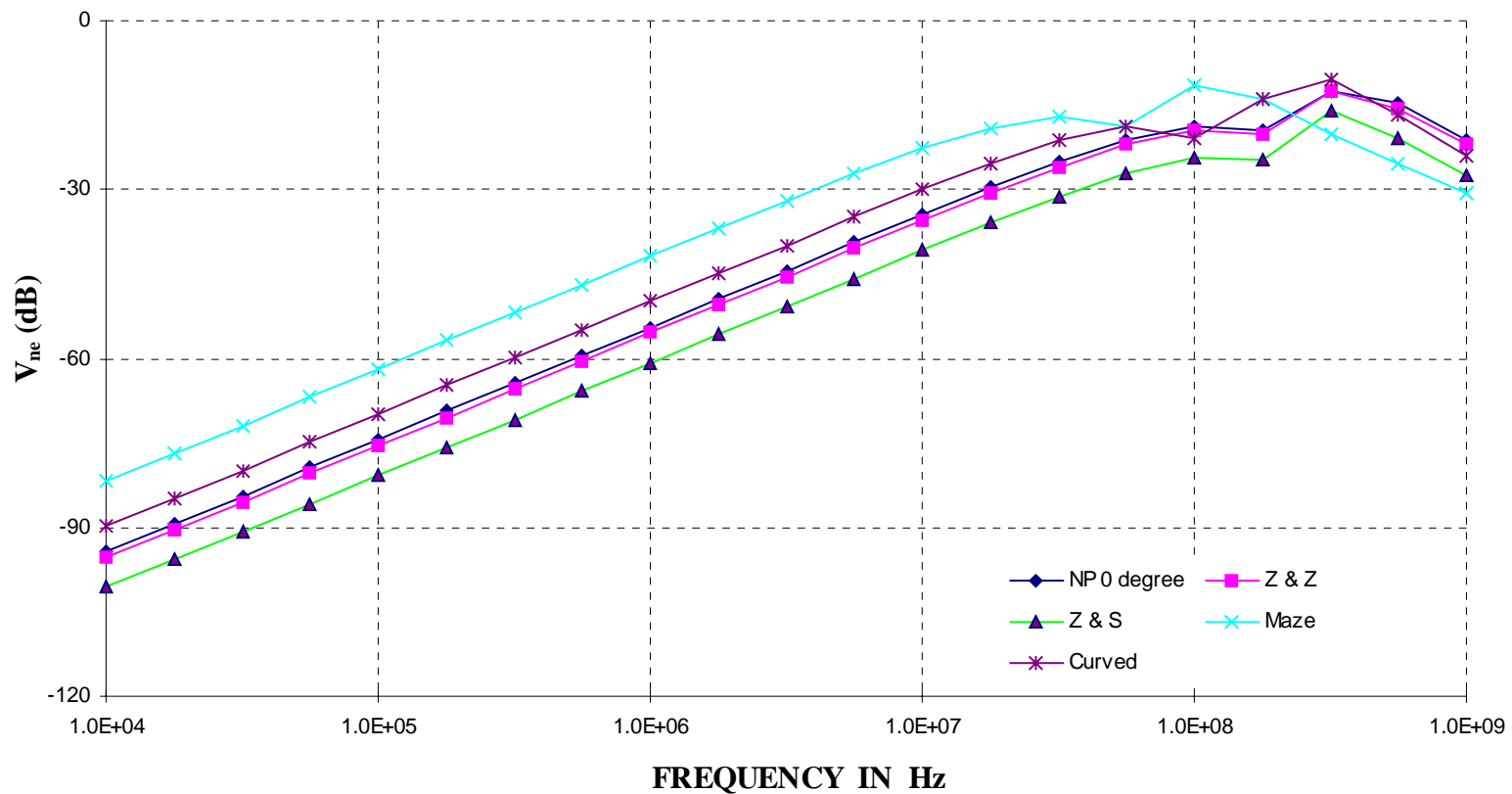


Figure 3.28. Simulated Frequency Domain Near End Crosstalk for  $d = 2$  mms.

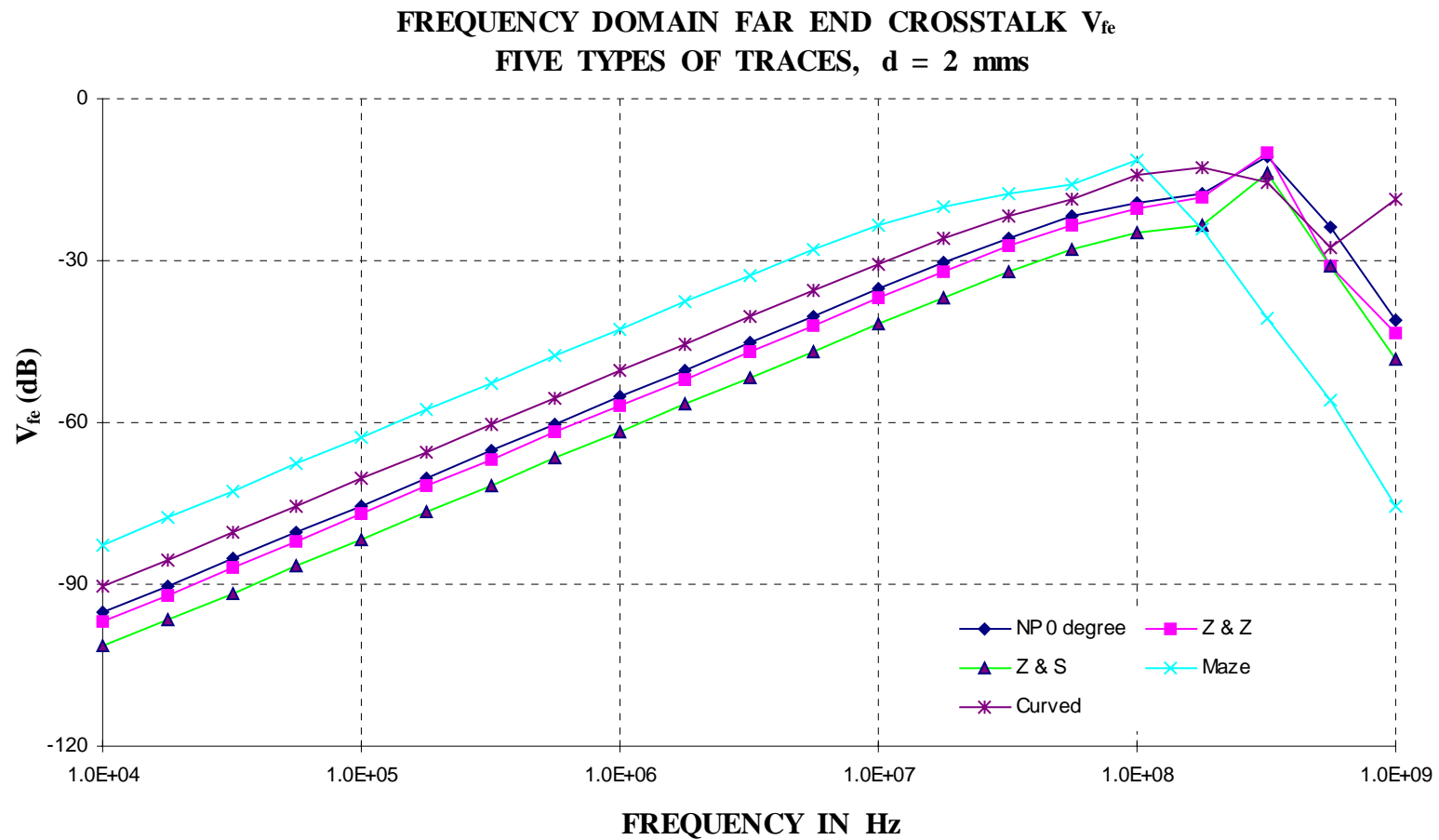


Figure 3.29. Simulated Frequency Domain Far End Crosstalk for  $d = 2$  mms.

**FREQUENCY DOMAIN NEAR END CROSSTALK  $V_{ne}$**   
**FIVE TYPES OF TRACES,  $d = 5$  mm**

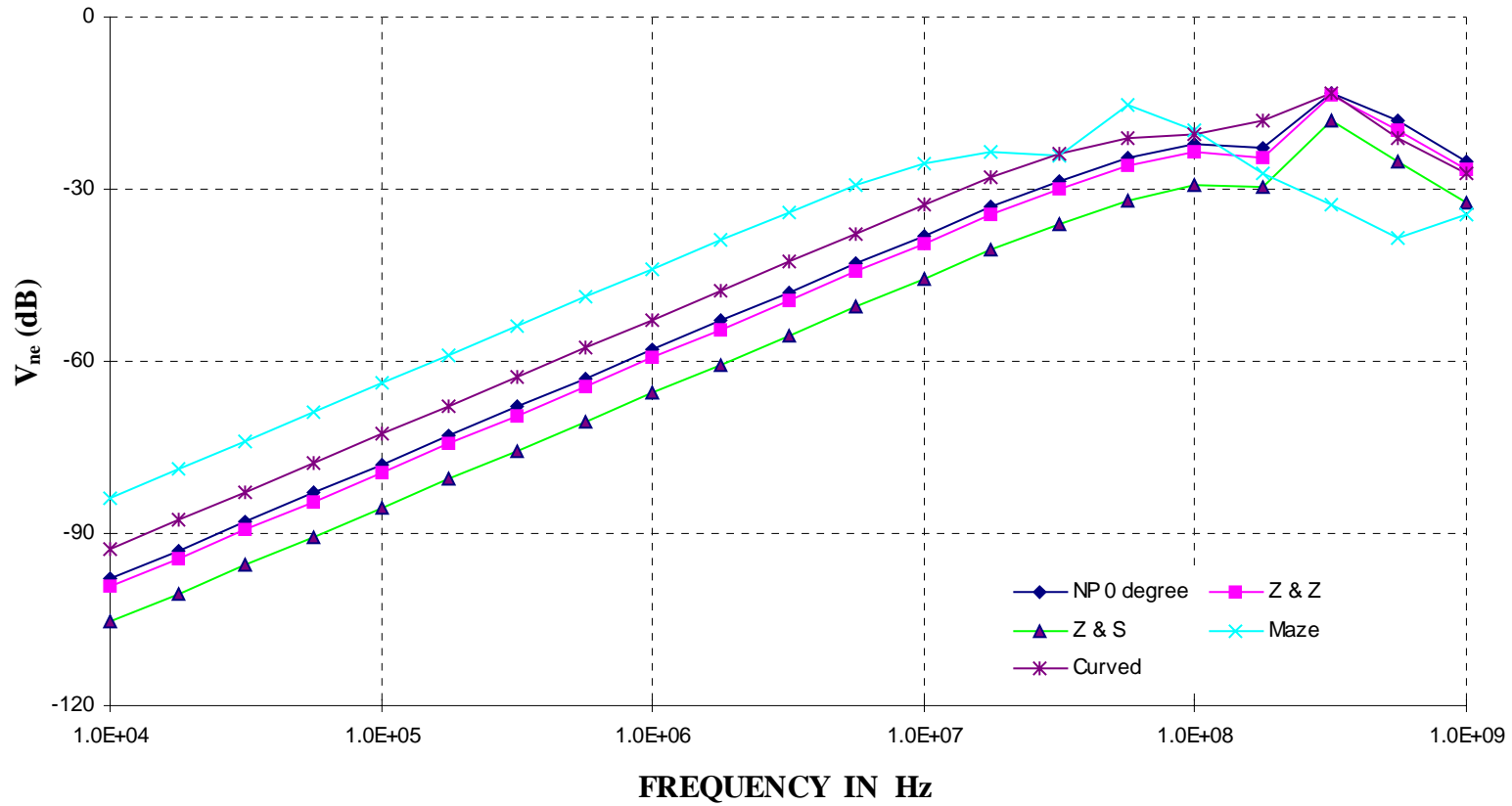


Figure 3.30. Simulated Frequency Domain Near End Crosstalk for  $d = 5$  mm.

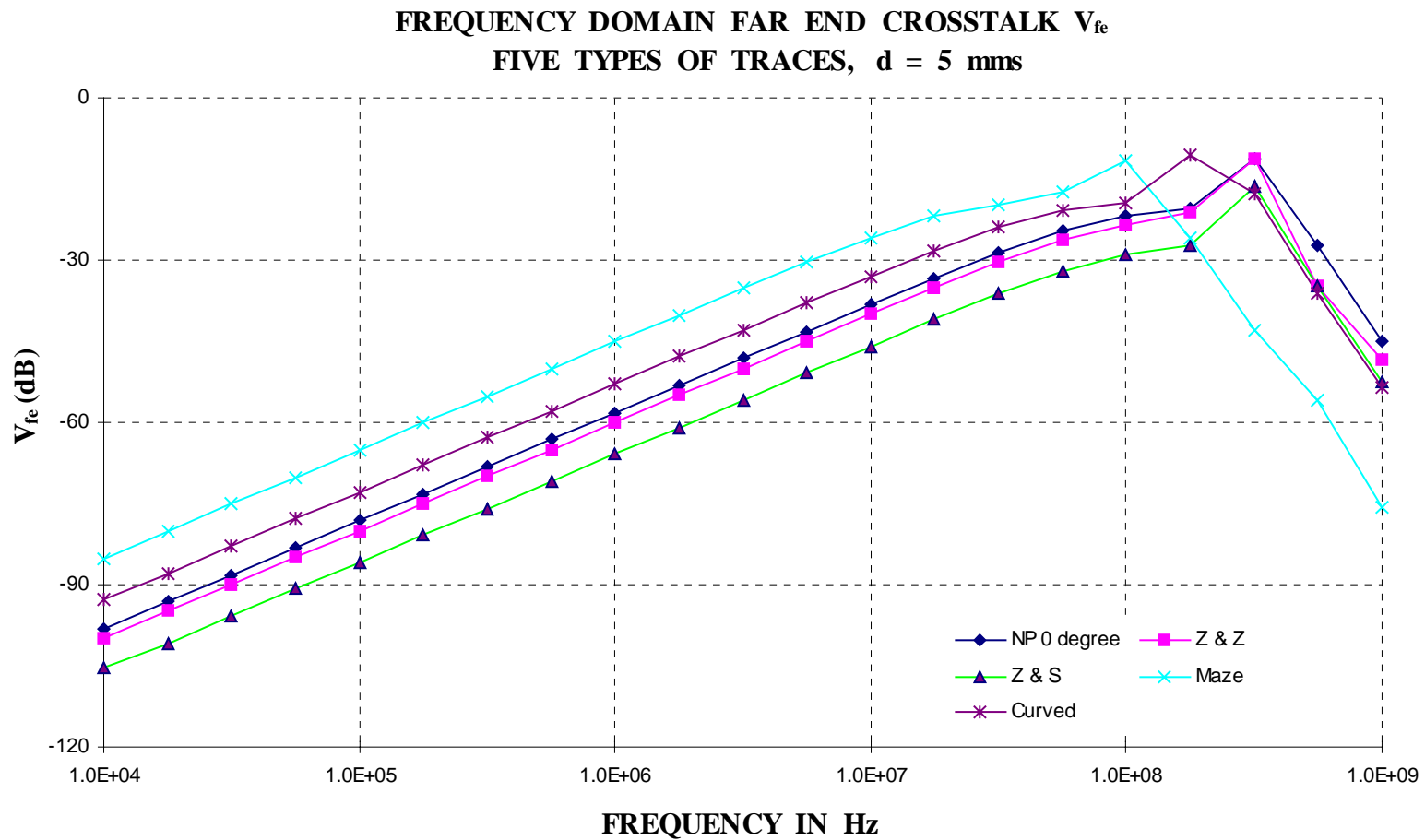


Figure 3.31. Simulated Frequency Domain Far End Crosstalk for  $d = 5$  mm.

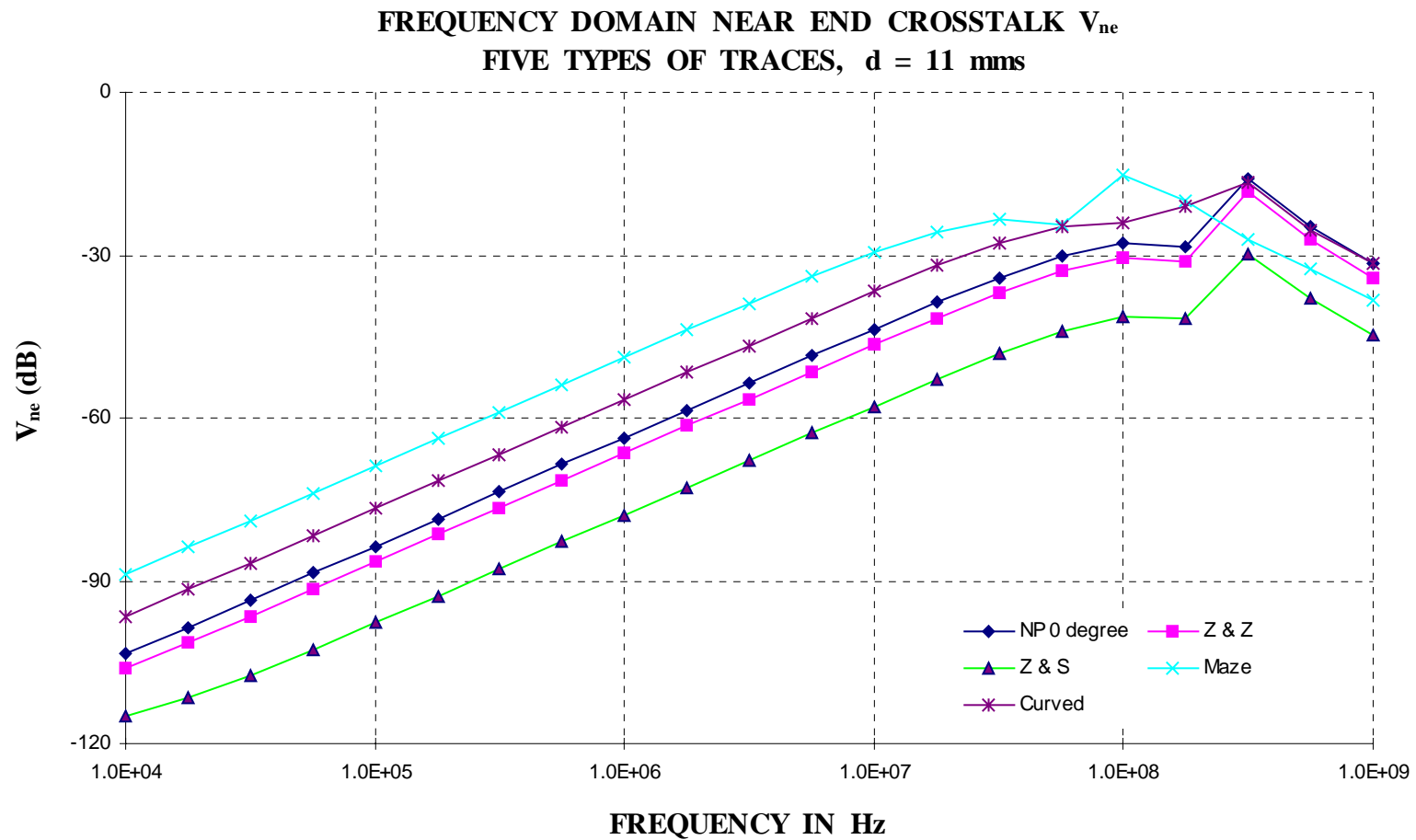


Figure 3.32. Simulated Frequency Domain Near End Crosstalk for  $d = 11$  mms.

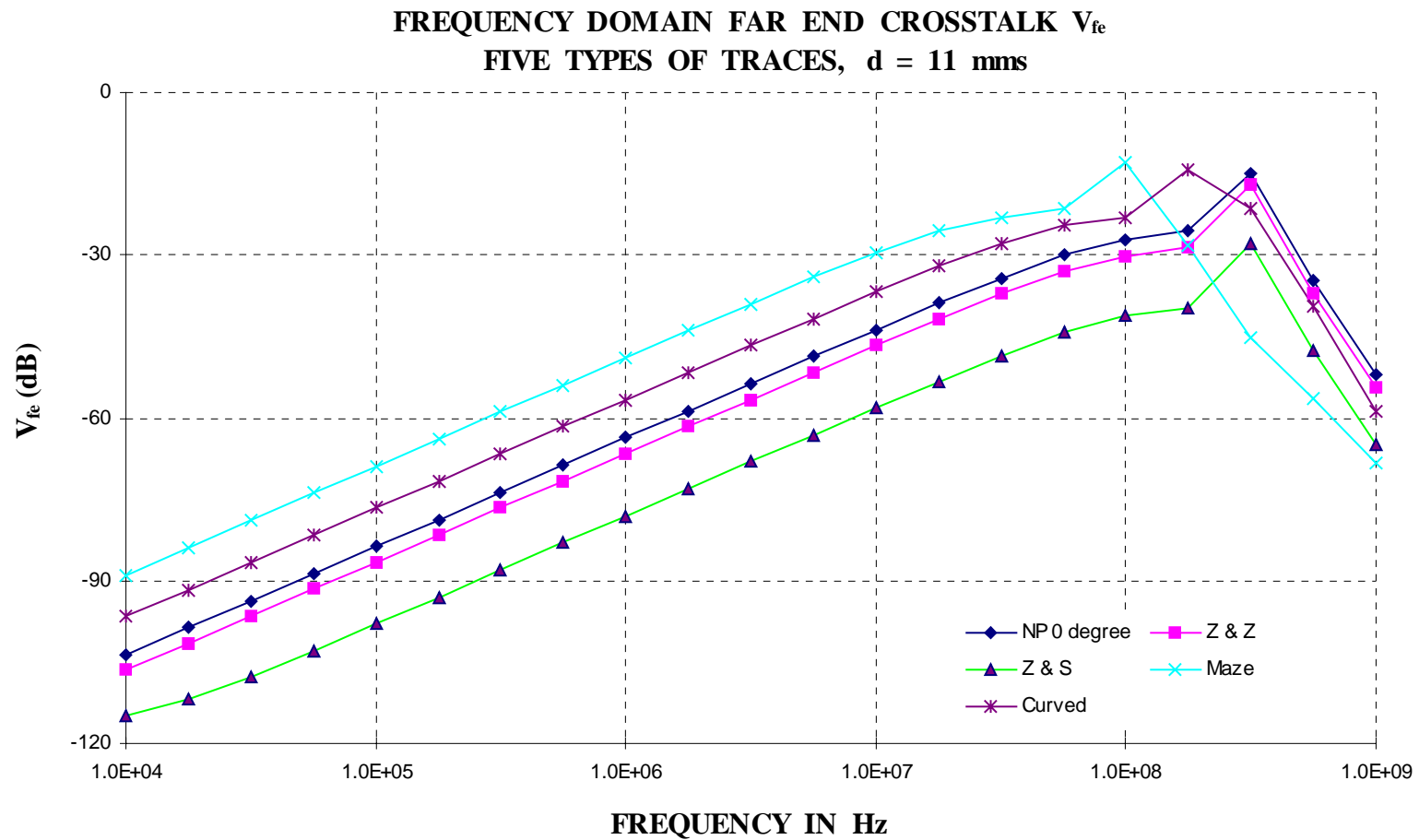


Figure 3.33. Simulated Frequency Domain Far End Crosstalk for  $d = 11$  mm.

**FREQUENCY DOMAIN NEAR END CROSSTALK  $V_{ne}$**   
**FIVE TYPES OF TRACES,  $d = 23$  mms**

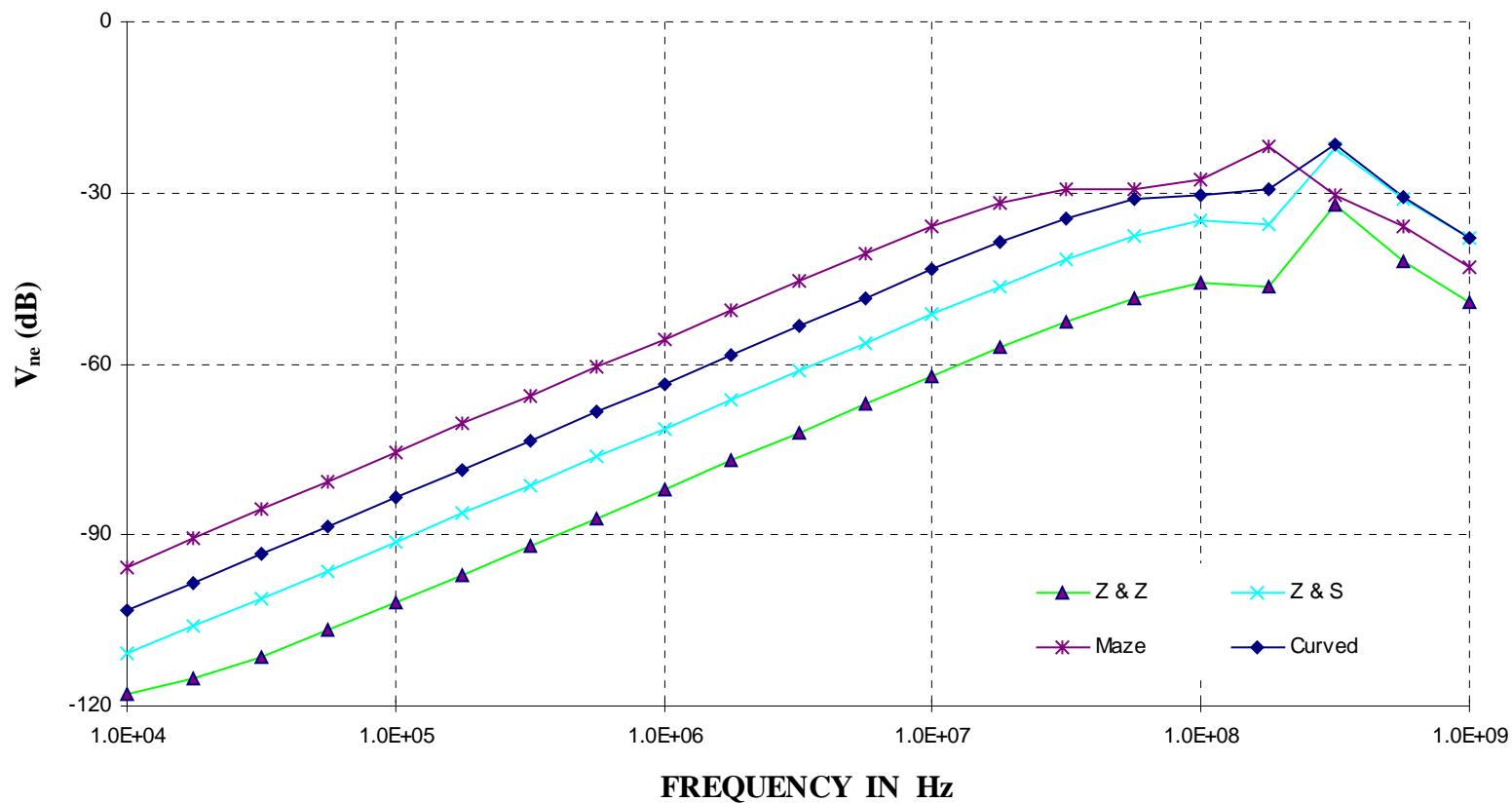


Figure 3.34. Simulated Frequency Domain Near End Crosstalk for  $d = 23$  mms.

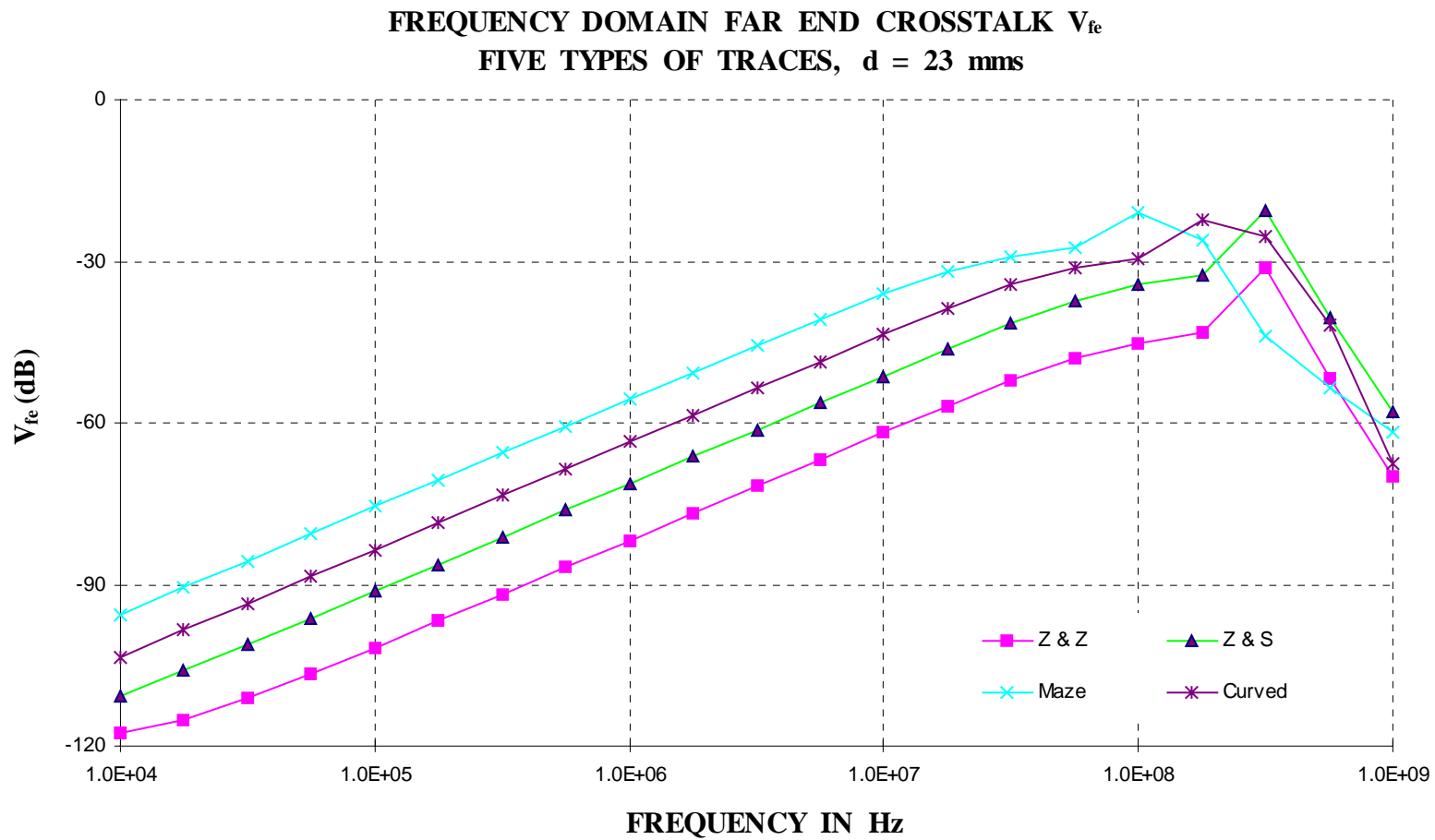


Figure 3.35. Simulated Frequency Domain Far End Crosstalk for  $d = 23$  mms.

FREQUENCY DOMAIN NEAR END CROSSTALK  $V_{ne}$   
FIVE TYPES OF TRACES,  $d = 44$  mms

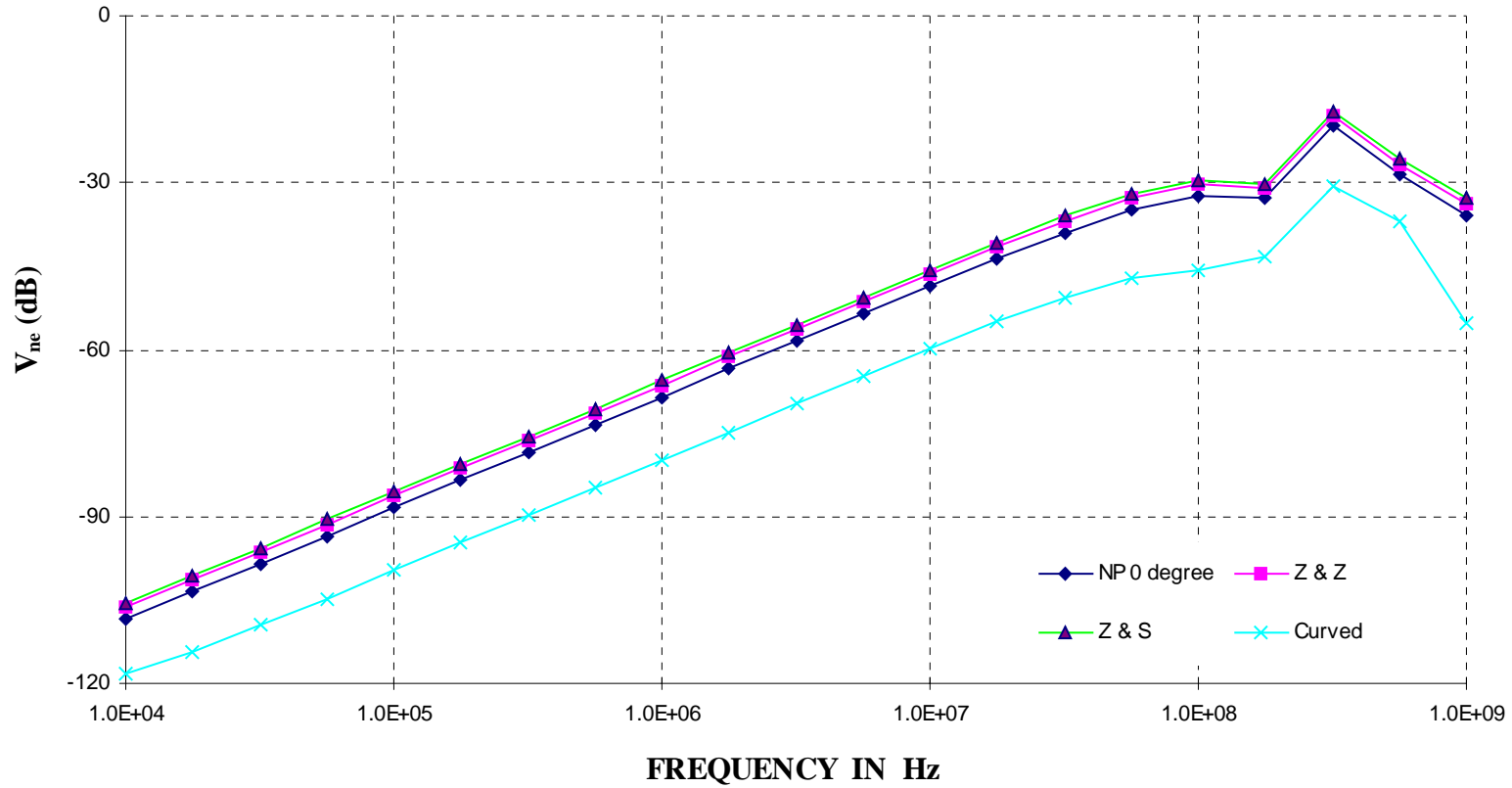


Figure 3.36. Simulated Frequency Domain Near End Crosstalk for  $d = 44$  mms.

**FREQUENCY DOMAIN FAR END CROSSTALK  $V_{fe}$**   
**FIVE TYPES OF TRACES,  $d = 44$  mms**

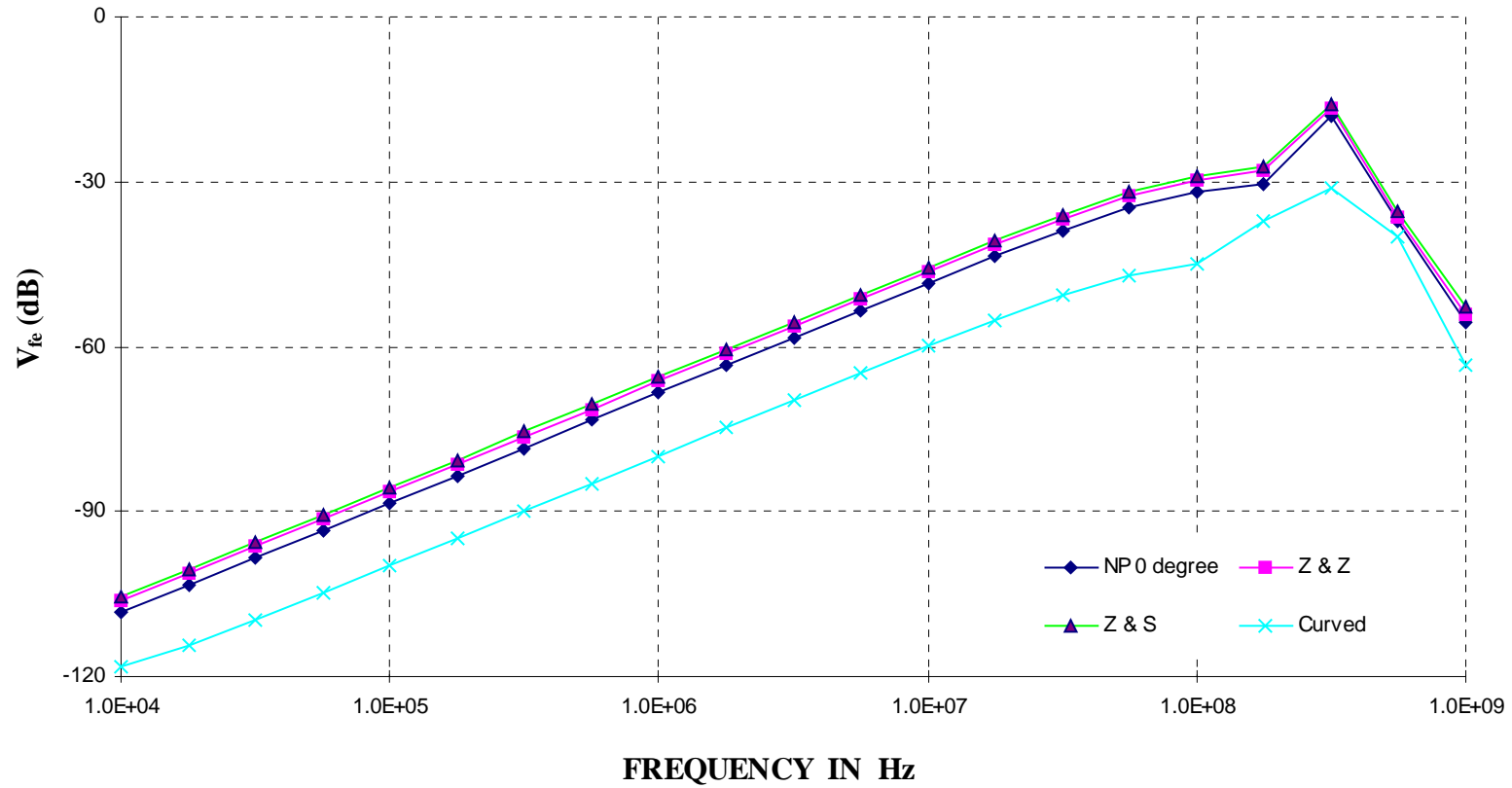


Figure 3.37. Simulated Frequency Domain Far End Crosstalk for  $d = 44$  mms.

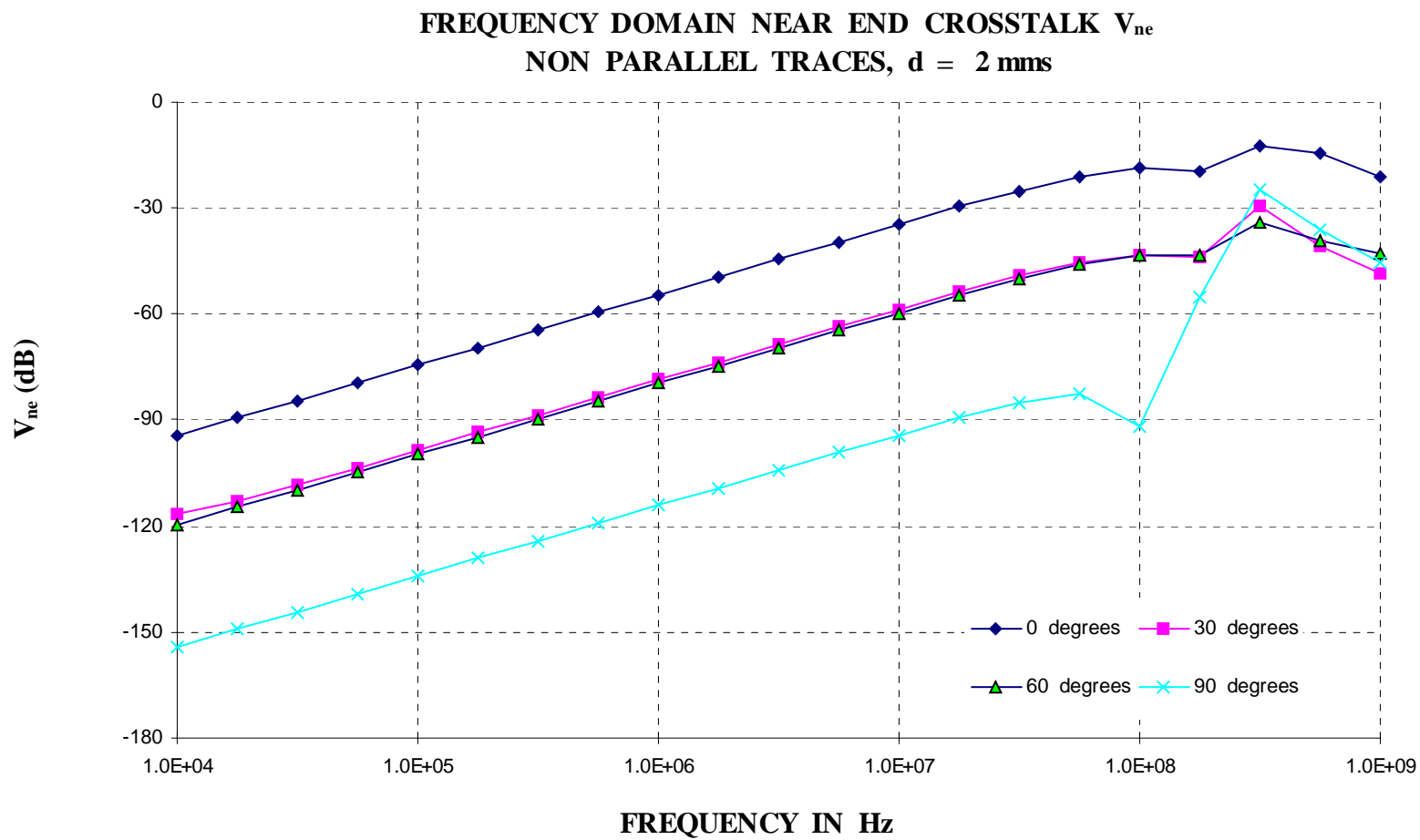


Figure 3.38. Simulated Frequency Domain Near End Crosstalk for Non Parallel Traces  $d = 2$  mms.

**FREQUENCY DOMAIN FAR END CROSSTALK  $V_{fe}$**   
**NON PARALLEL TRACES,  $d = 2$  mms**

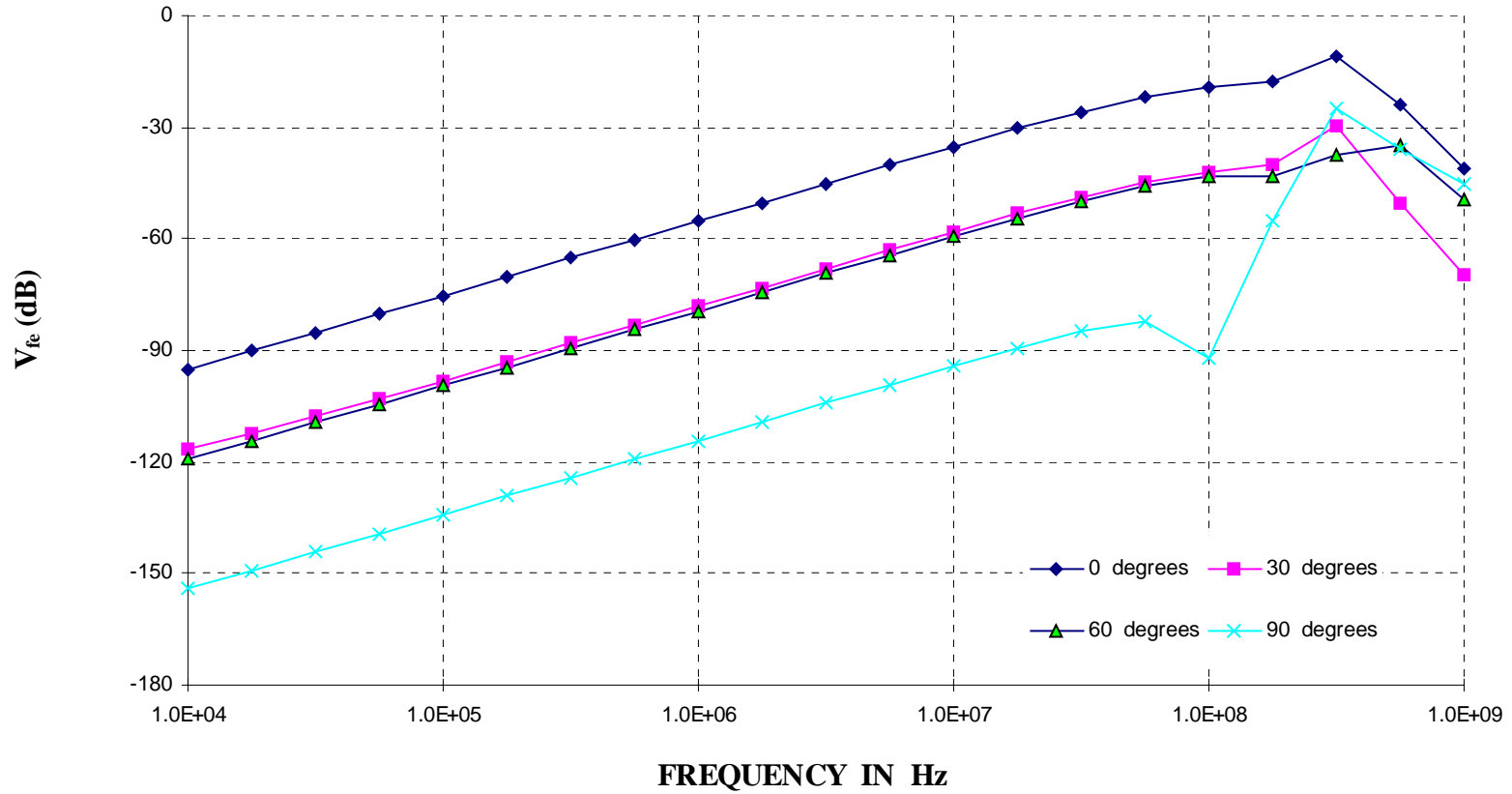


Figure 3.39. Simulated Frequency Domain Far End Crosstalk for Non Parallel Traces  $d = 2$  mms.

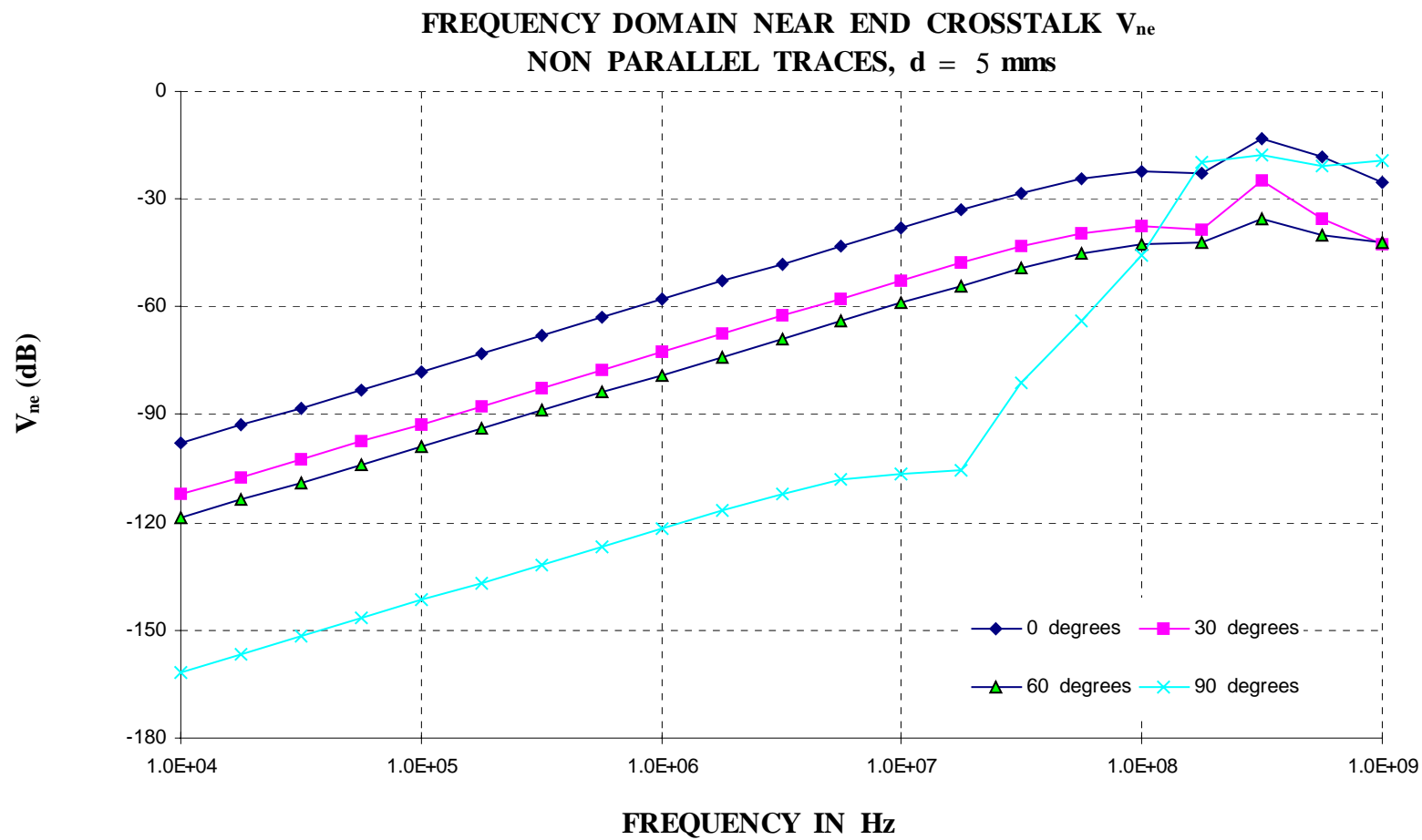


Figure 3.40. Simulated Frequency Domain Near End Crosstalk for Non Parallel Traces  $d = 5$  mms.

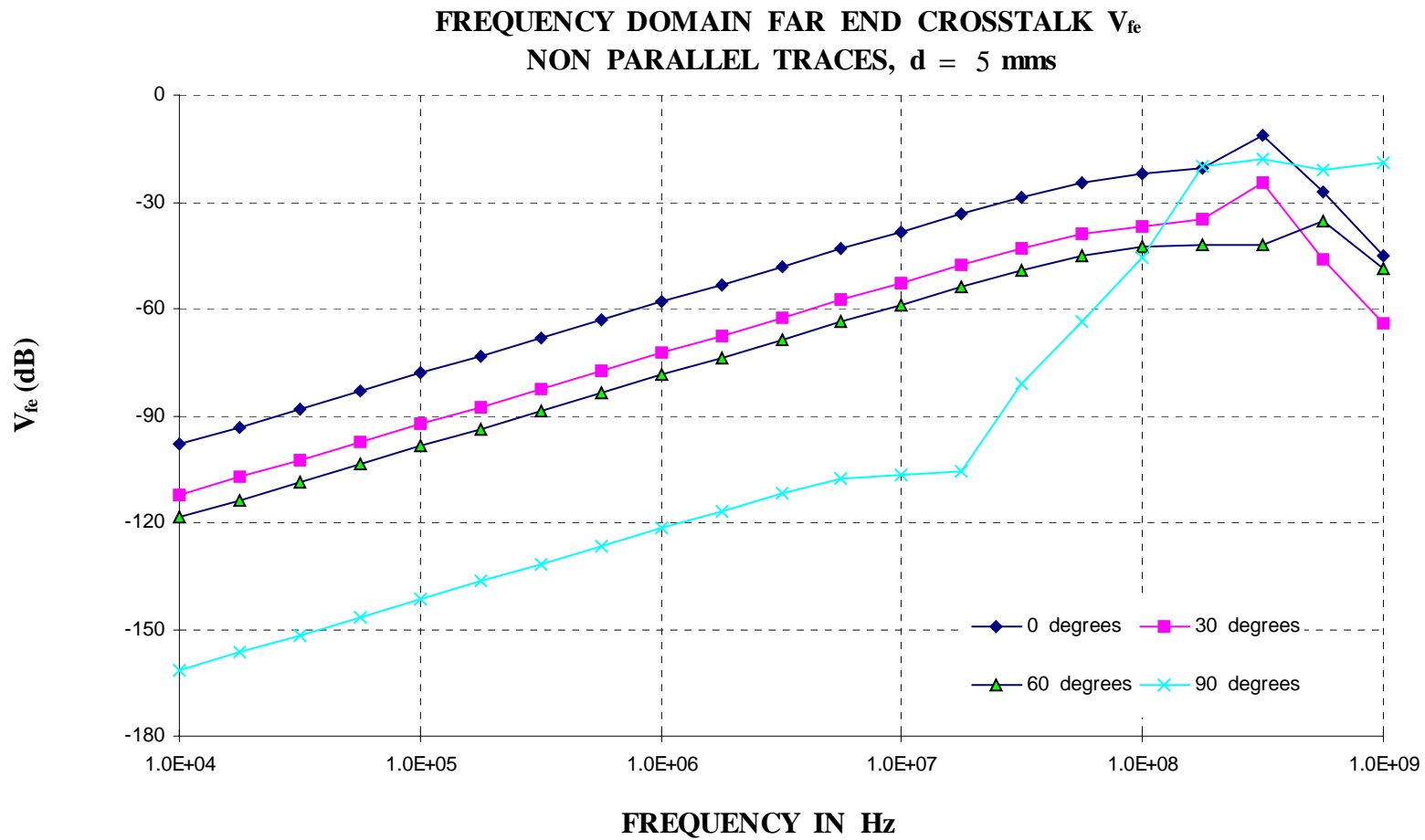
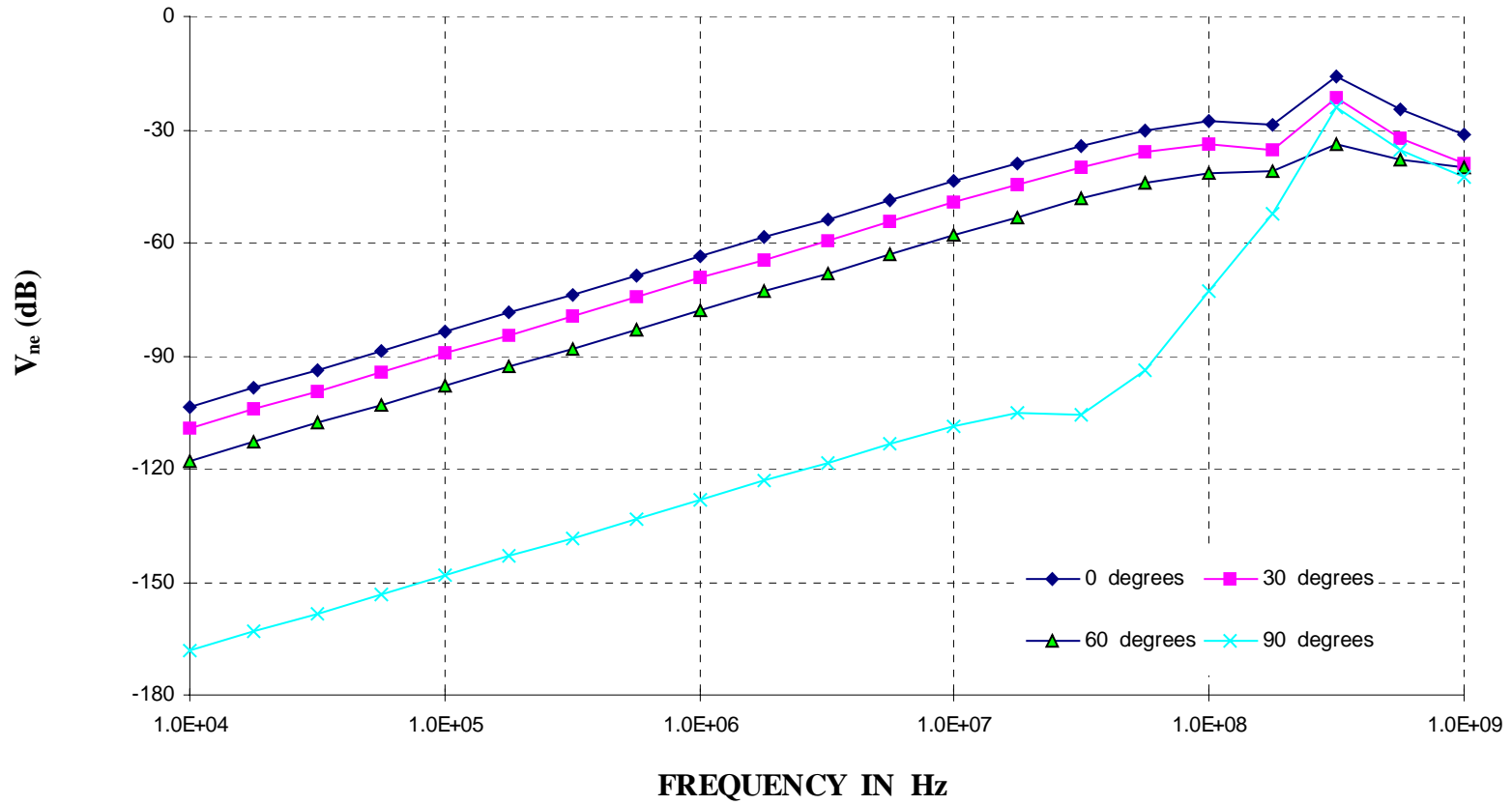


Figure 3.41. Simulated Frequency Domain Far End Crosstalk for Non Parallel Traces  $d = 5$  mms.

**FREQUENCY DOMAIN NEAR END CROSSTALK  $V_{ne}$**   
**NON PARALLEL TRACES,  $d = 11$  mms**



3.42. Simulated Frequency Domain Near End Crosstalk for Non Parallel Traces  $d = 11$  mms.

**FREQUENCY DOMAIN FAR END CROSSTALK  $V_{fe}$**   
**NON PARALLEL TRACES,  $d = 11$  mms**

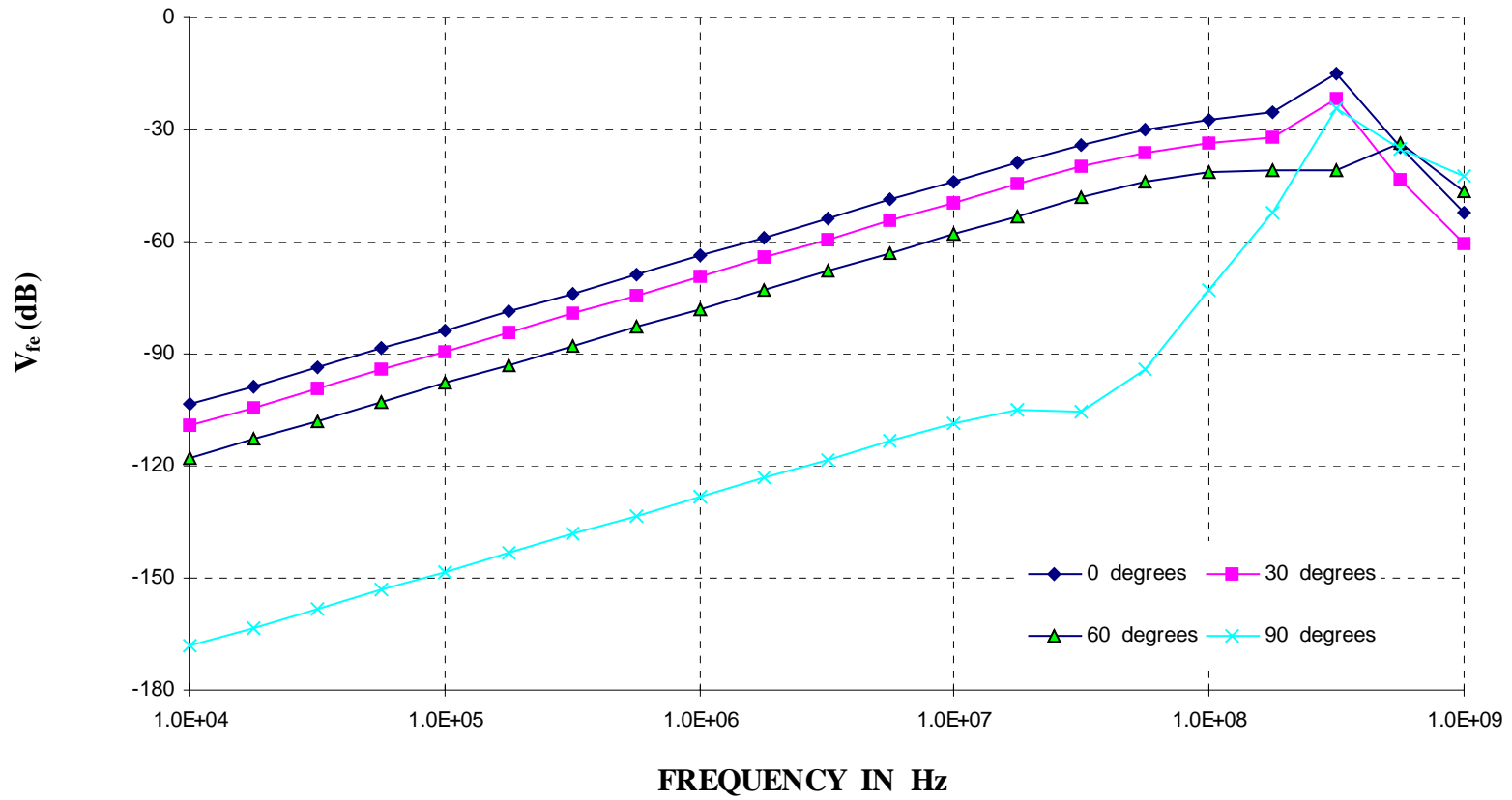


Figure 3Figure .43. Simulated Frequency Domain Far End Crosstalk for Non Parallel Traces  $d = 11$  mms.

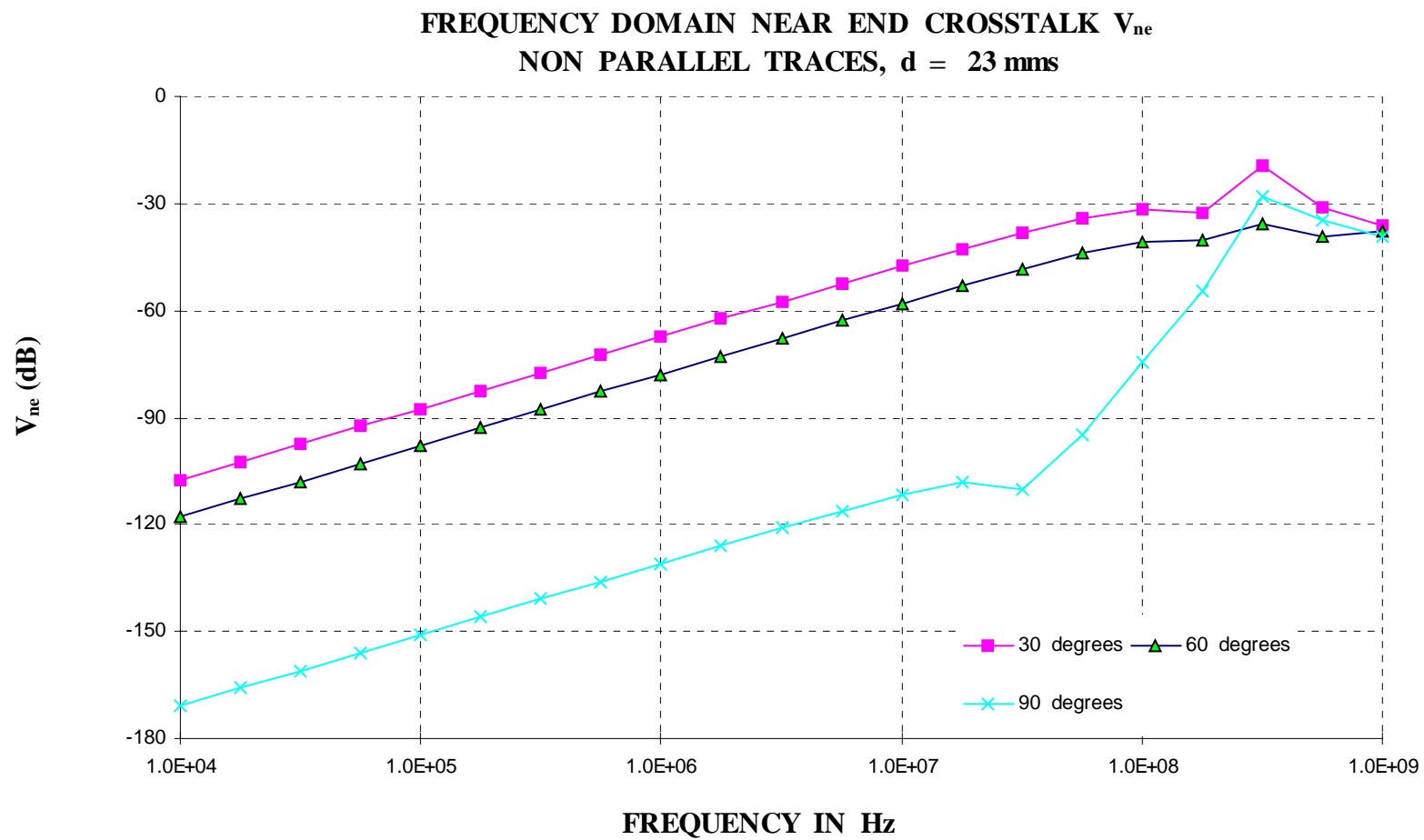


Figure 3.44. Simulated Frequency Domain Near End Crosstalk for Non Parallel Traces  $d = 23$  mms.

FREQUENCY DOMAIN FAR END CROSSTALK  $V_{fe}$   
NON PARALLEL TRACES,  $d = 23$  mms

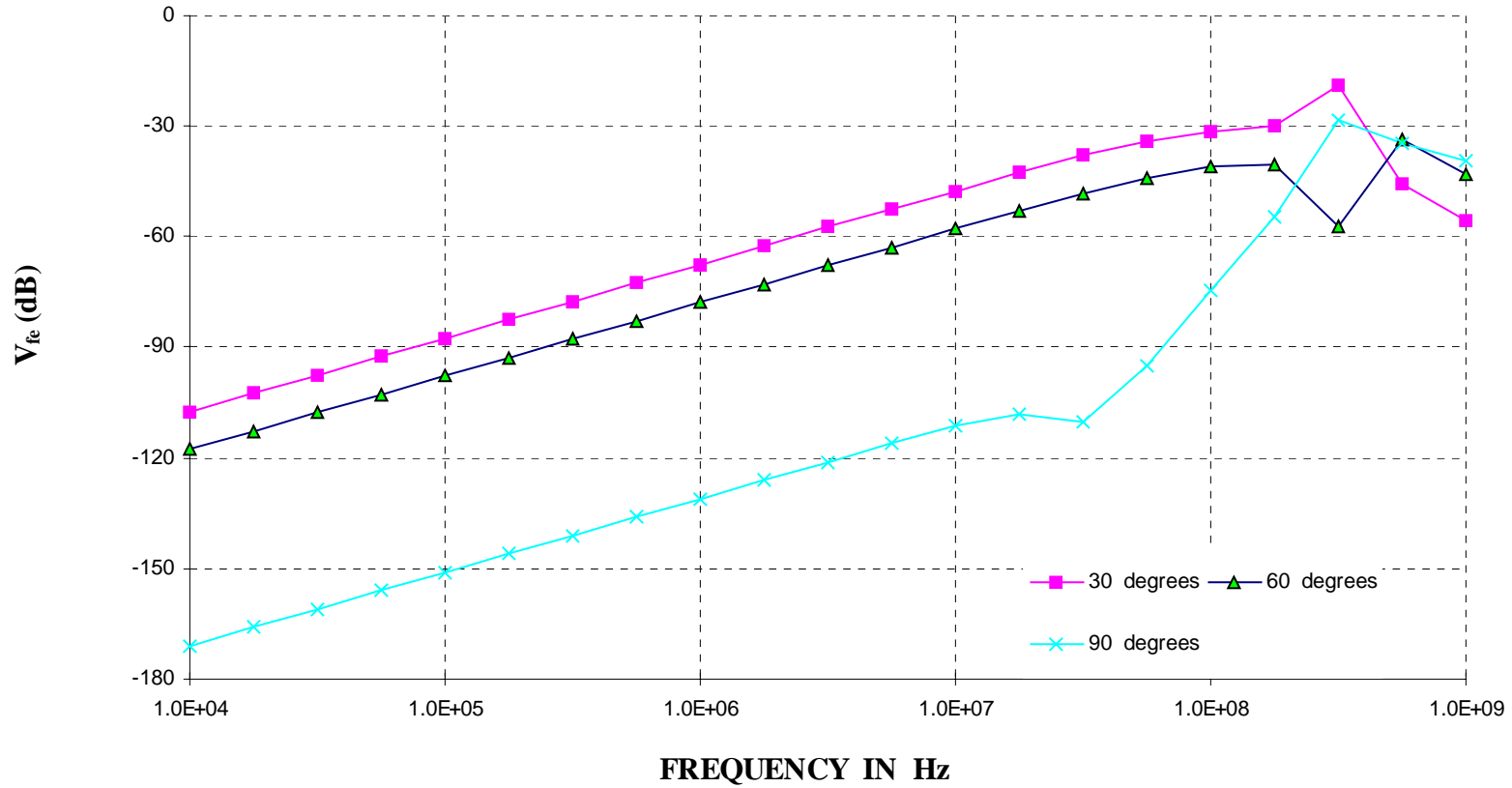


Figure 3.45. Simulated Frequency Domain Far End Crosstalk for Non Parallel Traces  $d = 23$  mms.

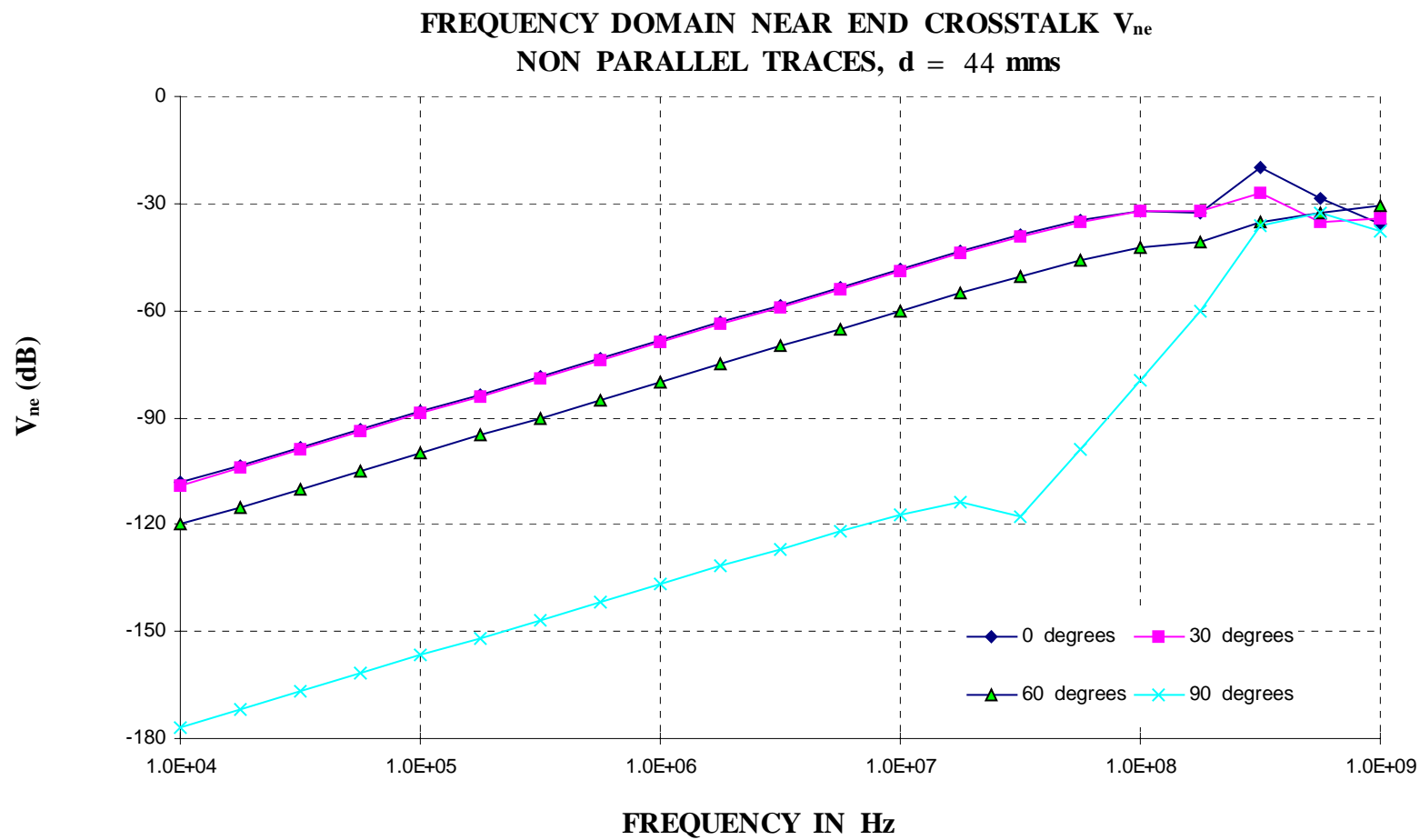


Figure 3.46. Simulated Frequency Domain Near End Crosstalk for Non Parallel Traces  $d = 44$  mms.

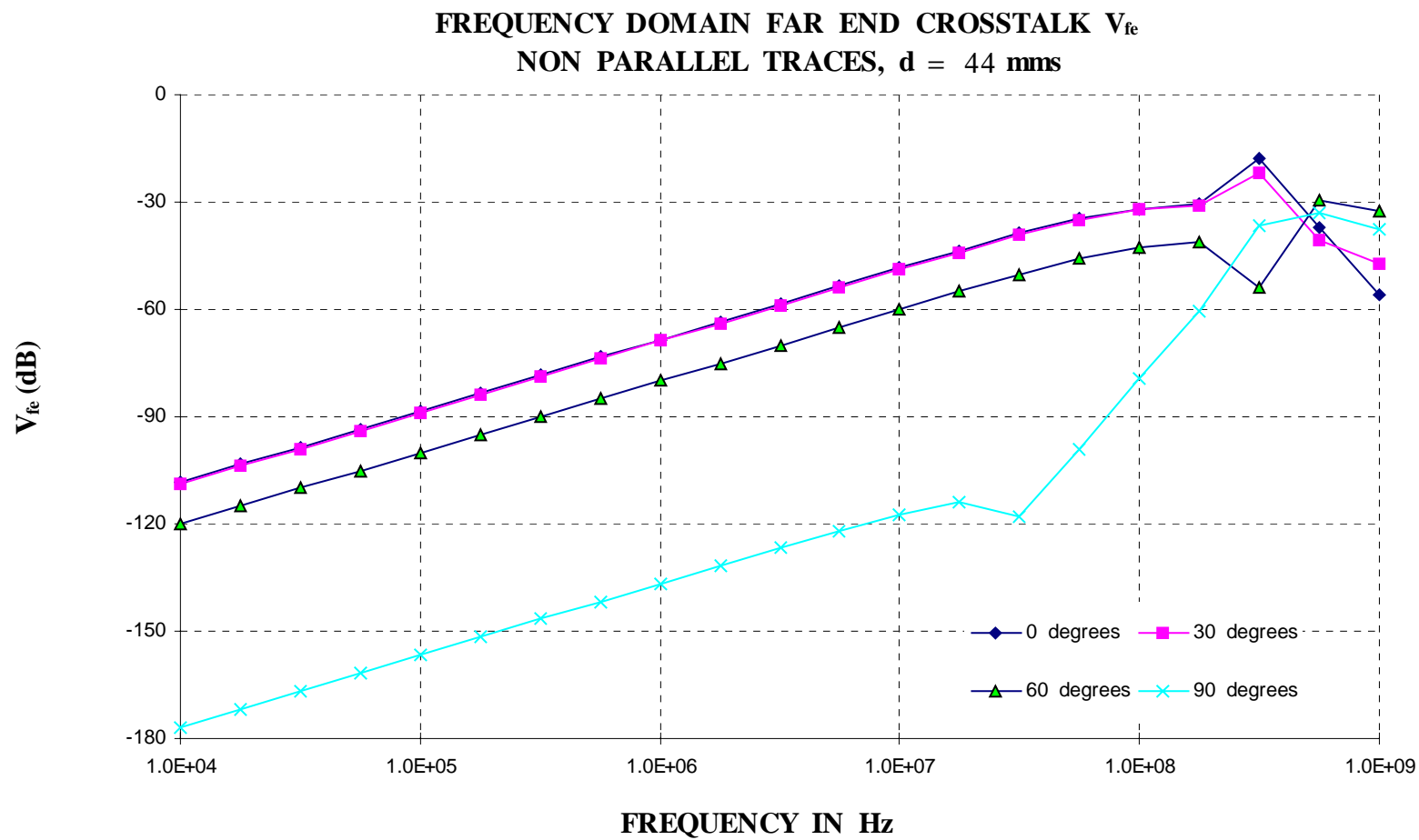


Figure 3.47. Simulated Frequency Domain Far End Crosstalk for Non Parallel Traces  $d = 44$  mms.

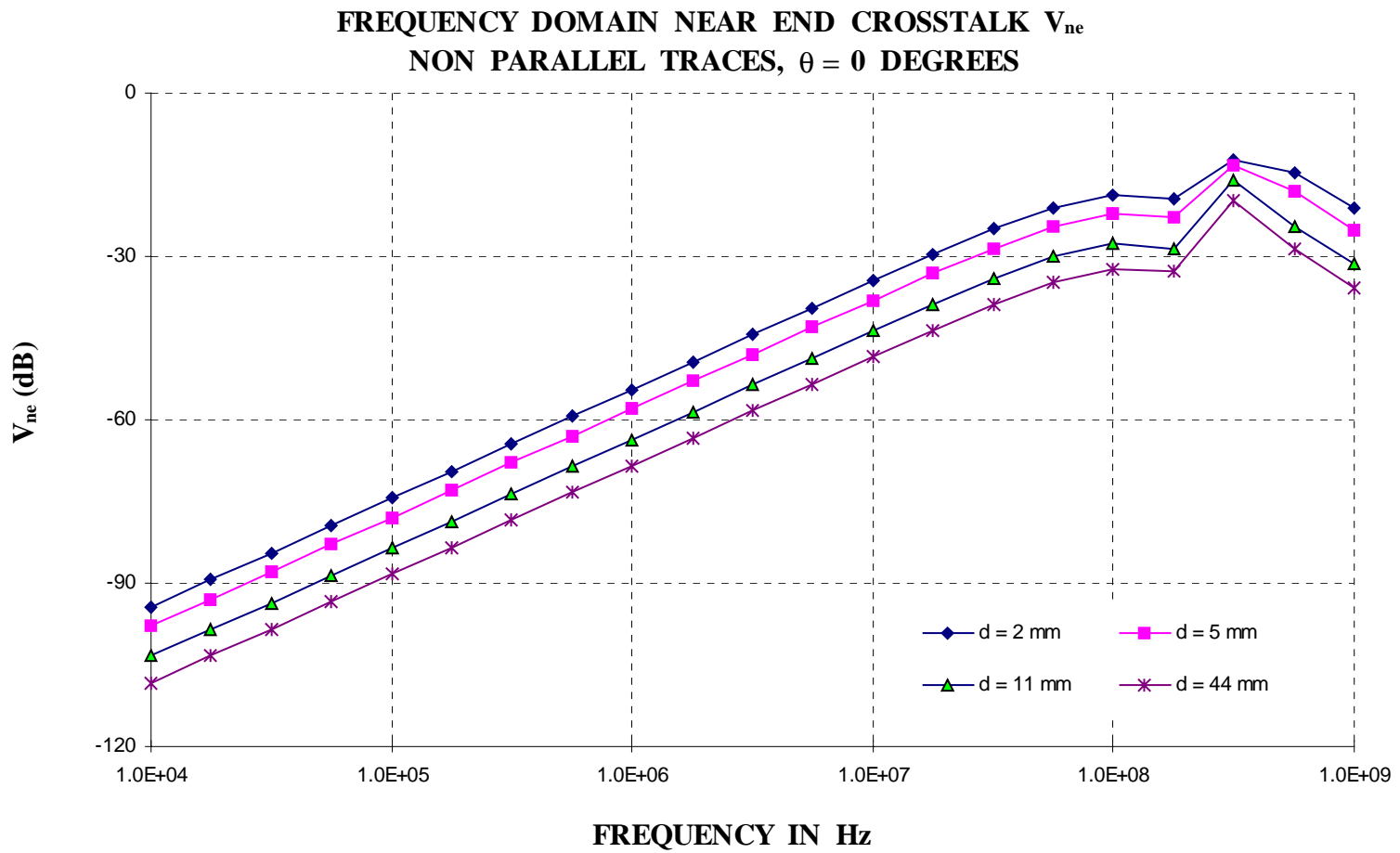


Figure 3.48. Simulated Frequency Domain Near End Crosstalk for Non Parallel Traces  $\theta =$  Degrees.

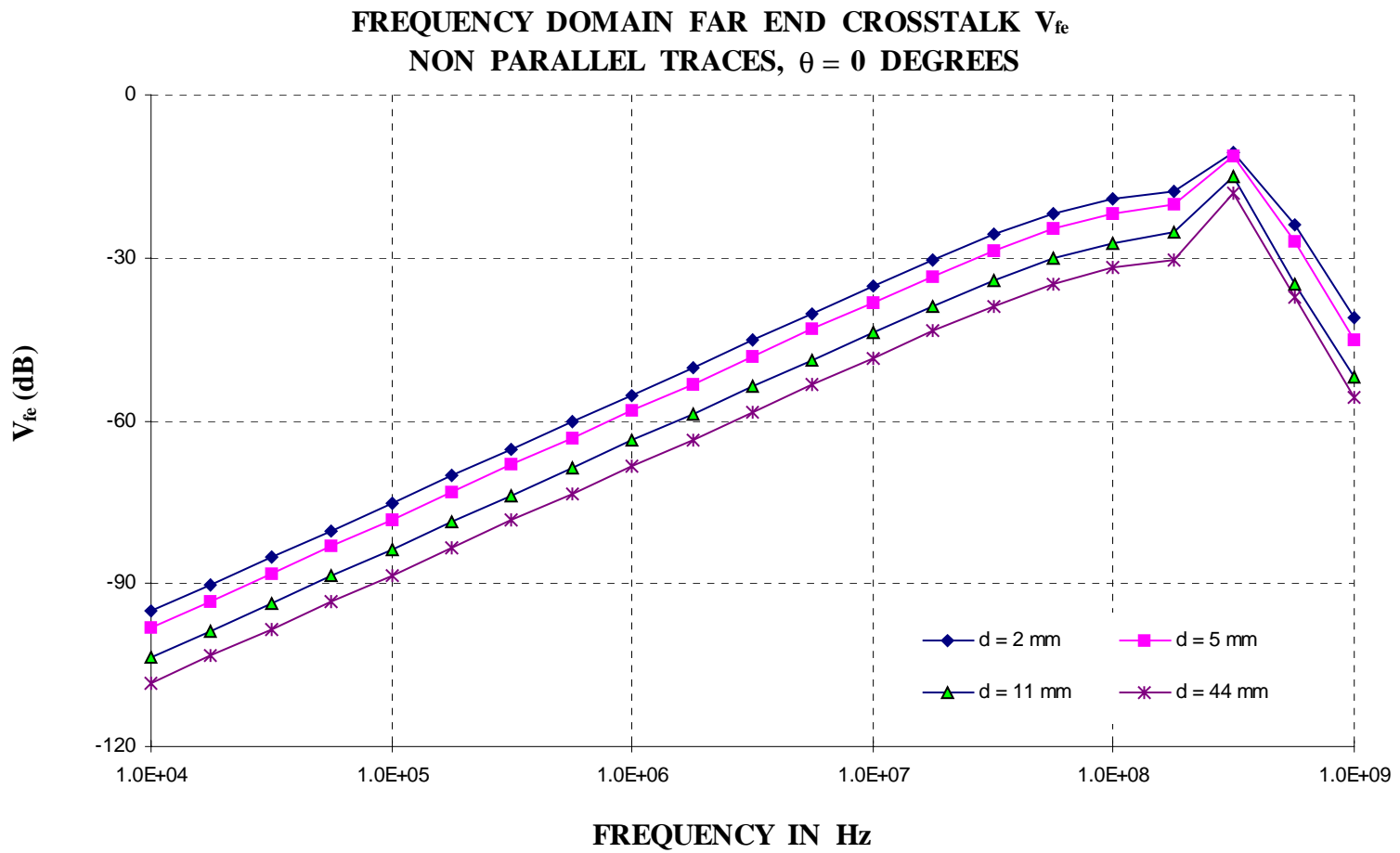


Figure 3.49. Simulated Frequency Domain Far End Crosstalk for Non Parallel Traces  $\theta = 0$  Degrees.

**FREQUENCY DOMAIN NEAR END CROSSTALK  $V_{ne}$   
NON PARALLEL TRACES.  $\Theta = 90$  DEGREES.**

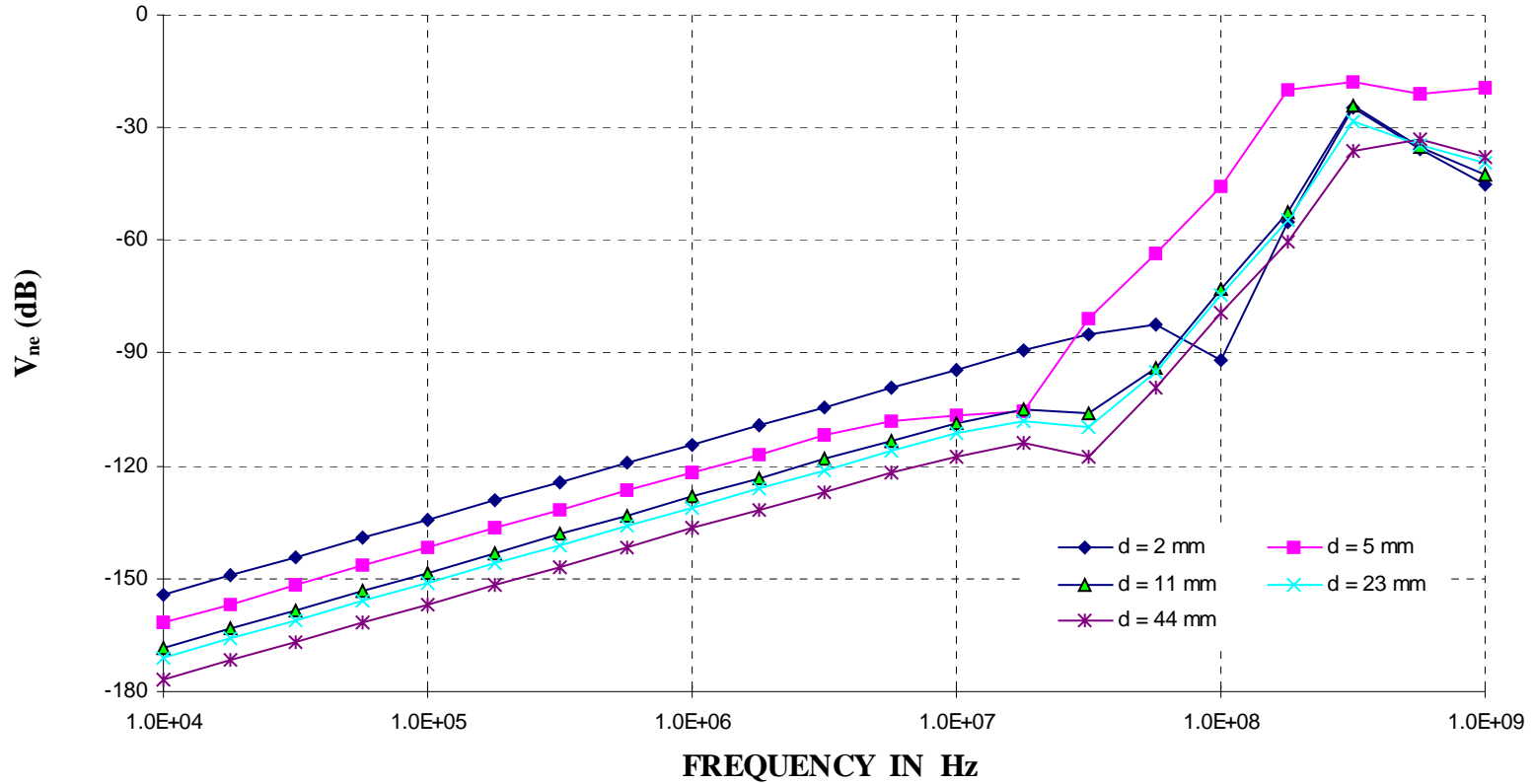


Figure 3.50. Simulated Frequency Domain Near End Crosstalk for Non Parallel Traces  $\theta = 90$  Degrees.

**FREQUENCY DOMAIN FAR END CROSSTALK  $V_{fe}$**   
**NON PARALLEL TRACES.  $\Theta = 90$  DEGREES.**

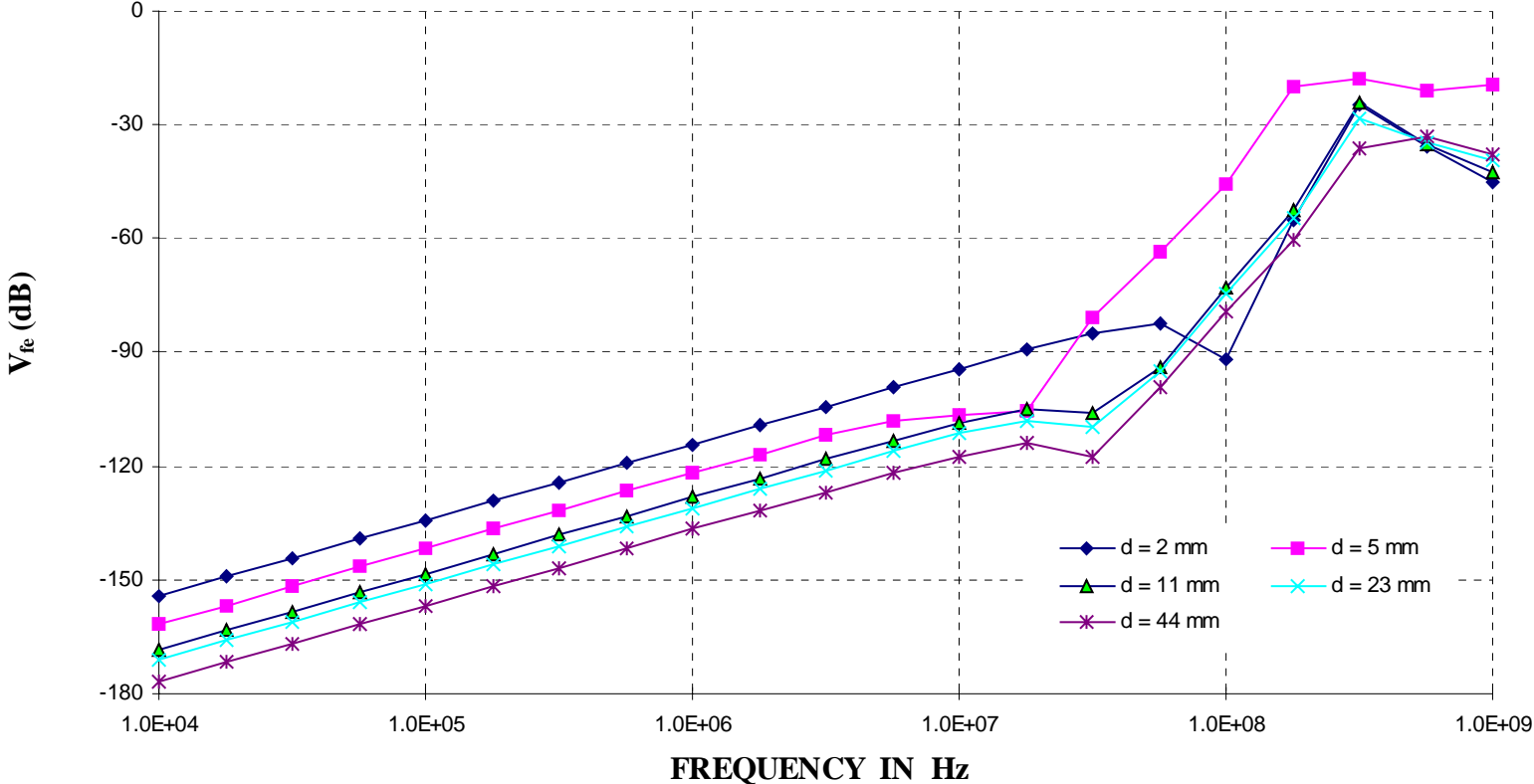


Figure 3.51. Simulated Frequency Domain Far End Crosstalk for Non Parallel Traces  $\theta = 90$  Degrees.

**FREQUENCY DOMAIN NEAR END CROSSTALK  $V_{ne}$**   
**PARALLEL TRACES WITH DISCONTINUITIES,  $\alpha = 0^\circ$**

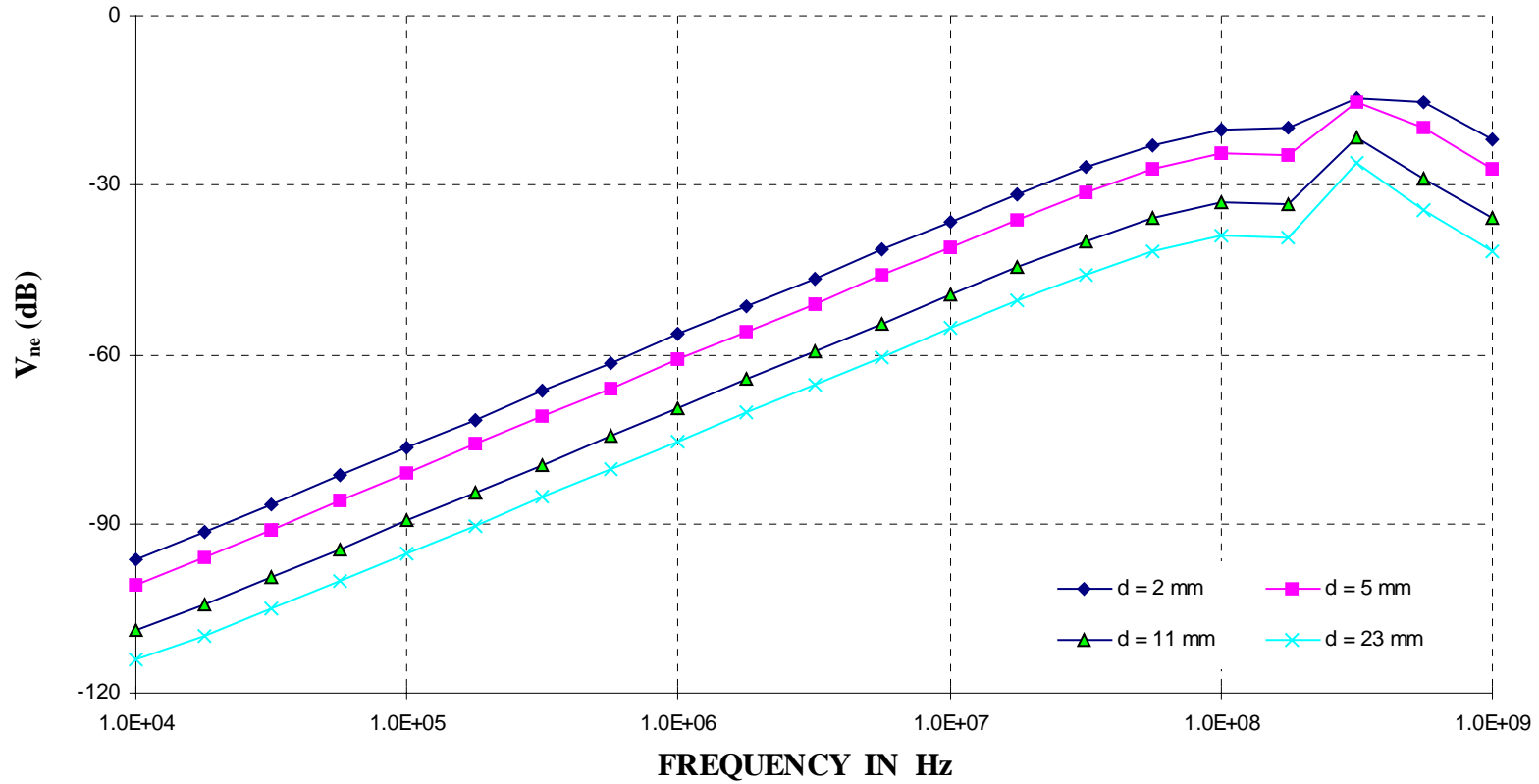


Figure 3.52. Simulated Frequency Domain Near End Crosstalk for Parallel Traces with Discontinuities  $\alpha = 0$  Degrees.

**FREQUENCY DOMAIN FAR END CROSSTALK  $V_{fe}$**   
**PARALLEL TRACES WITH DISCONTINUITIES,  $\alpha = 0^\circ$**

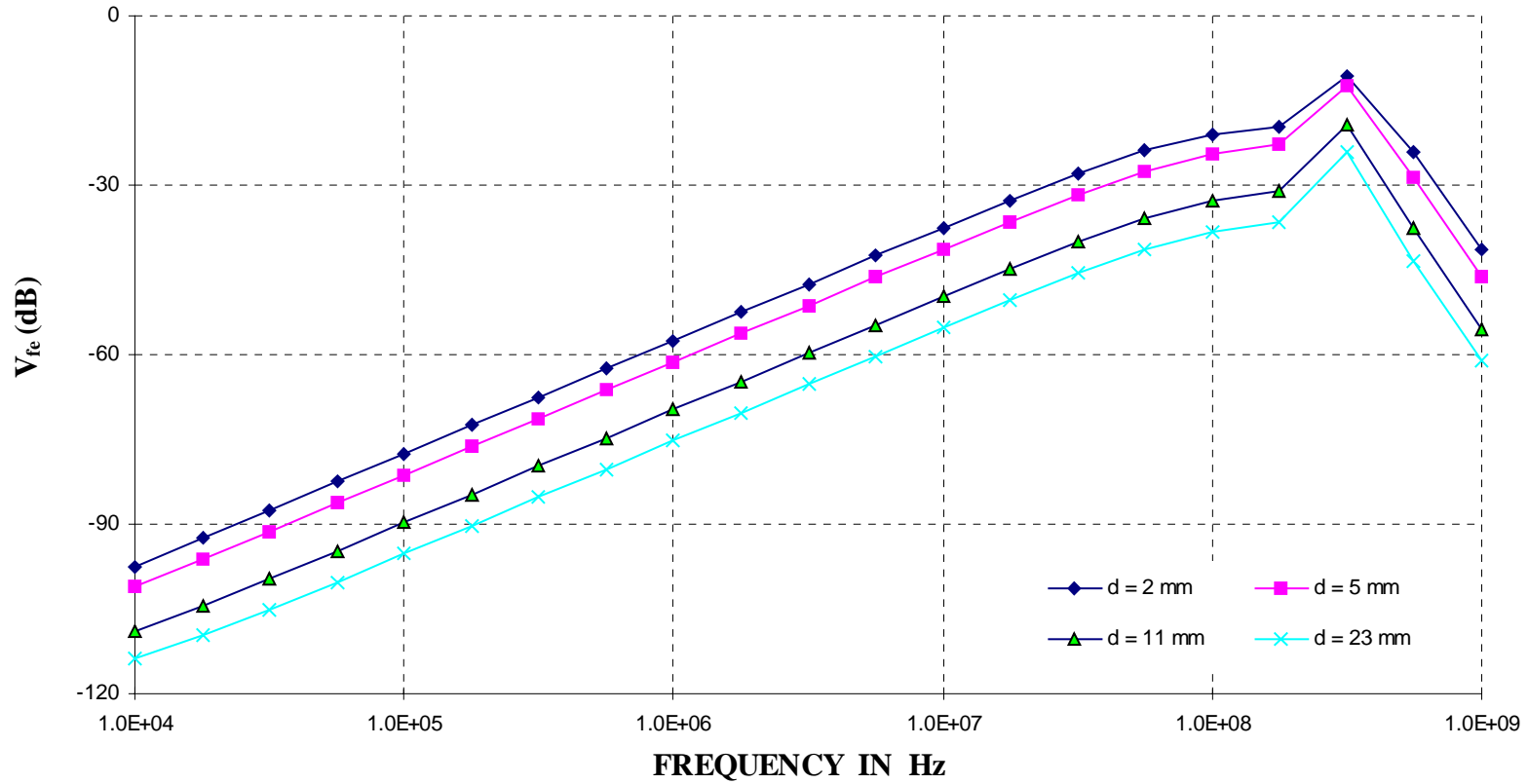


Figure 3.53. Simulated Frequency Domain Far End Crosstalk for Parallel Traces with Discontinuities  $\alpha = 0$  Degrees.

FREQUENCY DOMAIN NEAR END CROSSTALK  $V_{ne}$   
PARALLEL TRACES WITH DISCONTINUITIES,  $\alpha = 60^\circ$

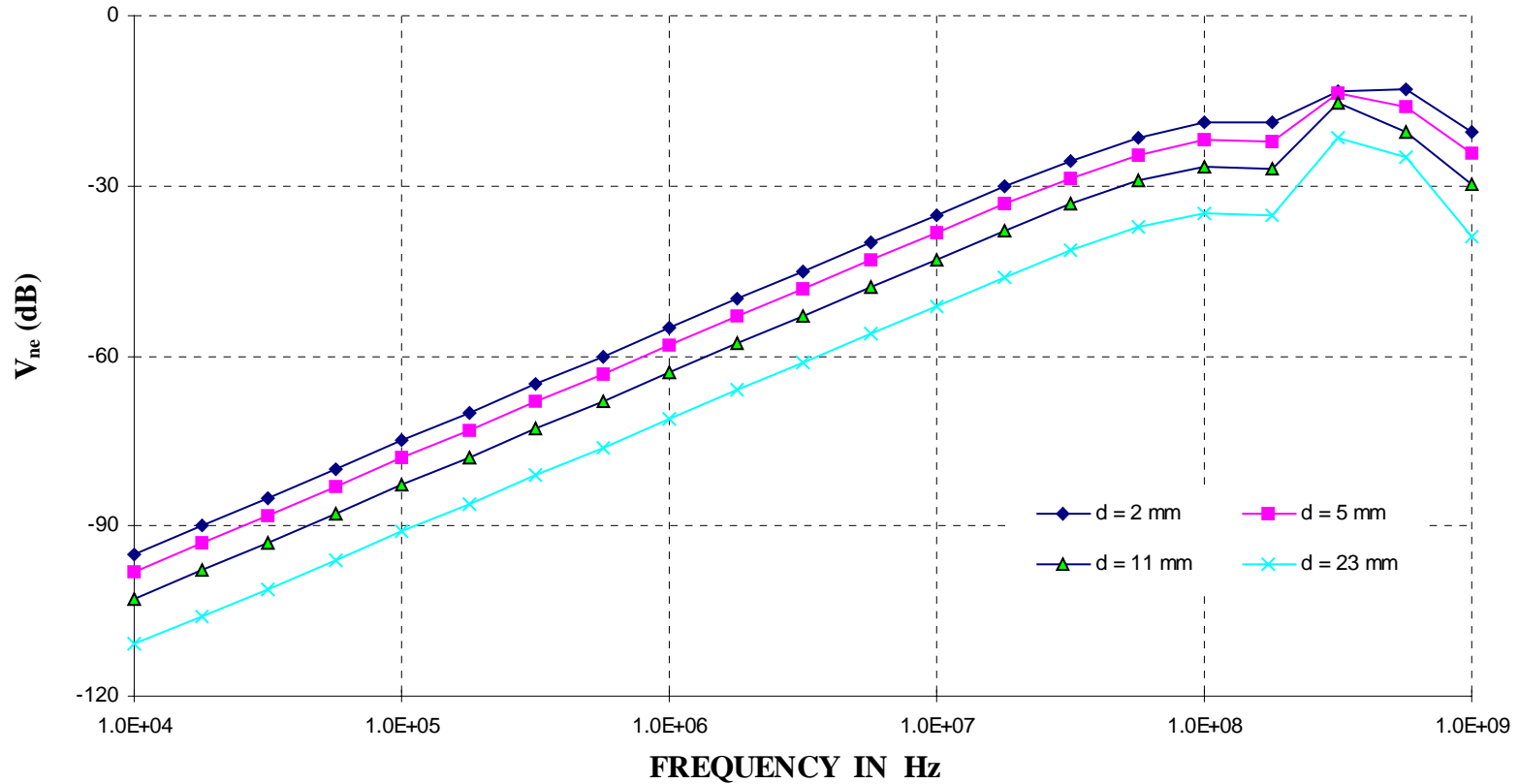


Figure 3.54. Simulated Frequency Domain Near End Crosstalk for Parallel Traces with Discontinuities  $\alpha = 60$  Degrees.

**FREQUENCY DOMAIN FAR END CROSSTALK  $V_{fe}$**   
**PARALLEL TRACES WITH DISCONTINUITIES,  $\alpha = 60^\circ$**

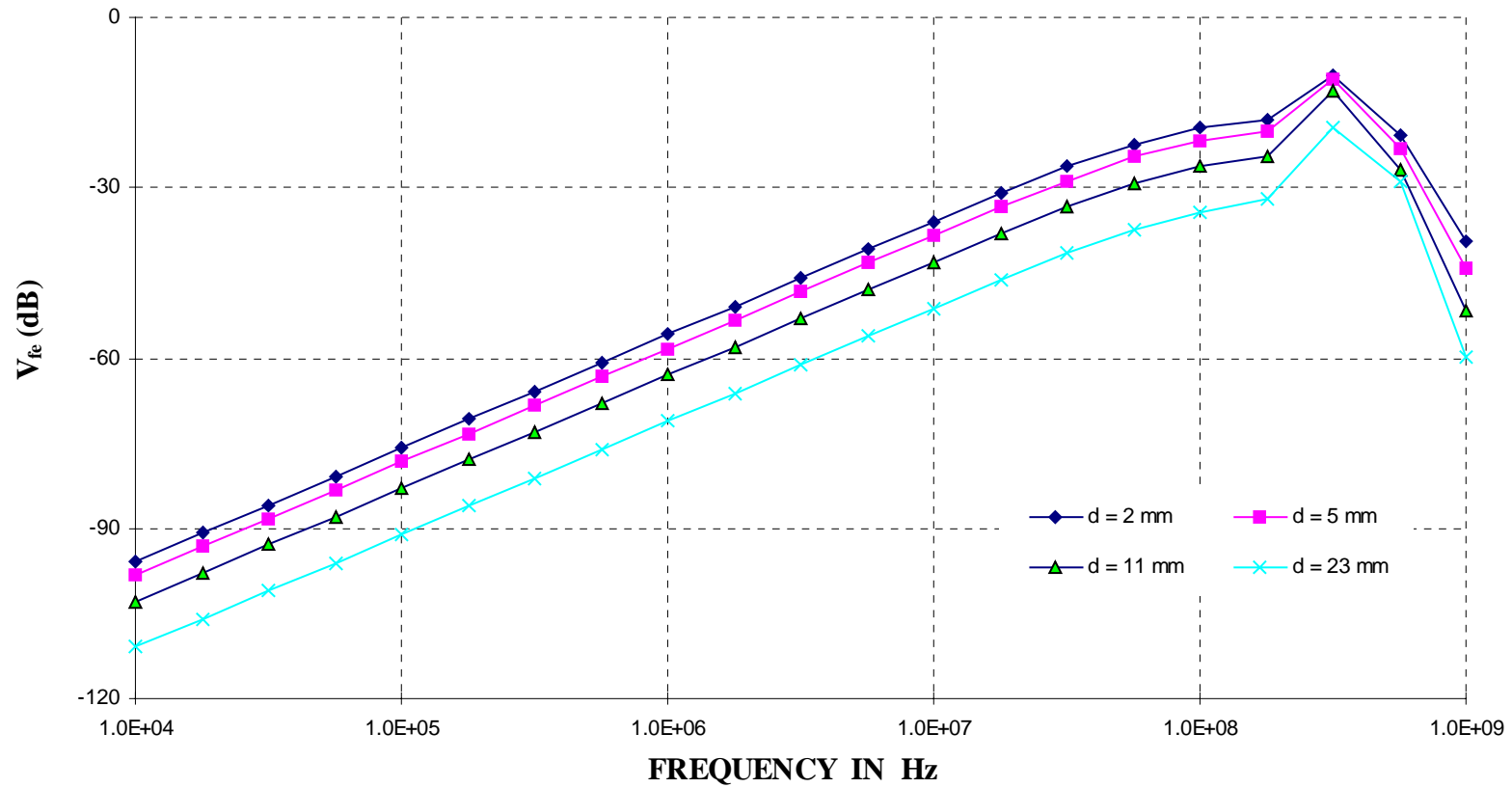


Figure 3.55. Simulated Frequency Domain Far End Crosstalk for Parallel Traces with Discontinuities  $\alpha = 60$  Degrees.

**FREQUENCY DOMAIN NEAR END CROSSTALK  $V_{ne}$**   
**PARALLEL TRACES WITH DISCONTINUITIES,  $\alpha = 90^\circ$**

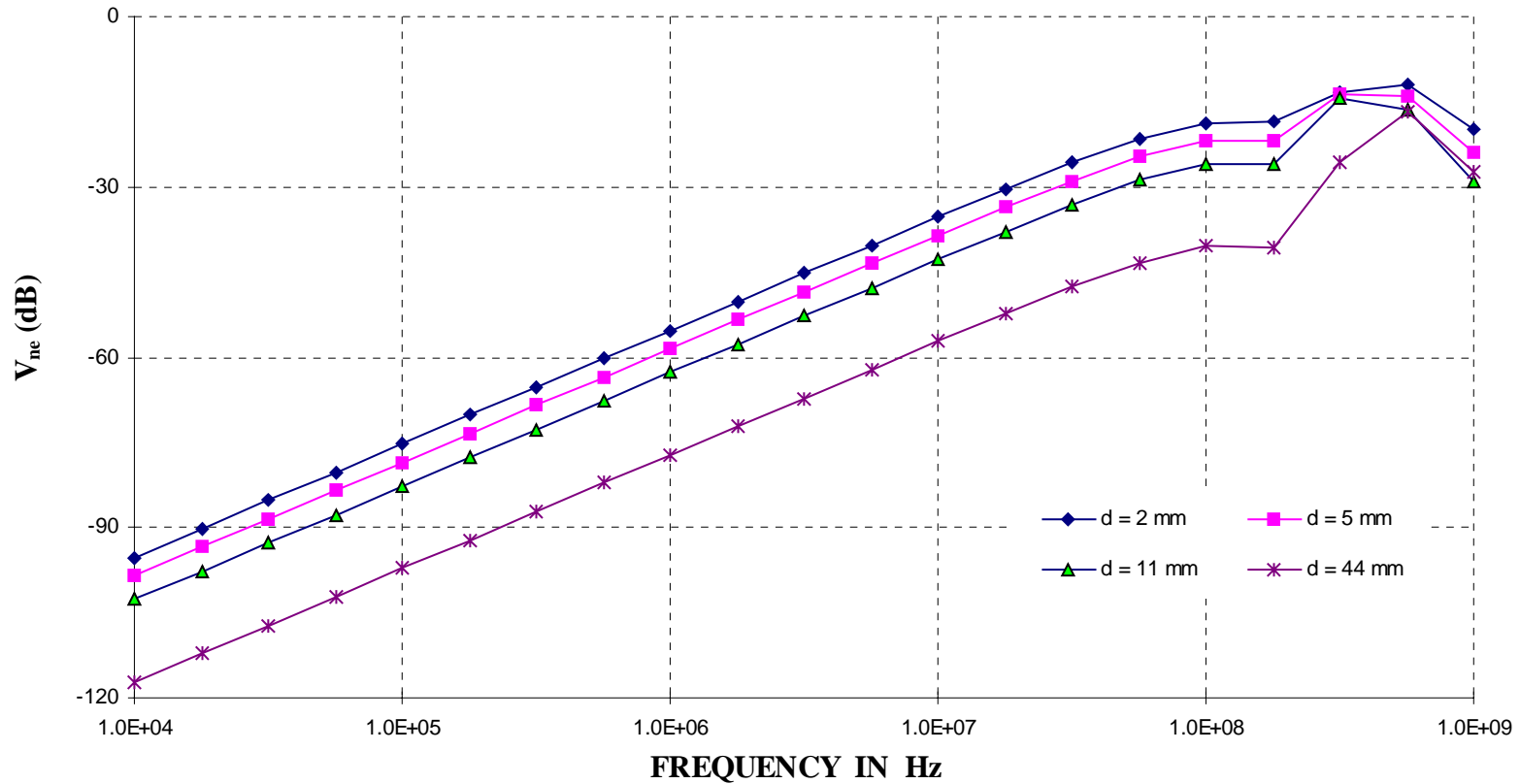


Figure 3.56. Simulated Frequency Domain Near End Crosstalk for Parallel Traces with Discontinuities  $\alpha = 90$  Degrees.

**FREQUENCY DOMAIN FAR END CROSSTALK  $V_{fe}$**   
**PARALLEL TRACES WITH DISCONTINUITIES,  $\alpha = 90^\circ$**

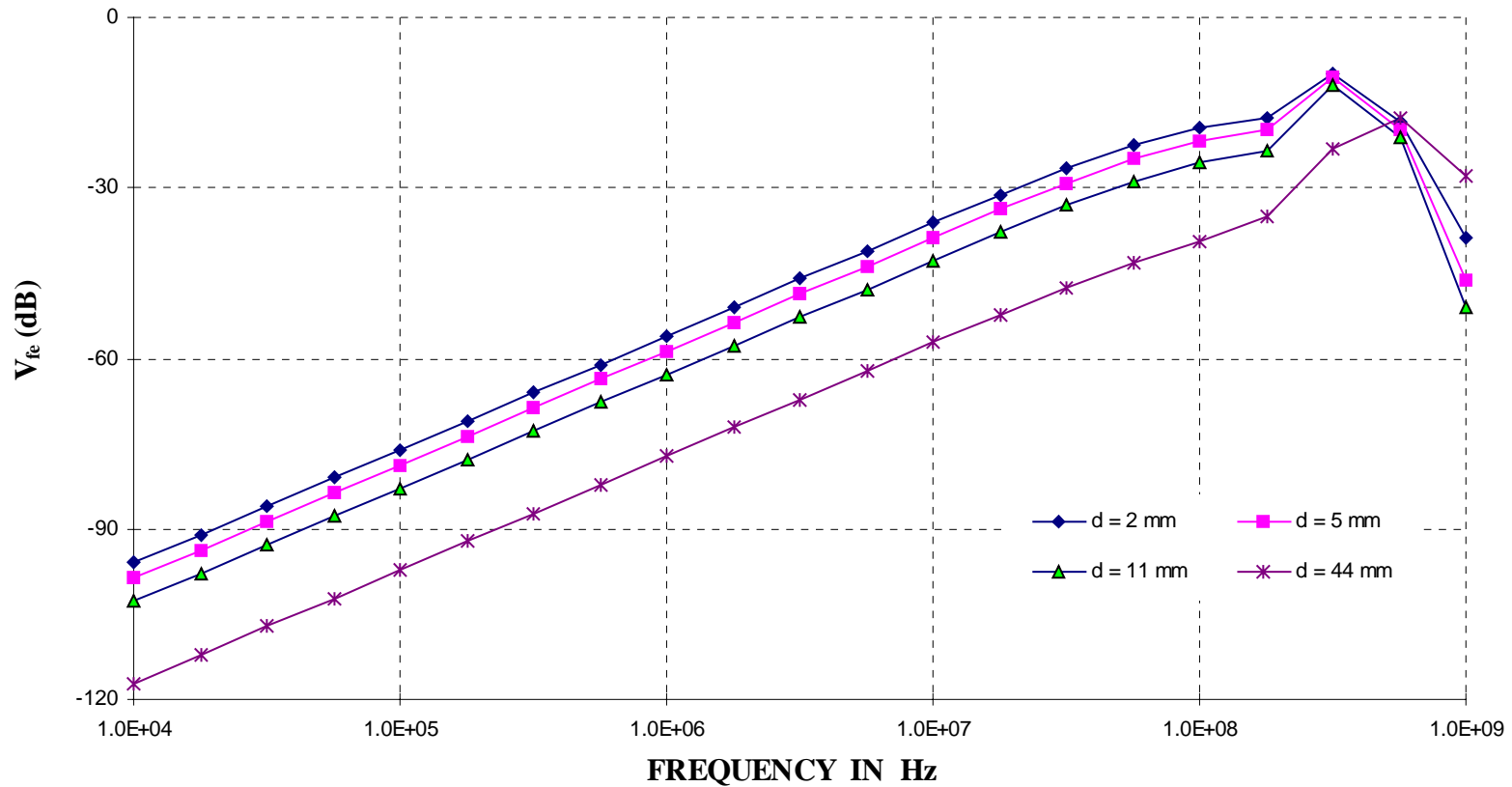


Figure 3.57. Simulated Frequency Domain Far End Crosstalk for Parallel Traces with Discontinuities  $\alpha = 90$  Degrees.

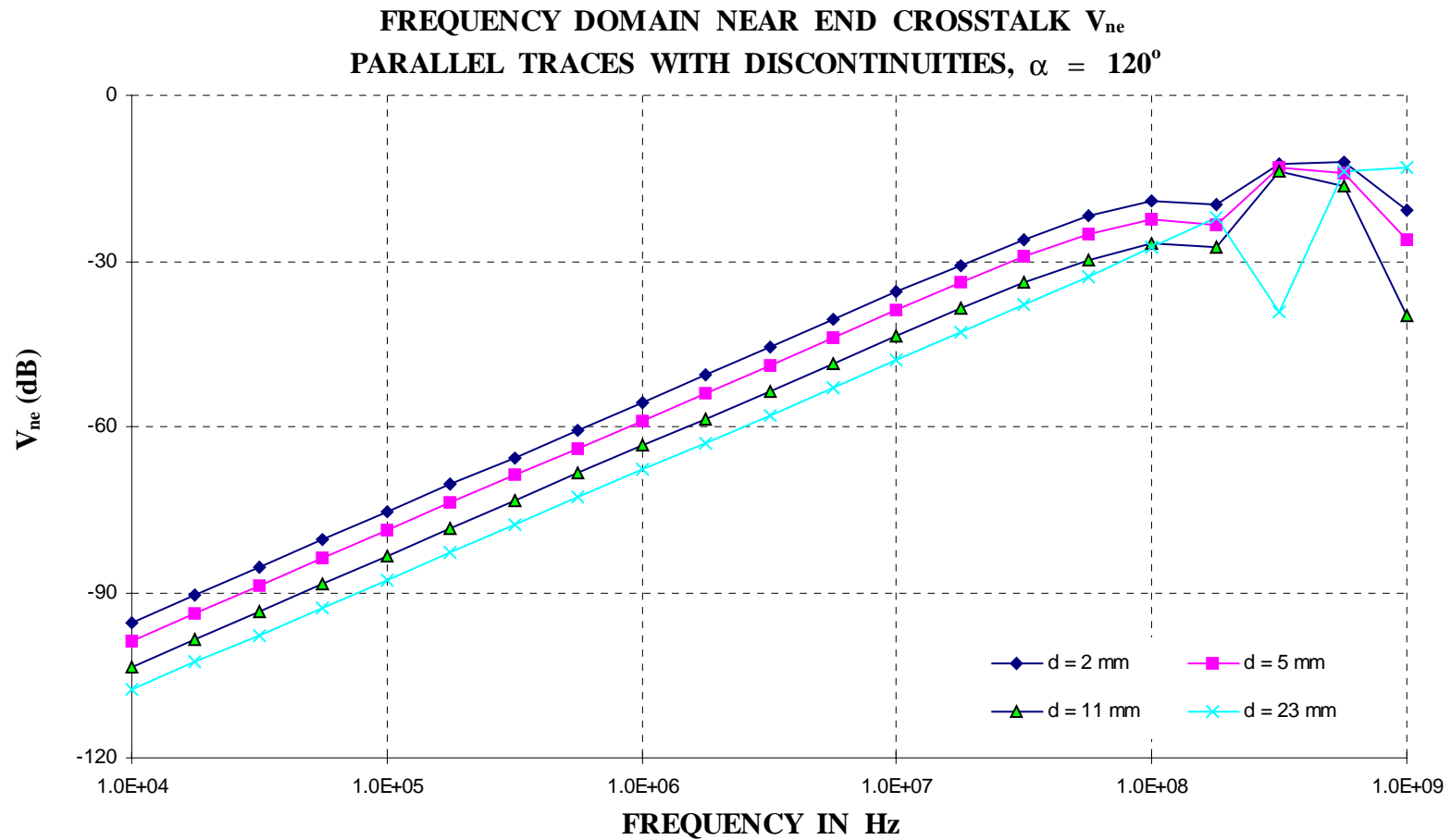


Figure 3.58. Simulated Frequency Domain Near End Crosstalk for Parallel Traces with Discontinuities  $\alpha = 120$  Degrees.

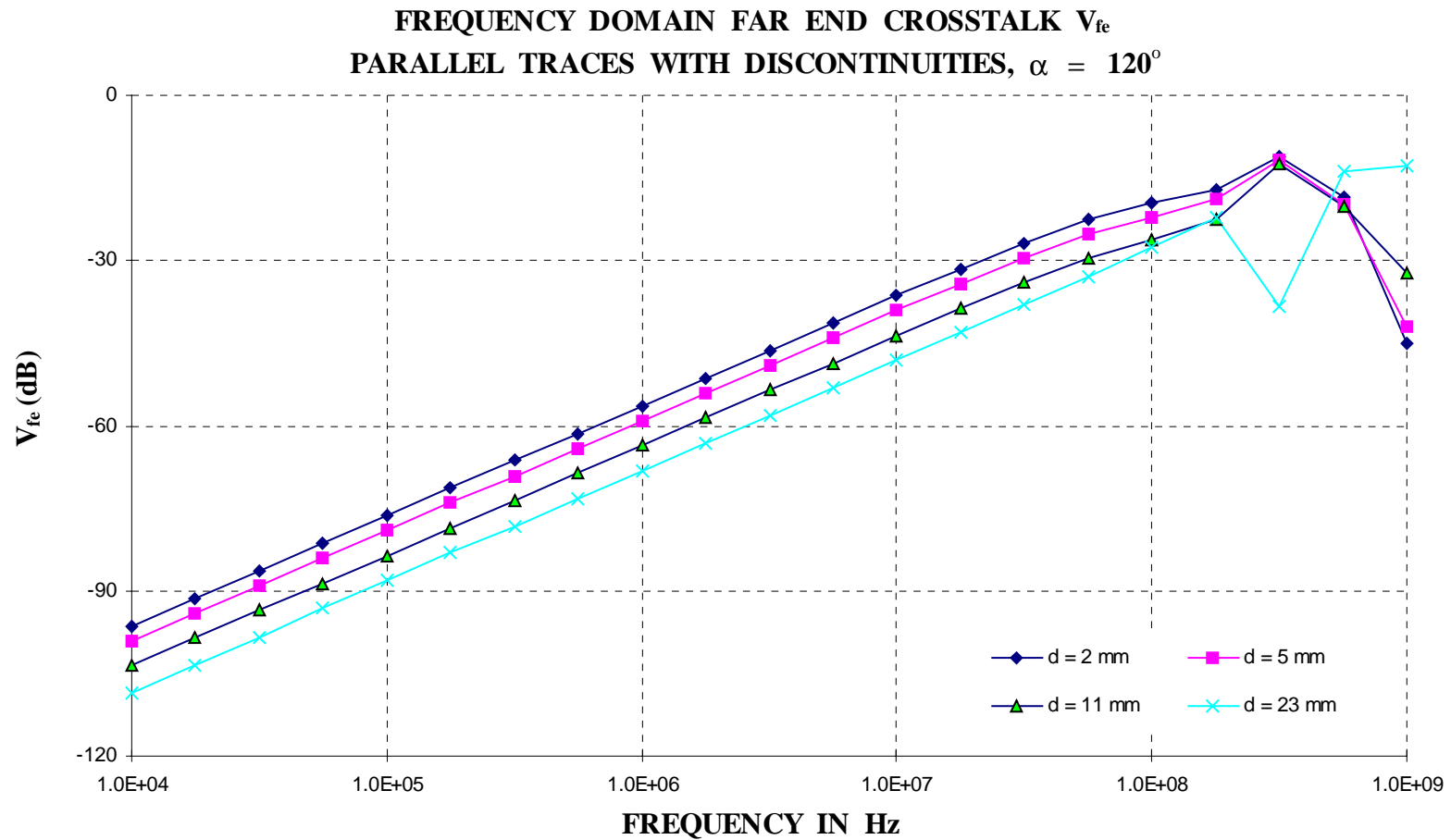


Figure 3.59. Simulated Frequency Domain Far End Crosstalk for Parallel Traces with Discontinuities  $\alpha = 120$  Degrees.

**FREQUENCY DOMAIN NEAR END CROSSTALK  $V_{ne}$   
PARALLEL TRACES WITH DISCONTINUITIES,  $d = 2$  mms**

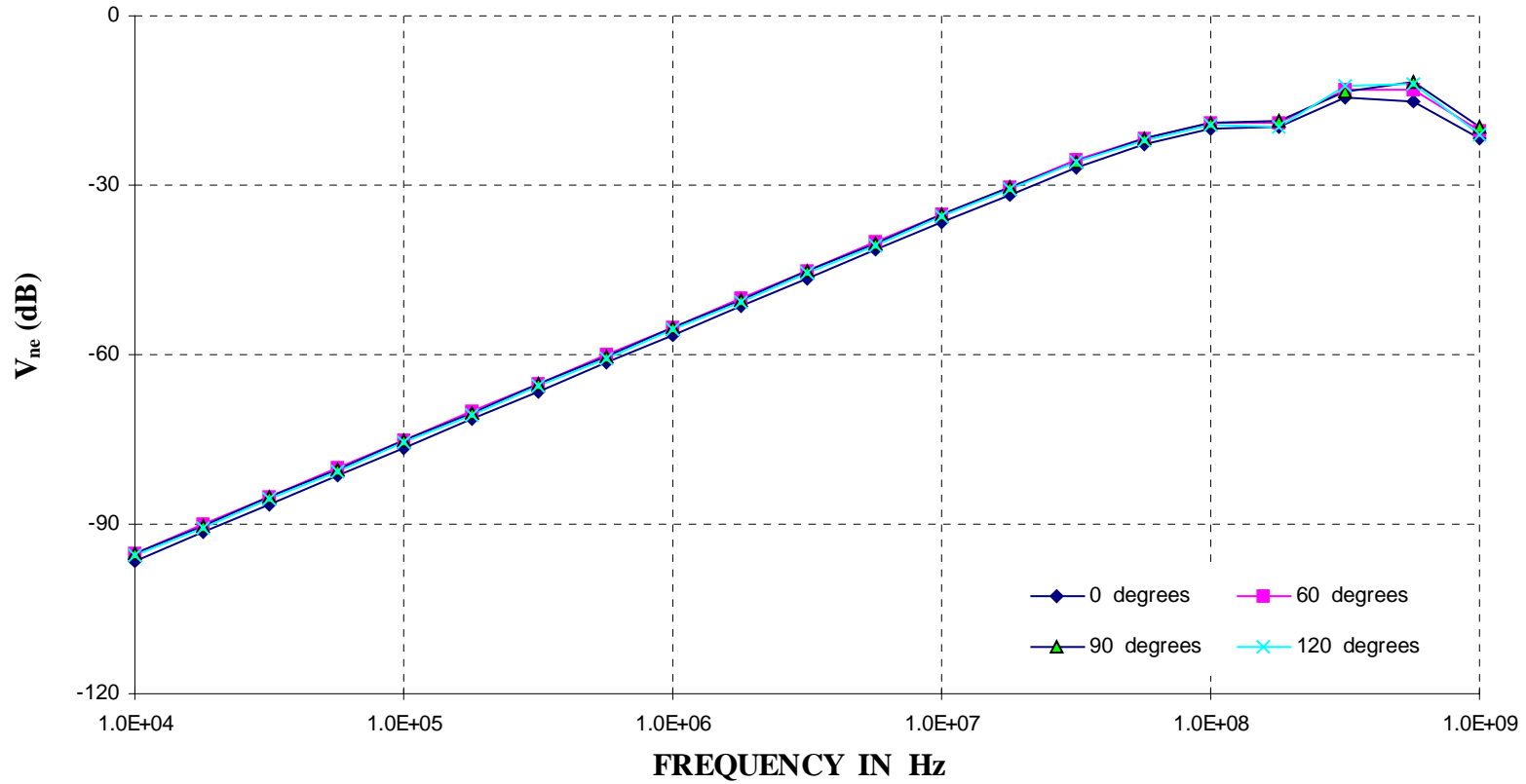


Figure 3.60. Simulated Frequency Domain Near End Crosstalk for Parallel Traces with Discontinuities  $d = 2$  mms.

**FREQUENCY DOMAIN FAR END CROSSTALK  $V_{fe}$**   
**PARALLEL TRACES WITH DISCONTINUITIES,  $d = 2$  mms**

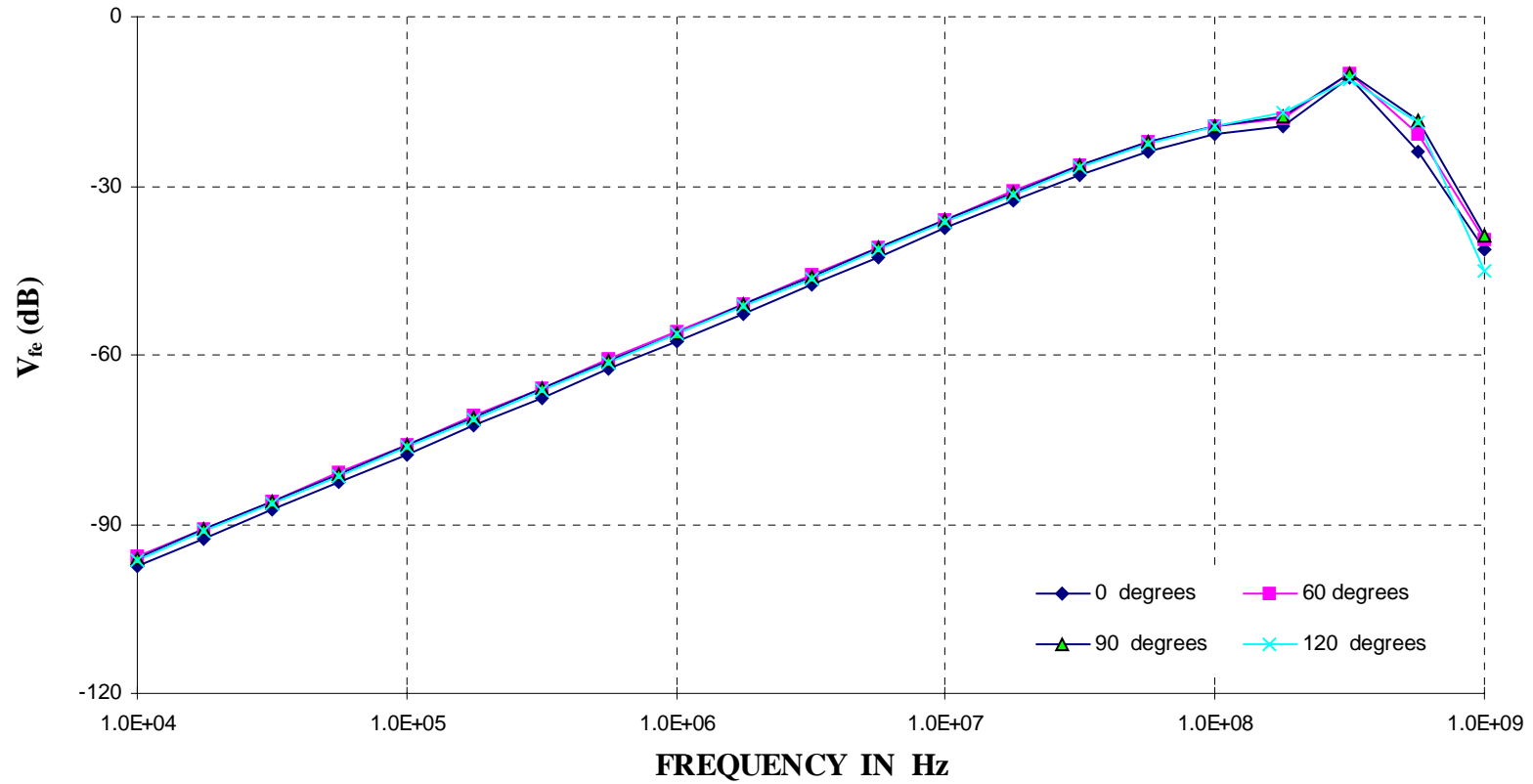


Figure 3.61. Simulated Frequency Domain Far End Crosstalk for Parallel Traces with Discontinuities  $d = 2$  mms.

**FREQUENCY DOMAIN NEAR END CROSSTALK  $V_{ne}$   
PARALLEL TRACES WITH DISCONTINUITIES,  $d = 5$  mms**

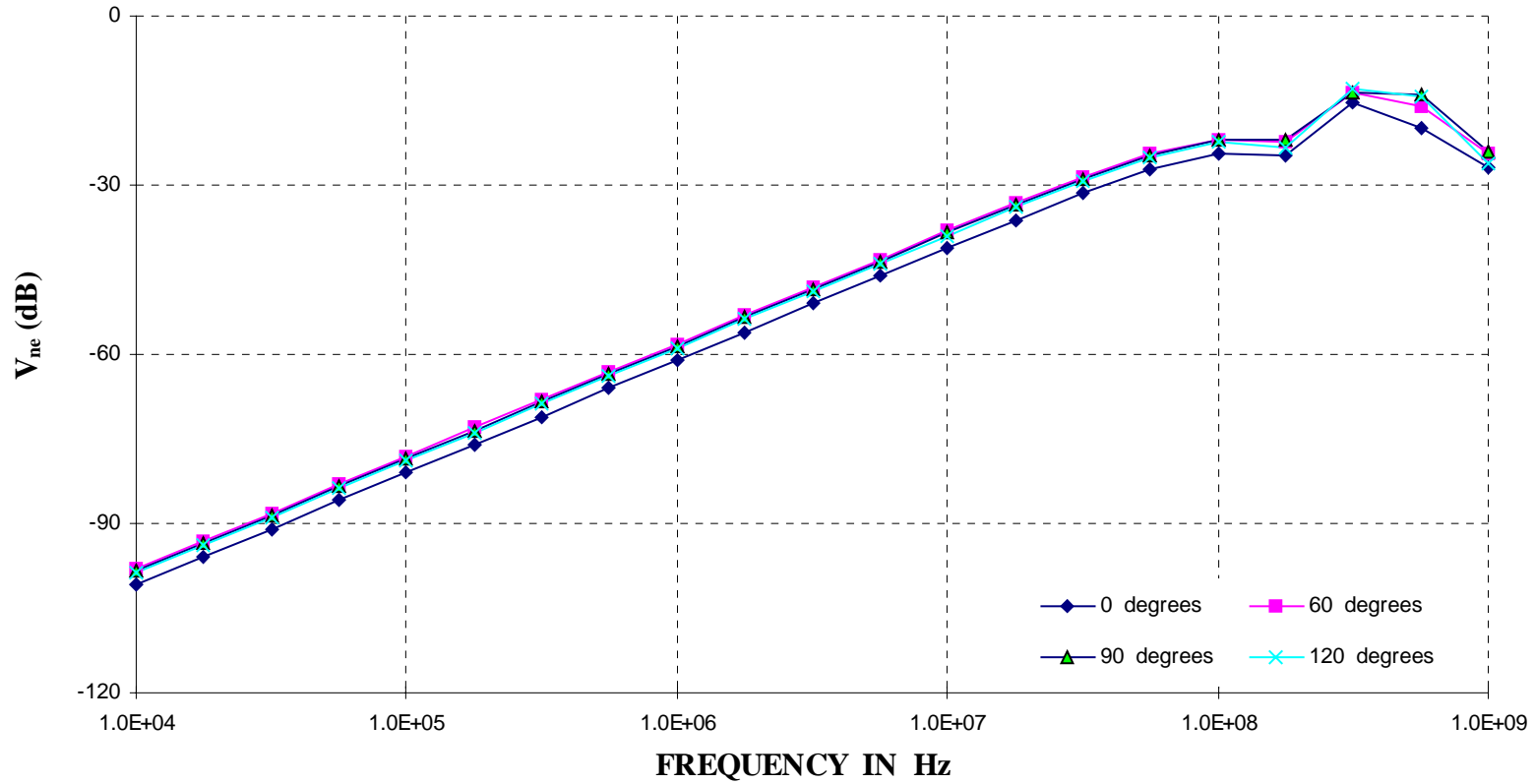


Figure 3.62. Simulated Frequency Domain Near End Crosstalk for Parallel Traces with Discontinuities  $d = 5$  mms.

**FREQUENCY DOMAIN FAR END CROSSTALK  $V_{fe}$   
PARALLEL TRACES WITH DISCONTINUITIES,  $d = 5$  mms**

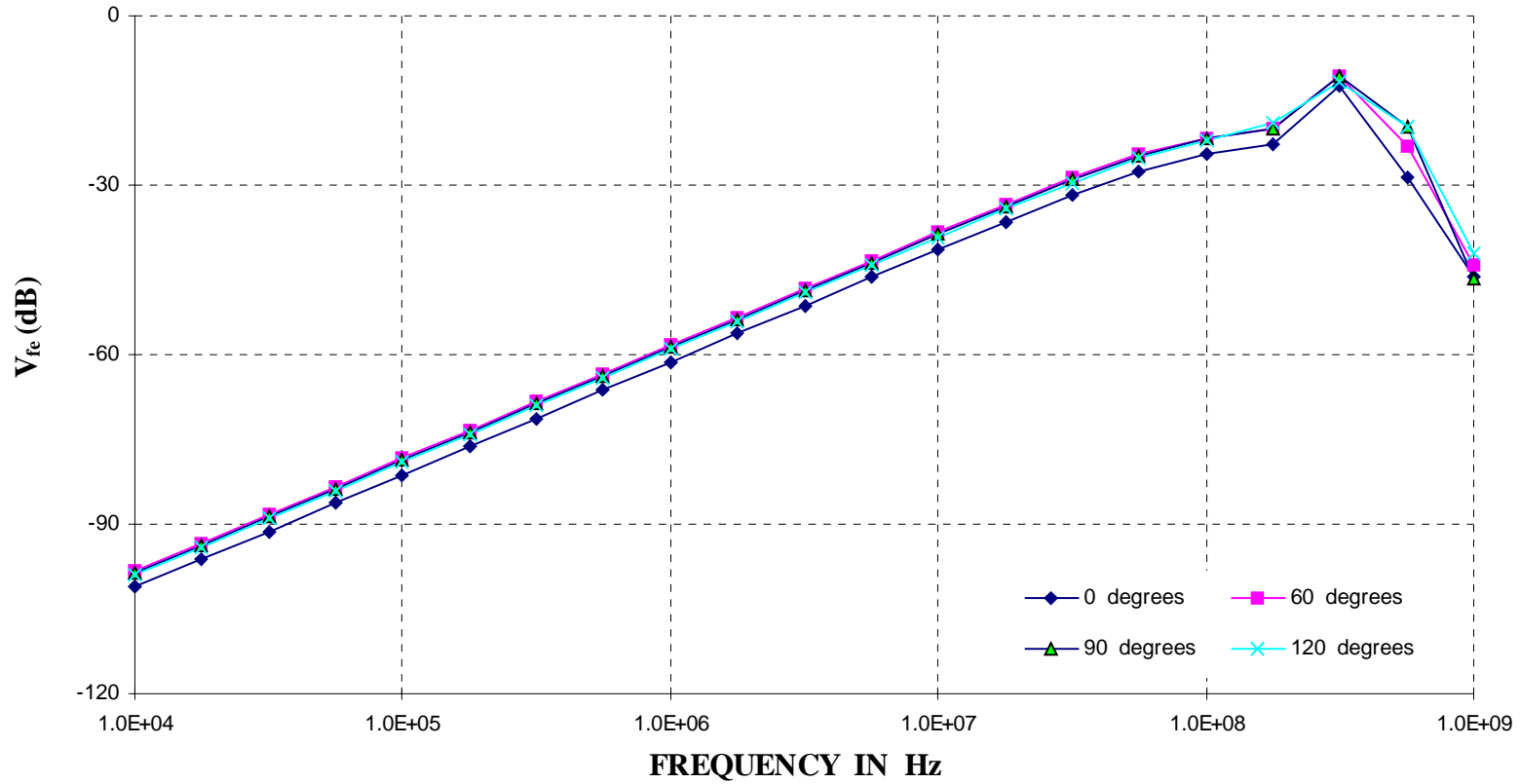


Figure 3.63. Simulated Frequency Domain Far End Crosstalk for Parallel Traces with Discontinuities  $d = 5$  mms.

#### IV. RADIATED EMI SIMULATIONS

The phenomenon of Radiated EMI from a single trace card was investigated by Ramchandani et al (1996). Consider a printed circuit board consisting of a single trace and a ground plane as shown in Figure 4.1. Hubing and Kaufman (1989) have shown that a trace on a circuit board is essentially a dipole. The correlation between a trace on a circuit board and a dipole is shown in Figure 4.2. Ramchandani et al (1996) used this model to determine the radiated EMI from a single trace shown in Figure 4.1.

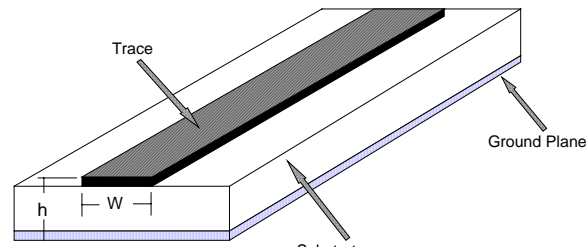


Figure 4.1. Geometry of a Single Trace Card for Radiated EMI.

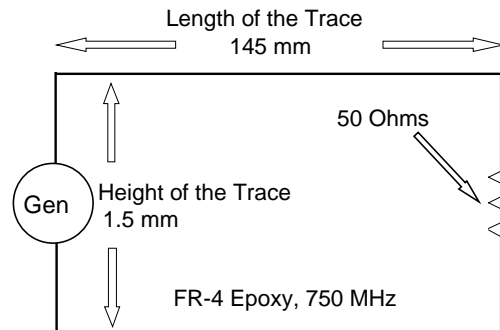


Figure 4.2. Single Trace as a Radiation Source.

## A. SIMULATION GEOMETRIES

Six geometries with different levels of complexities were selected for radiated EMI simulations. The first objective in the selection of these six geometries was to develop confidence and usage expertise with the commercial software packages. The second objective was to select geometries whose radiated fields could be theoretically modeled with relative ease. The third objective in the selection of these six geometries was their PEBB relevance. All six geometries are an extension of the geometry used to determine the radiated EMI from a single trace card by Ramchandani et al (1996). The six geometries are shown in Figure 4.3.

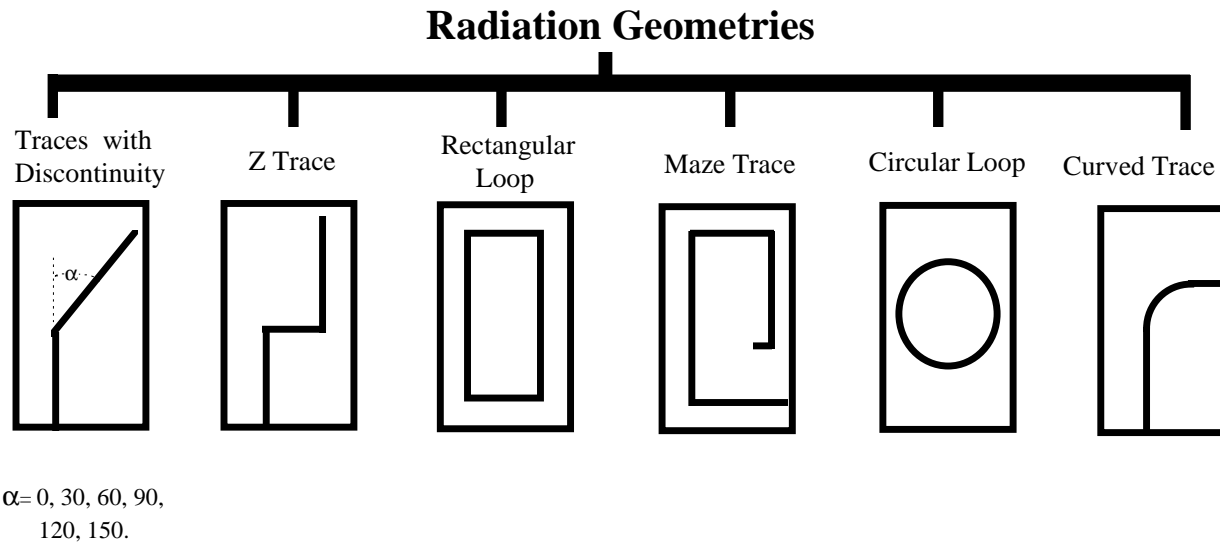


Figure 4.3. The Six Geometries for Radiated EMI Simulations.

#### 1. Traces with Discontinuity

This geometry comprises of a trace with one angular discontinuity. The PEBB is going to have numerous trace discontinuities. Thus, this type of geometry would be PEBB relevant. Another

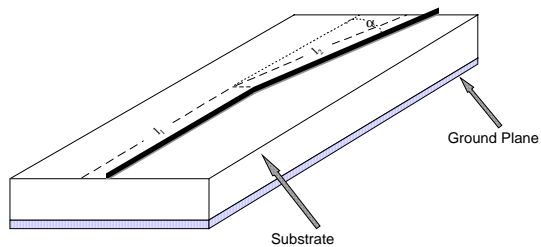


Figure 4.4. Printed Circuit Board Geometry for a Trace with Discontinuity.

reason for selecting this type of discontinuity was to see what effects the angular variation ( $\alpha$ ) would have on the radiated EMI. The Printed Circuit Board Geometry of the Trace with Discontinuity is shown in Figure 4.4. For theoretical purposes, this geometry consists of two dipoles oriented at an angle of  $\alpha$  relative to each other. The theoretical far fields from these two dipoles can be accurately determined. The lengths  $l_1$  and  $l_2$  of the dipoles in Figure 4.4 were approx. 6 cms each. For dipoles to be small as compared to the wavelength, the simulation frequency was chosen to be 750 MHz. At 750 MHz the wavelength is 40 cms. This wavelength is approx. seven times greater than the length of each dipole. Thus, the far field condition is satisfied: the length of the dipole is small compared to the radiation wavelength.

## 2. Z Trace

This geometry comprises of two abrupt 90 degree discontinuities. The PEBB is going to have numerous such abrupt discontinuities. One other reason for selecting this geometry was to compare the EMI from this Z trace with the EMI resulting from a straight trace with no discontinuity. The Printed Circuit Board Geometry of the Z Trace is shown in Figure 4.5.

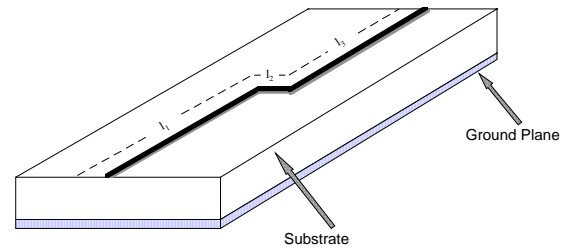


Figure 4.5. Printed Circuit Board Geometry for a Z Trace.

For theoretical purposes, this geometry consists of three dipoles oriented at ninety degrees relative to each other. The theoretical far fields from these three dipoles can be accurately determined. The lengths  $l_1$ ,  $l_2$  and  $l_3$  of the three dipoles in Figure 4.5 were approx. 7, 2.75, and 7 cms respectively. For dipoles to be small compared to the wavelength, the simulation frequency was again chosen to be 750 MHz. Thus the far field condition is satisfied: the length of the dipole is small compared to the radiation wavelength.

### 3. Rectangular Trace

This geometry possesses four abrupt 90 degree discontinuities and encloses a radiation surface. The PEBB is going to have numerous rectangular traces forming radiation surfaces. The Printed Circuit Board Geometry of the Rectangular Loop is shown in Figure 4.6. For theoretical purposes, this geometry can be considered as a small rectangular loop antenna. The theoretical far fields from a small rectangular loop antenna can be accurately determined. The lengths  $l_1$  and  $l_2$  of

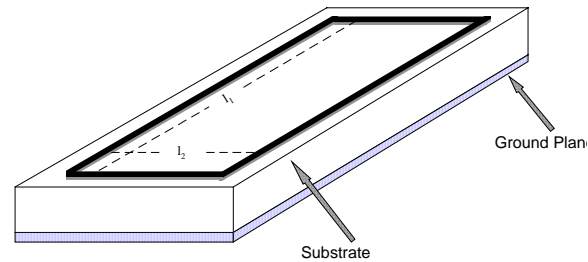


Figure 4.6. Printed Circuit Board Geometry for a Rectangular Loop.

the two sides of the rectangle in Figure 4.6 were approx. 13 cms and 10 cms respectively. Essentially a rectangular loop consists of four dipole elements. Consequently, the simulation frequency for this geometry was chosen to be 200 MHz. At 200 MHz the wavelength is 150 cms. This wavelength is approx. eleven times greater than the largest rectangular side. Thus the far field condition is satisfied: the length of the dipole is small compared to the radiation wavelength.

### 4. Maze Trace

This geometry incorporates more trace complexities. The PEBB is going to have numerous complex traces. The Printed Circuit Board Geometry of the Maze Trace is shown in Figure 4.7.

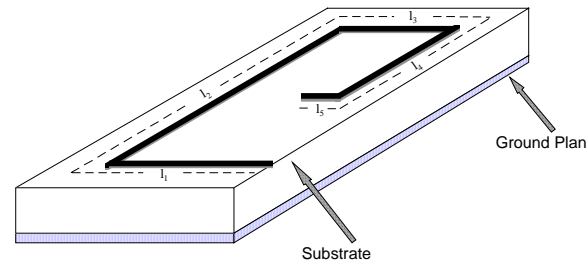


Figure 4.7. Printed Circuit Board Geometry for a Rectangular Loop.

For theoretical purposes, this geometry can be considered as an assembly of five dipoles oriented at ninety degrees. The theoretical far fields from the Maze Trace can also be accurately determined. The lengths  $l_1$ ,  $l_2$ ,  $l_3$ ,  $l_4$  and  $l_5$  in Figure 4.7 were approx. 10, 13, 10, 6, and 5 cms respectively. The simulation frequency for this geometry was also chosen to be 200 MHz. At this frequency the largest length in the Maze Trace is approx. 1/ 11 of the simulation wavelength. Thus the far field condition is satisfied: the length of the dipole is small compared to the radiation wavelength.

## 5. Circular Loop

This geometry possesses curvature with no discontinuities. The PEBB is going to have traces with

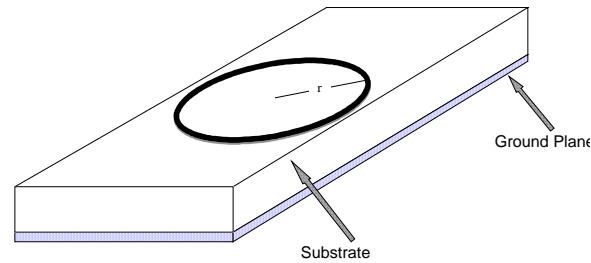


Figure 4.8. Printed Circuit Board Geometry for a Circular Loop.

all types of curvatures. Circle, being one of the simplest curvatures, was chosen as a starting point. The Printed Circuit Board Geometry of the Circular Loop is shown in Figure 4.8. For theoretical purposes, this geometry can be considered as a small circular loop antenna. The theoretical far fields from a small circular loop antenna can be accurately determined. The radius of the circle in Figure 4.8 was approx. 5 cms. For uniformity purposes, the simulation frequency for this geometry was also chosen to be 200 MHz. At this frequency the circumference of the loop is approx. one fifth of the simulation wavelength. Thus, satisfying the far field condition.

#### 6. Curved Trace

This geometry incorporates curvature with straight traces. The PEBB is going to have traces which could be simplified to this situation. The Printed Circuit Board Geometry of the Curved Trace is shown in Figure 4.9. Essentially the Curved Trace consists of three dipoles of lengths  $l_1$ ,

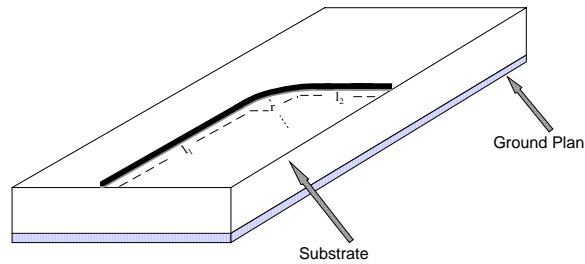


Figure 4.9. Printed Circuit Board Geometry for a Curved Trace.

$l_2$  and a quarter circle. The lengths  $l_1$ , and  $l_2$ , were approx. 6.2 and 3 cms respectively. The radius of the quarter circle in Figure 4.9 was approx. 4.4 cms.. Again, for purposes of uniformity, the simulation frequency for this geometry was also chosen to be 200 MHz. At this frequency all three dipoles satisfy the far field condition.

## B. THEORETICAL MODELS OF THE SIX GEOMETRIES

The complete set of fields for any of the above six geometries are quite complicated. The objective here is to develop theoretical models of the far fields produced by the above six geometries. In the far zone the electric and magnetic field intensities are given by:

$$\mathbf{E} = \mathbf{H} Z_c$$

where

|            |   |  |                                  |
|------------|---|--|----------------------------------|
| <b>E</b>   | = | Electric field Intensity in Volts/meter.                           |                                  |
| <b>H</b>   | = | Magnetic field Intensity in Amps/meter.                            |                                  |
| $Z_c$      | = | $(\mu/\epsilon)^{1/2}$ = Characteristic Impedance of the medium in |                                  |
|            |   | Ohms.  |                                  |
| $\mu$      | = | Permeability in Henries per meter                                  | = $4\pi \cdot 10^{-7}$ H/m.      |
| $\epsilon$ | = | Permittivity in Farads per meter                                   | = $(1/36\pi) \cdot 10^{-9}$ F/m. |
|            |   |  | .....(4.1)                       |

1. Trace with Discontinuity

From the Printed Circuit Board Geometry of Figure 4.4 it can be seen that there are two distinct traces oriented at an angle of  $\alpha$  relative to each other. For radiation purposes, each trace is a radiative element. In effect, for this geometry, we have two distinct Hertzian dipoles oriented at an angle of  $\alpha$  relative to each other, lying in the  $z = 0$  plane. For determining the far fields, consider the two dipoles (traces) lying in x-y plane as shown in Figure 4.10.

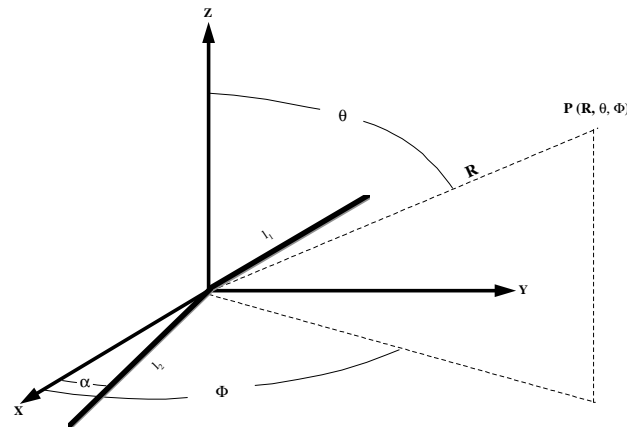


Figure 4.10. Two Dipoles at an angle of  $\alpha$  in the x-y Plane.

The far region electric field resulting from sources with a surface current distribution is given by (Balanis, 1982):

$$\mathbf{E} = -j \omega \mu \frac{e^{-jkR}}{4\pi R} \iint [\mathbf{J}_s - (\mathbf{J}_s \cdot \mathbf{a}_R) \mathbf{a}_R] e^{-jk\rho \cdot \mathbf{a}_R} ds'$$

where

$\mathbf{E}$  = Far region electric field in Volts/meter.

$\mathbf{a}_R$  = Unit vector of the spherical coordinate system  $(r, \theta, \phi)$ .

$\mathbf{a}_\theta$  = Unit vector of the spherical coordinate system  $(r, \theta, \phi)$ .

$\mathbf{a}_\phi$  = Unit vector of the spherical coordinate system  $(r, \theta, \phi)$ .

$\omega = 2 \pi f$  = Angular velocity in radians per second.

- f = Frequency in Hertz.
- $\mu$  = Permeability in Henries per meter =  $4\pi \cdot 10^{-7}$  H/m.
- k =  $2\pi/\lambda$  = Propagation constant.
- $\lambda$  = Wavelength in meters.
- $\mathbf{J}_s$  = Surface current density of the sources in Amps/m<sup>2</sup>.
- s' = Source surface, meters<sup>2</sup>.
- $\rho$  = Distance between source and observation points in meters.

.....(4.2)

Applying this to the geometry of the two dipoles in Figure 4.10 and solving the integral equation we get:

$$\mathbf{E} = -j \omega \mu \frac{I l}{2\pi R} \frac{e^{-jkR}}{R} \text{Cos}(\alpha/2) [\text{Cos}(\theta)\text{Cos}(\phi-\alpha/2) \mathbf{a}_\theta - \text{Sin}(\phi-\alpha/2) \mathbf{a}_\phi]$$

Volts/meter

where

- $\mathbf{E}$  = Far region electric field in Volts/meter.
- I = Current of the dipoles in Amps.
- l =  $l_1 = l_2 =$  Length of each dipole in meters.

.....(4.3)

## 2. Z Trace

From the Printed Circuit Board Geometry of Figure 4.5 it can be seen that there are three distinct traces oriented at 90 degrees to each other. For radiation purposes, each of the three traces are radiative elements. In effect, for this geometry, we have three distinct Hertzian dipoles oriented at 90 degrees relative to each other, and lying in the  $z = 0$  plane. For determining the far fields, consider the three dipoles (traces) lying in x-y plane as shown in Figure 4.11.

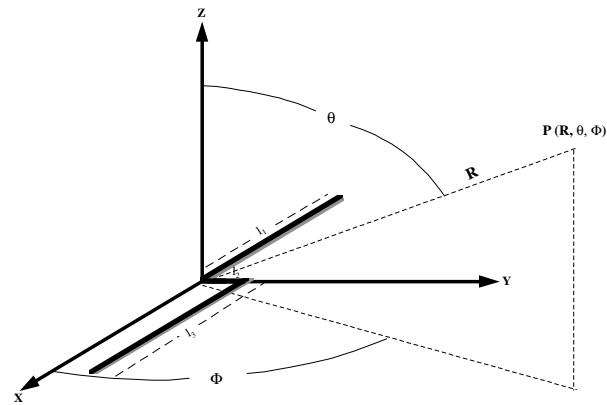


Figure 4.11. Three Dipoles forming a Z Trace in the x-y Plane.

For theoretical purposes, the Z trace is simply an extension of the previous case of traces with discontinuity. Applying Eqn. 4.2 to the three dipoles in Figure 4.11 and solving the integral Eqn. 4.2, we get:

$$\mathbf{E} = -j \omega \mu I \left[ \frac{e^{-jkR}}{4\pi R} l_1 \{ \cos(\theta)\cos(\phi) \mathbf{a}_\theta - \sin(\phi) \mathbf{a}_\phi \} + \right. \\ \left. l_2 \{ \cos(\theta)\sin(\phi) \mathbf{a}_\theta + \cos(\phi) \mathbf{a}_\phi \} + l_3 \{ \cos(\theta)\cos(\phi) \mathbf{a}_\theta - \sin(\phi) \mathbf{a}_\phi \} \right]$$

where

- $\mathbf{E}$  = Far region electric field in Volts/meter.
- $\mathbf{a}_\phi$  = Unit vector of the spherical coordinate system  $(r, \theta, \phi)$ .
- $\mathbf{a}_\theta$  = Unit vector of the spherical coordinate system  $(r, \theta, \phi)$ .
- $\omega$  =  $2 \pi f$  = Angular velocity in radians per second.
- $f$  = Frequency in Hertz.
- $\mu$  = Permeability in Henries per meter =  $4\pi \cdot 10^{-7}$  H/m.
- $k$  =  $2 \pi/\lambda$  = Propagation constant.
- $l_1$  = Length of one dipole of the Z Trace in meters.
- $l_2$  = Length of the second dipole of the Z Trace in meters.

$l_3$  = Length of the third dipole of the Z Trace in meters.

$\lambda$  = Wavelength in meters.

$I$  = Current of the dipoles in Amps.

.....(4.4)

### 3. Rectangular Loop

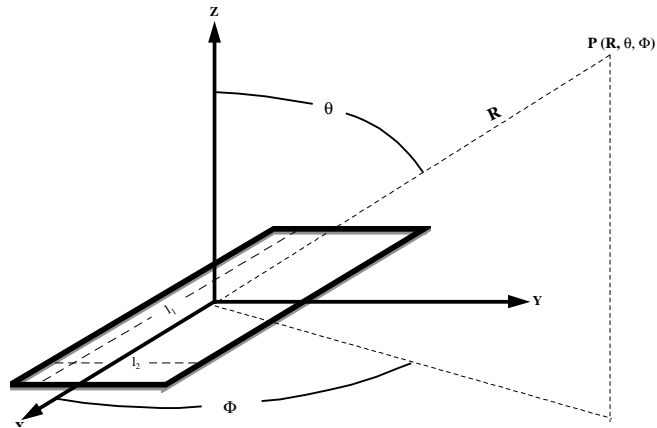


Figure 4.12. Rectangular Loop in the x-y Plane.

From the Printed Circuit Board Geometry for Rectangular Loop in Figure 4.6 it can be seen that the rectangular trace essentially acts as a loop antenna. In effect, we have a rectangular loop lying in the  $z = 0$  plane with its center at the origin as shown in Figure 4.12. Each side of this rectangle will act as a radiative element. Thus, each side of the rectangle can be considered as a Hertzian dipole. The net far fields produced by this rectangle will be the vector sum of the four far fields resulting from each of the four sides of the rectangle. The resultant Electric Field Intensity in the far region will have only the  $\phi$  component and is given by (Paul and Nasar, 1987):

$$\mathbf{E}_\phi = -j \omega \mu k I l_1 \frac{e^{-jkR}}{4\pi R} l_2 \sin(\theta) \mathbf{a}_\phi$$

where

$\mathbf{E}_\phi$  = Far field  $\phi$  component of the electric field in Volts/meter.

$\mathbf{a}_\phi$  = Unit vector of the spherical coordinate system  $(r, \theta, \phi)$ .

$\omega$  =  $2\pi f$  = Angular velocity in radians per second.

$f$  = Frequency in Hertz.

$\mu$  = Permeability in Henries per meter =  $4\pi \cdot 10^{-7}$  H/m.

$k$  =  $2\pi/\lambda$  = Propagation constant.

$\lambda$  = Wavelength in meters.

- I = Current of the loop in Amps.
- $l_1$  = Length of the side of the rectangle in meters.
- $l_2$  = Length of the other side of the rectangle in meters.

.....(4.5)

#### 4. Maze Trace

From the Printed Circuit Board Geometry of Figure 4.7 it can be seen that essentially there are five distinct traces oriented at 90 degrees to each other. For radiation purposes, each of the five traces are radiative elements. In effect, for this geometry, we have five distinct Hertzian dipoles oriented at 90 degrees relative to each other and lying in the  $z = 0$  plane. For determining the far fields, consider the five dipoles (traces) lying in x-y plane as shown in Figure 4.13.

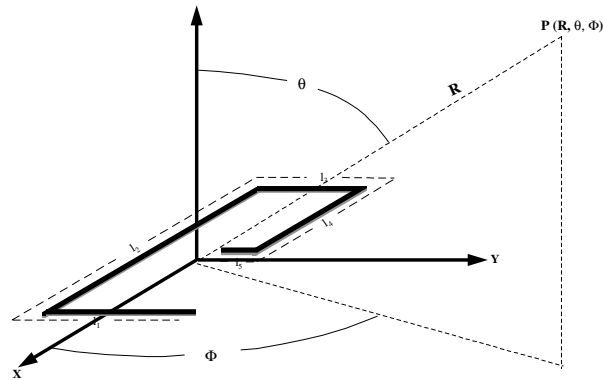


Figure 4.13. Maze Trace in the x-y Plane.

One way to determine the far fields of these five dipoles is by extending the three dipole technique used for the Z trace. Algebraically this would be very demanding and not quite effective. A simpler but effective approach would be to consider the Maze as comprising of two parts: i) a dipole of length  $l_5$ , ii) a rectangle of sides  $l_1 \times l_2$ , but less a dipole of length  $(l_2 - l_4)$ . In effect, the far fields of the Maze would be far fields of dipole  $l_5$ , plus the far fields of the rectangle  $l_1 \times l_2$  and minus the far fields from a fictitious dipole of length  $(l_2 - l_4)$ . For the Maze Trace, the resulting far fields after applying Eqn 4.2 to the two dipoles  $l_5$  and  $(l_2 - l_4)$  in conjunction with the rectangular loop are given by:

$$\begin{aligned}
 \mathbf{E} &= -j \omega \mu k I l_1 l_2 \frac{e^{-jkR}}{4\pi R} \sin(\theta) \mathbf{a}_\phi \\
 &+ \\
 &-j \omega \mu k I l_5 \frac{e^{-jkR}}{4\pi R} \{ \cos(\theta)\sin(\phi) \mathbf{a}_\theta + \cos(\phi) \mathbf{a}_\phi \} \\
 &- \\
 &-j \omega \mu k I (l_2 - l_4) \left\{ \frac{e^{-jkR}}{4\pi R} \cos(\theta)\cos(\phi) \mathbf{a}_\theta - \sin(\phi) \mathbf{a}_\phi \right\}
 \end{aligned}$$

where

$\mathbf{E}$  = Far region electric field in Volts/meter.

$\mathbf{a}_\phi$  = Unit vector of the spherical coordinate system  $(r, \theta, \phi)$ .

- $\mathbf{a}_\theta$  = Unit vector of the spherical coordinate system  $(r, \theta, \phi)$ .
  - $\omega$  =  $2 \pi f$  = Angular velocity in radians per second.
  - $f$  = Frequency in Hertz.
  - $\mu$  = Permeability in Henries per meter =  $4\pi 10^{-7}$  H/m.
  - $k$  =  $2 \pi/\lambda$  = Propagation constant.
  - $l_1$  = Length of one side of the Maze Trace in meters.
  - $l_2$  = Length of second side of the Maze Trace in meters.
  - $l_3$  = Length of the third side of the Maze Trace in meters.
  - $l_4$  = Length of the fourth side of the Maze Trace in meters.
  - $l_5$  = Length of the fifth side of the Maze Trace in meters.
  - $\lambda$  = Wavelength in meters.
  - $I$  = Current of the dipoles in Amps.
- .....(4.6)

## 5. Circular Loop

From the Printed Circuit Board Geometry for the Circular Loop in Figure 4.8 it can be seen that the circular trace also acts as a loop antenna. In effect, we have a circular loop lying in the  $z = 0$  plane with its center at the origin as shown in Figure 4.14. A circular loop of radius "r" and carrying a current I constitutes a magnetic dipole of moment  $(I \pi r^2)$ . The far field from a magnetic dipole

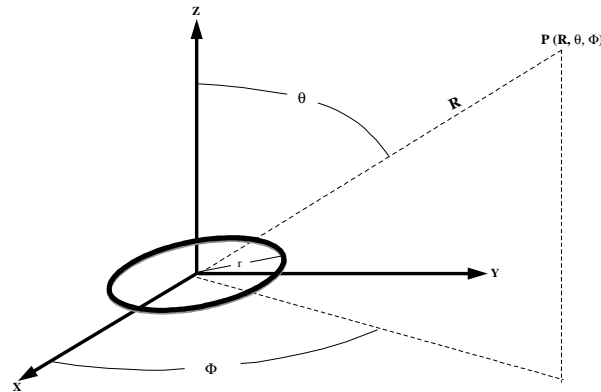


Figure 4.14. Circular Loop in the x-y Plane.

can be easily determined by using Reciprocity Theorem. This magnetic dipole is in effect the dual of the Hertzian dipoles used in the earlier cases. Like the rectangular loop, the Electric Field Intensity in the far region for the circular loop will have only the  $\phi$  component and is given by (Paul, 1992):

$$\mathbf{E}_\phi = -j \omega \mu k (I \pi r^2) \frac{e^{-jkR}}{4\pi R} \sin(\theta) \mathbf{a}_\phi$$

where

$\mathbf{E}_\phi$  = Far field  $\phi$  component of the electric field in Volts/meter.

$\mathbf{a}_\phi$  = Unit vector of the spherical coordinate system (r,  $\theta$ ,  $\phi$ ).

$\omega$  =  $2 \pi f$  = Angular velocity in radians per second.

f = Frequency in Hertz.

$\mu$  = Permeability in Henries per meter =  $4\pi \cdot 10^{-7}$  H/m.

k =  $2 \pi / \lambda$  = Propagation constant.

$\lambda$  = Wavelength in meters.

I = Current of the loop in Amps.

r = Radius of the circular loop in meters.

$(I \pi r^2)$  = Magnetic dipole moment of the circular loop.

.....(4.7)

## 6. Curved Trace

From the Printed Circuit Board Geometry of Figure 4.9 it can be seen that essentially there are three distinct traces. For radiation purposes, each of the three traces are radiative elements. In effect, for this geometry, we now have three distinct Hertzian dipoles lying in the  $z = 0$  plane. For determining the far fields, consider the three dipoles (traces) lying in  $x$ - $y$  plane as shown in Figure 4.15. For theoretical purposes, the Curved trace is also an extension of the previous cases. Applying Eqn. 4.2 to the three dipoles in Figure 4.15 and solving the integral Eqn. 4.2, we get:

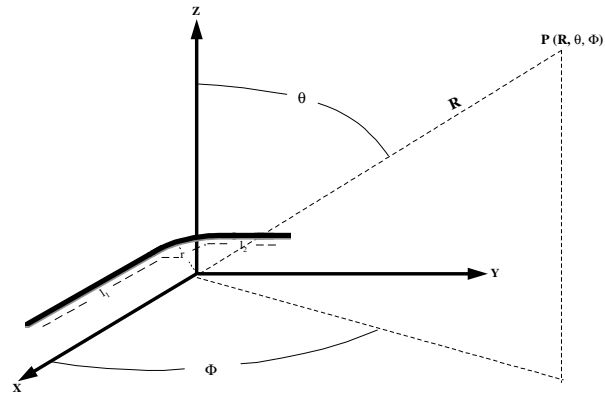


Figure 4.15. Curved Trace in the x-y Plane.

$$\mathbf{E} = -j \omega \mu I \left[ \frac{e^{-jkR}}{4\pi R} (l_1 + l_2) \cos(\pi/4) \{ \cos(\theta) \cos(\phi - \pi/4) \mathbf{a}_\theta - \sin(\phi - \pi/4) \mathbf{a}_\phi \} + \{ (\pi r/2) \sin(\theta) \mathbf{a}_\phi \} \right]$$

where

$\mathbf{E}_\phi$  = Far field  $\phi$  component of the electric field in Volts/meter.

$\mathbf{a}_\phi$  = Unit vector of the spherical coordinate system (r,  $\theta$ ,  $\phi$ ).

$\omega$  =  $2\pi f$  = Angular velocity in radians per second.

f = Frequency in Hertz.

$\mu$  = Permeability in Henries per meter =  $4\pi \cdot 10^{-7}$  H/m.

k =  $2\pi/\lambda$  = Propagation constant.

$\lambda$  = Wavelength in meters.

I = Current of the loop in Amps.

$l_1$  = Length of the side of the rectangle in meters.

$l_2$  = Length of the other side of the rectangle in meters.

r = Radius of the quarter circle in meters.

### C. COMPUTER SIMULATIONS

Computer simulation of an object using the commercial software packages require several basic steps which have to be followed in a structured format. The basic steps are: 1) Drawing the geometric model of the simulation object, 2) Assigning material properties to the simulation object, 3) Defining the boundary conditions of the object, 4) Setting up solution criteria of the simulation, 5) Solving for the fields, 6) Post Processing to view and analyze the results.

#### 1) Drawing the geometric model.

This step allows the creation of a 3D geometric model of the simulation object. In this step there are software commands to create just about any type of a 3D object. After the object is created, it can be viewed from different positions.

#### 2) Assigning material properties.

In this step material attributes, such as permeability and permittivity, are assigned to the different parts of the simulation object. The software packages have a database of the attributes of commonly used materials. However, the databases can be expanded to incorporate new materials.

#### 3) Defining the boundary conditions.

In this step the surfaces of the simulation object are assigned an appropriate boundary condition. Different boundary types, like perfect E or perfect H or radiation surface, are assigned to the different surfaces of the simulation object in this step.

#### 4) Setting up solution criteria.

In this step the starting mesh, the frequency range of the simulation and the stopping criteria are assigned. The starting mesh could be either adaptive or specified by the user. The adaptive mesh is an optimal starting mesh generated by the package for the stimulation object.

#### 5) Solving for the fields.

This step initiates the solution of the fields of the simulation object. The solution continues until the stopping criteria specified in the earlier step are fulfilled. One of the stopping criterion is the number of passes that are made on the mesh of the object. Usually, the more passes are specified the more accurate the solution tends to be. However, more passes mean more numerical computations. This in turn requires more computational time and more memory capacity of the computer. Typically, three passes produce a reasonably accurate solution. The majority of the simulations for this study took as much as 50 hours per simulation. Some took as much as 120 hours.

6) Post Processing to view and analyze the results.

This step displays the manner in which the solution converged. The solution convergence indicates the accuracy of the results of the simulation. In addition, this step processes the solution results to display the desired fields or other pertinent parameter.

The following simulations were done for the six geometries:

1. Traces with Discontinuities and the Z Trace were simulated at 750 MHz. For Traces with Discontinuities a simulation was done for each of the six angles ( $\alpha$ s). The six angles were: 0, 30, 60, 90, 120 and 150 degrees. One simulation was done for the Z Trace.
2. The Rectangular Loop, the Maze Trace, the Circular Loop and the Curved Trace were simulated at 200 MHz.

#### D. THEORETICAL AND COMPUTER SIMULATION RESULTS

1. Results for Traces with Discontinuity.

All theoretical computations and computer simulations of this geometry were done at 750 MHz. The far fields were computed by using the model developed in Eqn. 4.3. Computer simulations were done for both the near and the far fields. The entire set of near and far field computer simulations in conjunction with theoretical computations were performed for each of the six alphas ( $\alpha = 0, 30, 60, 90, 120, \text{ and } 150$ ). The results for this geometry are shown in Figures 4.16 through 4.23.

2. Results for Z Trace.

All theoretical computations and computer simulations of this geometry were also done at 750 MHz. The far fields were computed by using the model developed in Eqn. 4.4. Computer simulations were done for both the near and the far fields. The results for this geometry are shown in Figures 4.24 and 4.25.

| Type of Trace         | Simulated Near Fields 750 MHz | Simulated Far Fields, 750 MHz | Simulated & Theoretical Fields, 750 MHz |
|-----------------------|-------------------------------|-------------------------------|---|
| Discon $\alpha = 0$   | Figure 4.16                   | Figure 4.17                   | Figure 4.18                             |
| Discon $\alpha = 30$  | Figure 4.16                   | Figure 4.17                   | Figure 4.19                             |
| Discon $\alpha = 60$  | Figure 4.16                   | Figure 4.17                   | Figure 4.20                             |
| Discon $\alpha = 90$  | Figure 4.16                   | Figure 4.17                   | Figure 4.21                             |
| Discon $\alpha = 120$ | Figure 4.16                   | Figure 4.17                   | Figure 4.22                             |
| Discon $\alpha = 150$ | Figure 4.16                   | Figure 4.17                   | Figure 4.23                             |
| Z                     | Figure 4.24                   | Figure 4.25                   | Figure 4.25                             |

Table 4.1. Theoretical and Simulated Results at 750 MHz.

Table 4.1 summarizes the different results with their corresponding figures for the above two geometries at 750 MHz.

### 3. Results for Rectangular Loop, Maze Trace, Circular Loop and Curved Trace. .

All theoretical computations and computer simulations of these four geometries were done at 200 MHz. The far fields were computed by using the respective models developed in Eqns. 4.5 through 4.8. Computer simulations were done for both the near and the far fields. The

results for these geometries are shown in Figures 4.26 through 4.33. Table 4.2 summarizes the different results with their corresponding figures for the four geometries at 200 MHz.

| Type of Trace    | Simulated Near Fields, 200 MHz | Simulated and Theoretical Far Fields, 200 MHz |
|------------------|--------------------------------|---|
| Rectangular Loop | Figure 4.26                    | Figure 4.27                                   |
| Maze Trace       | Figure 4.28                    | Figure 4.29                                   |
| Circular Loop    | Figure 4.30                    | Figure 4.31                                   |
| Curved Trace     | Figure 4.32                    | Figure 4.33                                   |

Table 4.2. Theoretical and Simulated Results at 200 MHz.

#### 4. Results of Frequency Sweeps for all six geometries.

The computer drawings of the six geometries developed for earlier simulations were then used to conduct a simulation of frequency sweeps. A Frequency Sweep ranging from 150 MHz to 900 MHz was simulated for Z Trace and Traces with Discontinuities. From these simulations, the electric fields were determined at  $R = 5$  cms, 10 cms, 5 meters, and 10 meters.  $R$  is shown in Figure 4.10. The frequency sweeps were conducted for the six alphas, ( $\alpha = 0, 30, 60, 90, 120, \text{ and } 150$ ). The results of these frequency sweeps are shown in Figures 4.34 through 4.37.

A Frequency Sweep ranging from 50 MHz to 300 MHz was simulated for Circular Loop and Curved Trace. From these simulations, the electric fields were again determined at  $R = 5$  cms, 10 cms, 5 meters, and 10 meters.  $R$  is shown in Figures 4.11 through 4.15 respectively. The results for these frequency sweeps are shown in Figures 4.38 through 4.41. Table 4.3 summarizes the different results with their corresponding figures for all six geometries. The simulations for the Rectangular Loop and the Maze Trace are currently in progress.

| Type of Trace               | Simulated Freq. Sweep at 5 cms. | Simulated Freq. Sweep at 10 cms. | Simulated Freq. Sweep at 5 M. | Simulated Freq. Sweep at 10 M. |
|-----------------------------|---------------------------------|----------------------------------|-------------------------------|--------------------------------|
| Traces with Discontinuities | Figure 4.34                     | Figure 4.35                      | Figure 4.36                   | Figure 4.37                    |
| Z Trace                     | Figure 4.34                     | Figure 4.35                      | Figure 4.36                   | Figure 4.37                    |
| Circular Loop               | Figure 4.38                     | Figure 4.39                      | Figure 4.40                   | Figure 4.41                    |
| Curved Trace                | Figure 4.38                     | Figure 4.39                      | Figure 4.40                   | Figure 4.41                    |

Table 4.3. Simulated Results of Frequency Sweeps at 5 cms, 10 cms, 5 M and 10 M.

## E. DISCUSSION AND CONCLUSIONS OF THE RESULTS

### 1. The agreement between theoretically computed and computer simulated far fields.

From Figures 4.18 through 4.23 it can be seen that theoretical and simulated results for the Traces with a Discontinuity are in close agreement with each other. From Figures 4.25, 4.27, 4.29, 4.31 and 4.33 it can be seen that theoretical and simulated results for Z Trace,

Rectangular Loop, Maze Trace, Circular Loop and Curved Trace are also in close agreement with each other. The by product of these agreements was the development of confidence in the usage of the commercial packages.

## 2. Extending the simulations to near fields.

Figure 4.16 shows the extension of the simulations to the near fields for the Traces with a Discontinuity. Figures 4.24, 4.26, 4.28, 4.30 and 4.32 show the extension of the simulations to the near fields for Z Trace, Rectangular Loop, Maze Trace, Circular Loop and Curved Trace respectively. There is no efficient way to theoretically determine the near fields for the six geometries and cross-check them with the near fields obtained by the simulations.

## 3. Extending the simulations to Frequency Sweeps.

Figures 4.34 through 4.41 show the extension of the simulations to scanning the six geometries over a frequency range and simulating the fields at the four specified points in space (5cms, 10 cms, 5 Meters, and 10 Meters). For a given geometry, these four points could be either in the far zone or the near zone depending on the frequency. In effect, the Frequency Sweep figures provide near zone and far zone fields at the four specified points in space.

## 4. Acquiring confidence in the near field simulations and Frequency Sweeps.

To acquire confidence in the Frequency Sweeps a cross-check was made with the far fields obtained by the Frequency Sweeps in Figures 4.34 through 4.41 and the far fields obtained from the figures in #1 above. For all six geometries, the cross-checks established a close agreement in the far fields obtained either from the Frequency Sweep figures or the far field figures in #1 above. This built confidence in the Frequency Sweep figures in #3 above. The same process was repeated by cross checking the near field values obtained by the Frequency Sweeps with the values from the near field figures in #2 above. For all six geometries, the cross-checks established a close agreement in the near fields obtained either from the Frequency Sweep figures in item #3 above or the near field figures in item #2 above. This established confidence in the near fields obtained by simulations in item #2 above.

## 5. The fields from a straight trace are higher than the fields from a trace with a discontinuity.

From Figures 4.16 and 4.17 it can be seen that at any given point in space, the near fields and the far fields from the straight trace are the highest. Both, the near fields and the far fields reduce as  $\alpha$  increases. Near fields and far fields from the trace with a discontinuity of 150

degrees are the lowest. The conclusion is that a straight trace is an efficient radiator. As the trace discontinuity angle ( $\alpha$ ) increases the trace becomes less efficient radiator. This conclusion is reinforced by recognizing that the net radiative current in a trace with a discontinuity is less than the radiative current in a straight trace. Thus, to minimize Radiated EMI discontinuities need to be incorporated in a trace.

#### 6. Dependence of Radiated EMI on the length of a trace.

For Traces with Discontinuity, Z Trace, Maze Trace and Curved Trace.

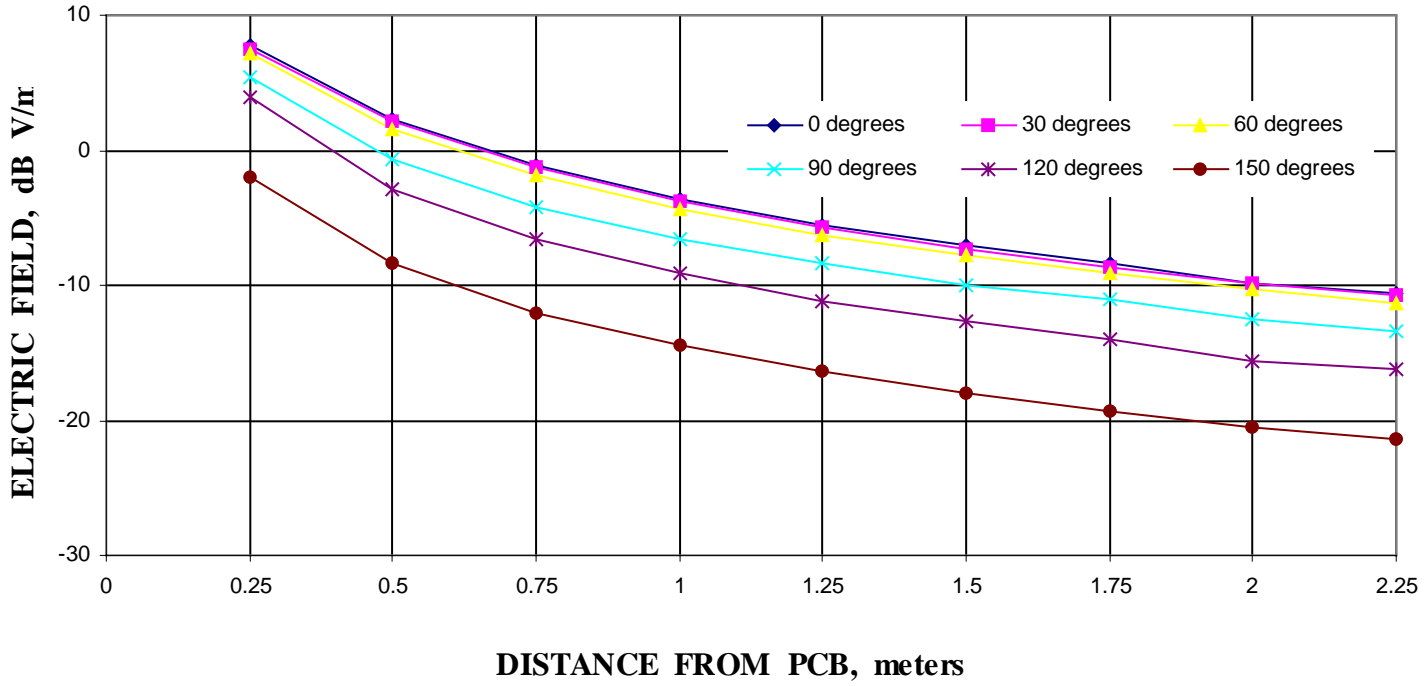
Only one model for each of these geometries was simulated. Consequently, the simulations give results for only one set of lengths for each trace. However, the simulations for each of these geometries are accurate and reflect the respective theoretical models in Eqns. 4.1 through 4.8. Examining these equations it can be seen that the radiated fields are directly proportional to the length of the respective trace. The conclusion is that to minimize the Radiated EMI the lengths of these traces need to be minimized.

#### 7. Dependence of Radiated EMI on the area of a loop.

For Rectangular and Circular Loops.

For both geometries only one model was simulated. Consequently, the simulations give results for only one rectangle and one circle. However, the simulations for each of these geometries are accurate and reflect the respective theoretical models in Eqns. 4.5 and 4.7 respectively. By examining these equations it can be seen that the radiated fields are directly proportional to the area of the respective loop. The conclusion is that to minimize the Radiated EMI the area of these loops need to be minimized.

**SIMULATED NEAR FIELDS AT 750 MHz  
TRACE WITH A DISCONTINUITY**



**SIMULATED FAR FIELDS AT 750 MHz  
TRACE WITH A DISCONTINUITY**

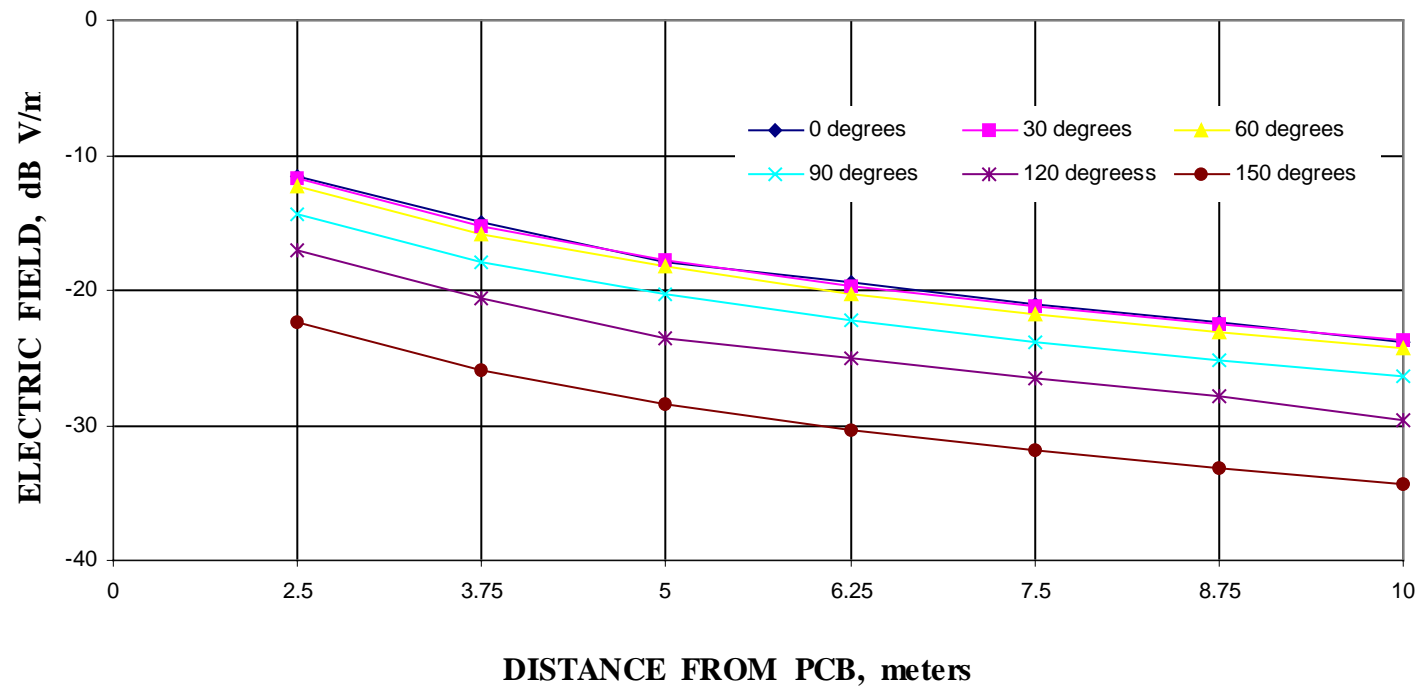


Figure 4.16. Simulated Near Fields at 750 MHz for Traces with Discontinuities.

**SIMULATED AND THEORETICAL FAR FIELDS AT 750 MHz  
TRACE WITH A DISCONTINUITY OF 0 DEGREES**

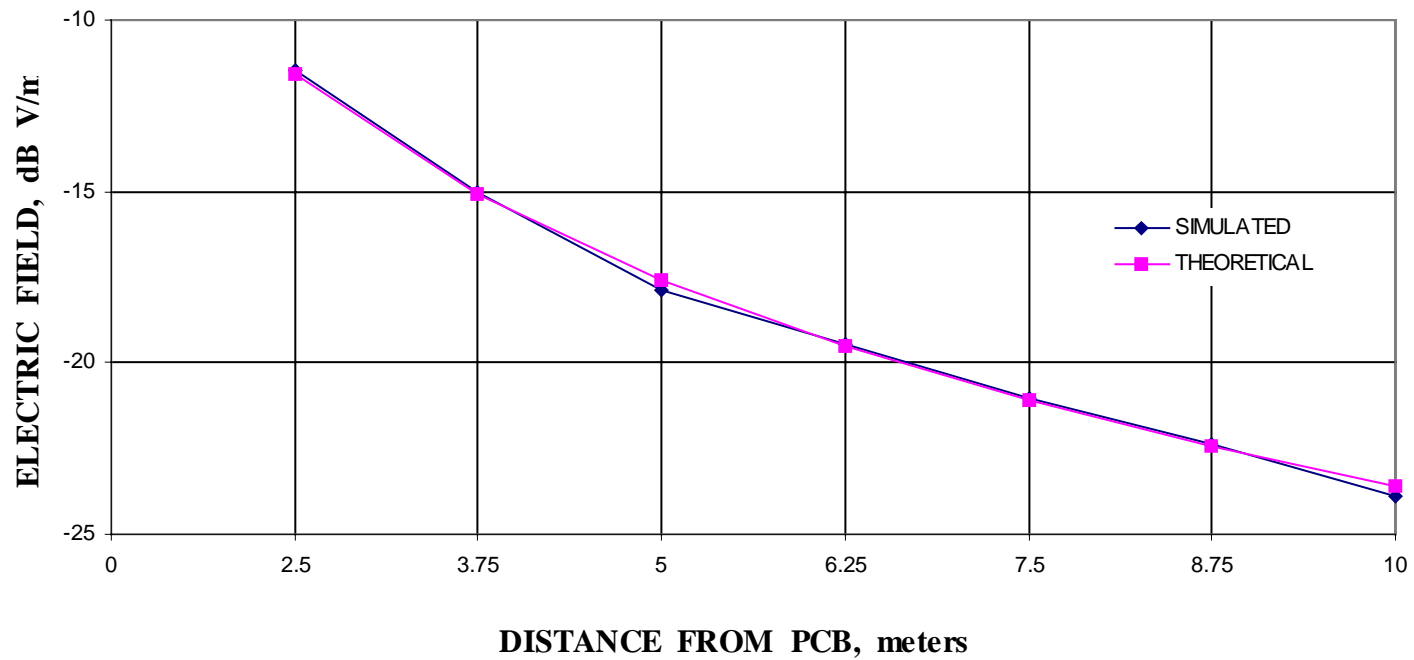


Figure 4.17. Simulated Far Fields at 750 MHz for Traces with Discontinuities.

Figure 4.18. Simulated and Theoretical Far Fields at 750 MHz for Trace with Discontinuity of 0 Degrees.

Figure 4.19 Simulated and Theoretical Far Fields at 750 MHz for Trace with Discontinuity of 30 Degrees.

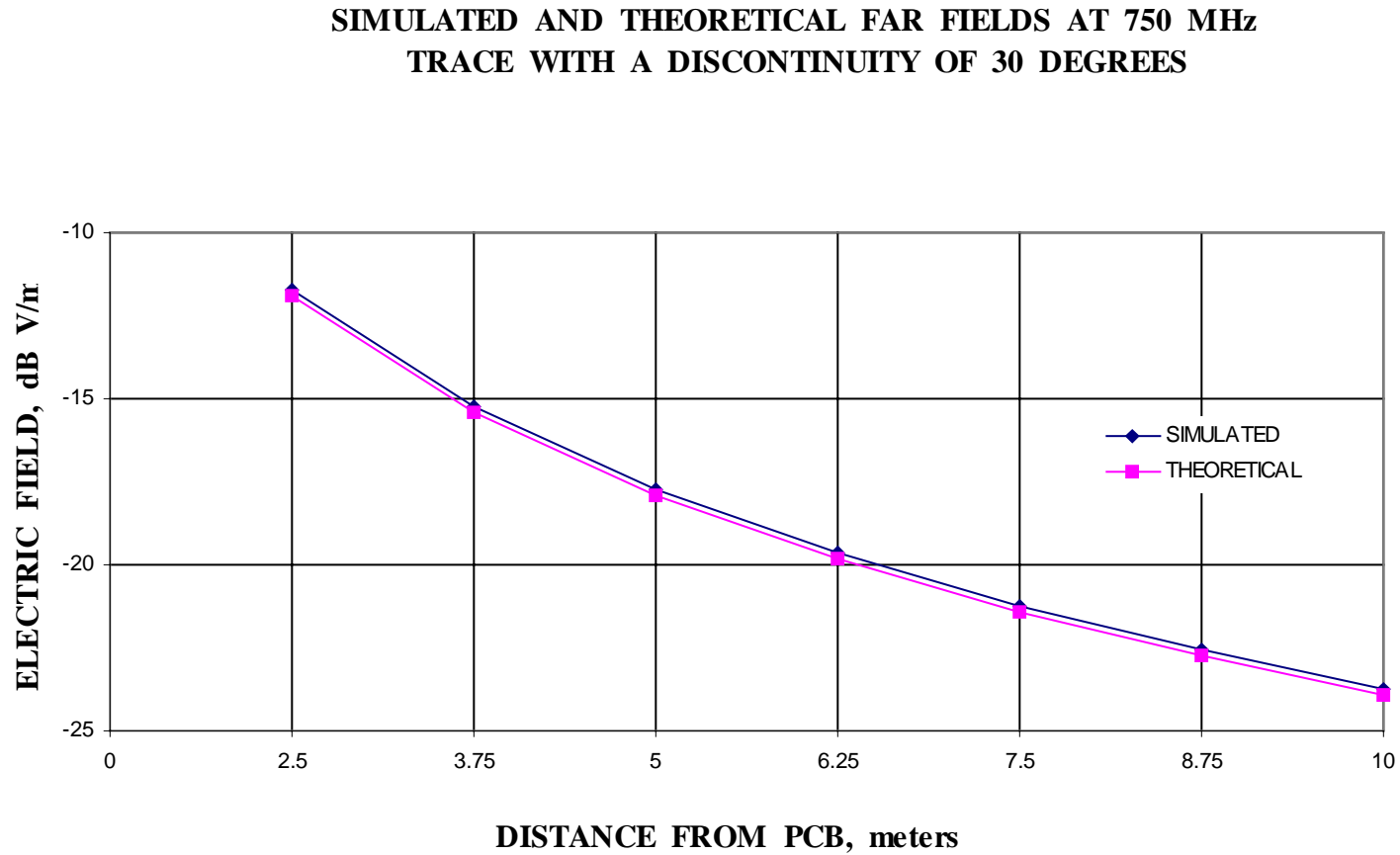


Figure 4.20. Simulated and Theoretical Far Fields at 750 MHz for Trace with Discontinuity of 60 Degrees.

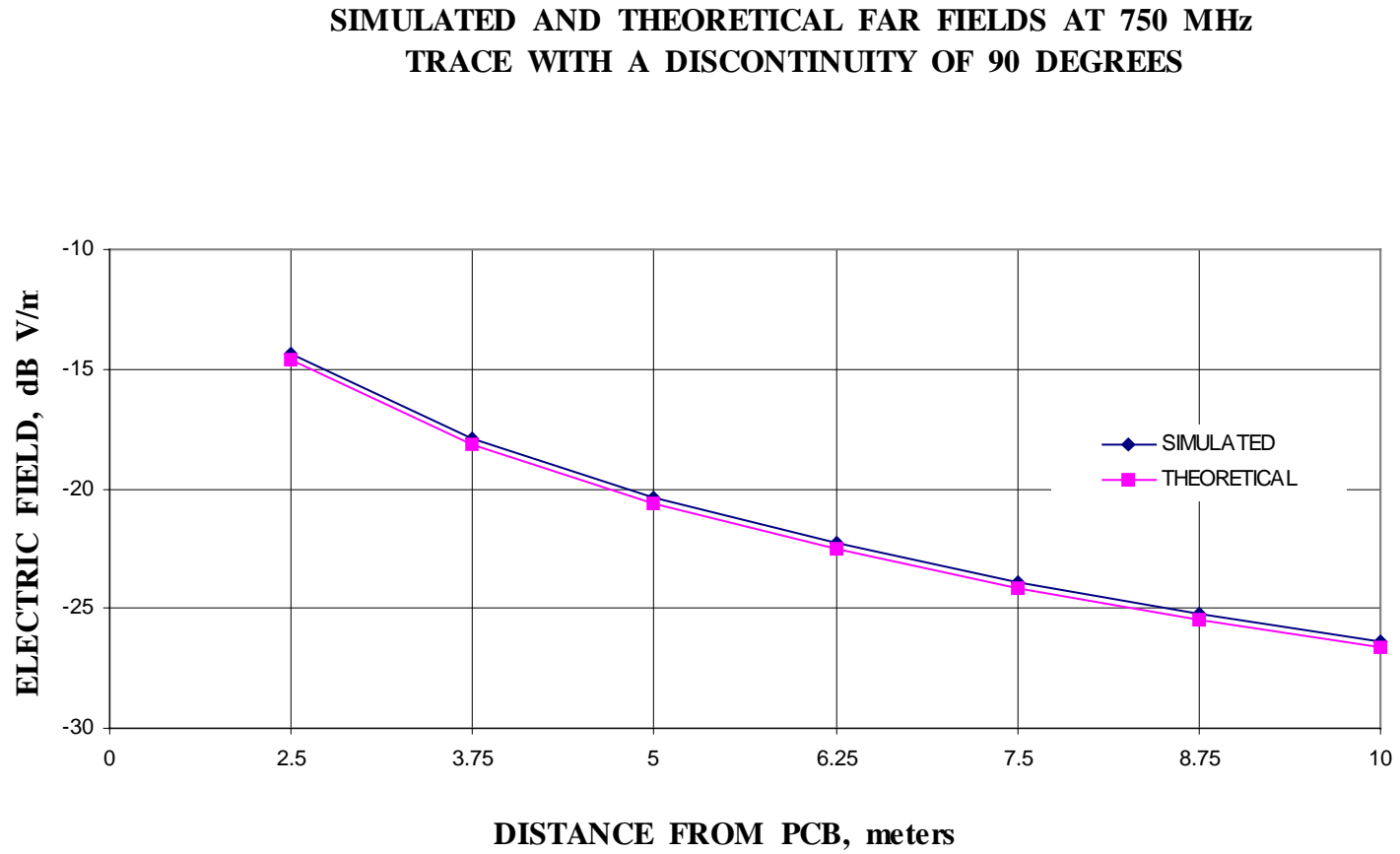


Figure 4.21. Simulated and Theoretical Far Fields at 750 MHz for Trace with Discontinuity of 90 Degrees.

Figure 4.22. Simulated and Theoretical Far Fields at 750 MHz for Trace with Discontinuity of 120 Degrees.

**SIMULATED AND THEORETICAL FAR FIELDS AT 750 MHz  
TRACE WITH A DISCONTINUITY OF 150 DEGREES**

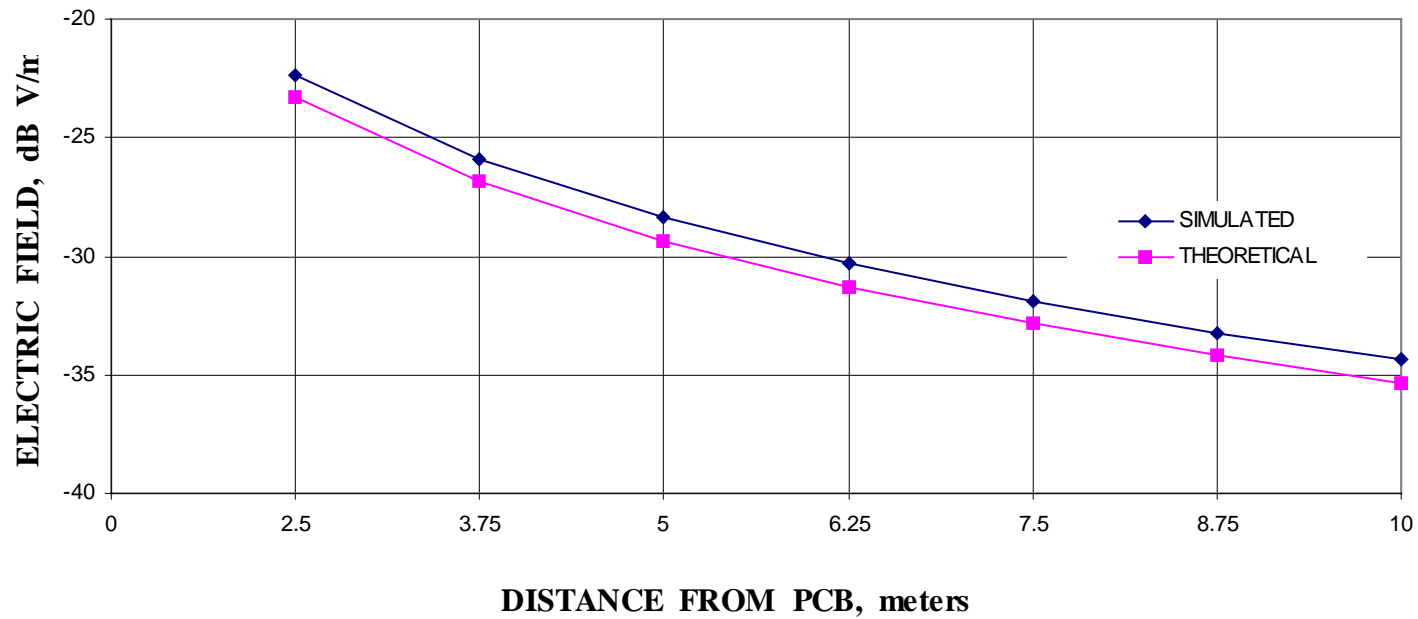


Figure 4.23. Simulated and Theoretical Far Fields at 750 MHz for Trace with Discontinuity of 150 Degrees.

**SIMULATED NEAR FIELDS AT 750 MHz  
Z TRACE**

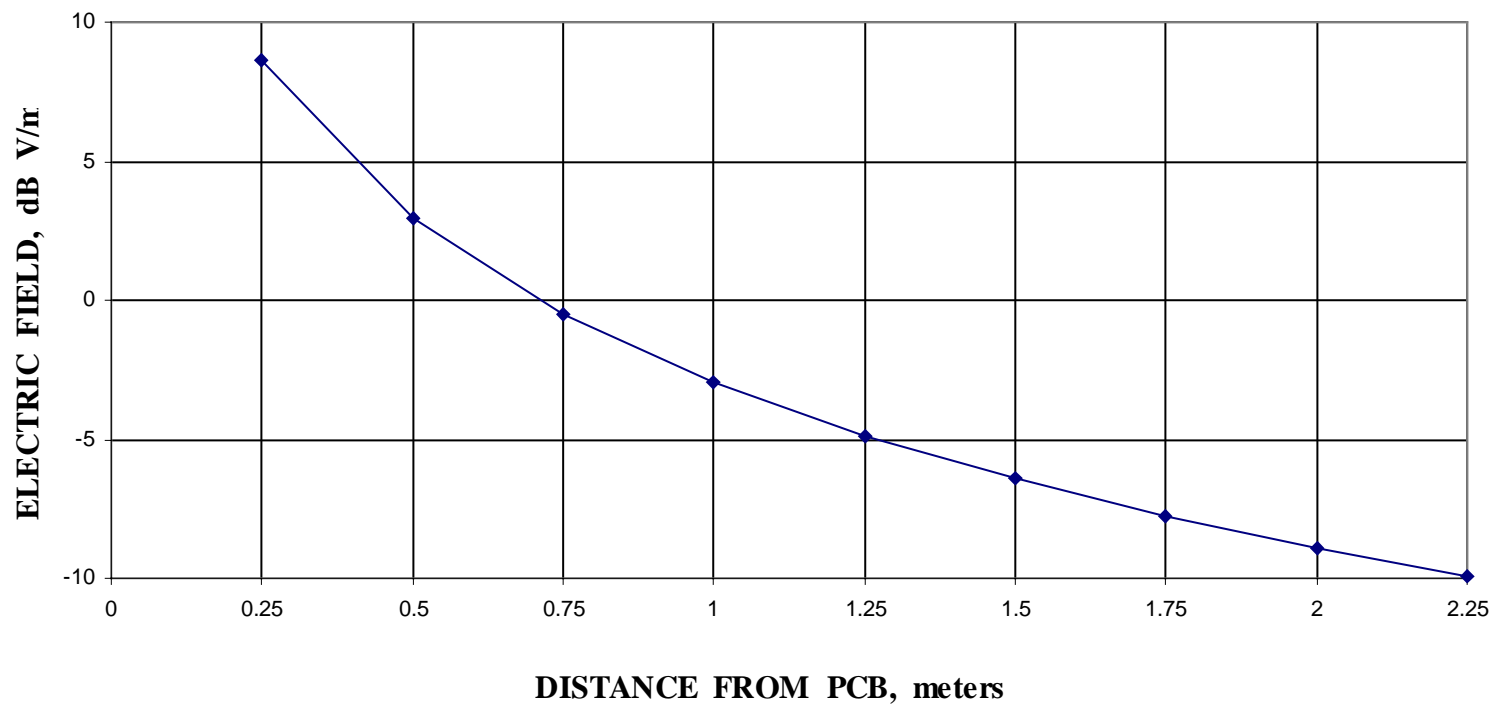


Figure 4.24. Simulated Near Fields at 750 MHz for the Z Trace.

**SIMULATED AND THEORETICAL FAR FIELDS AT 750 MHz  
Z TRACE**

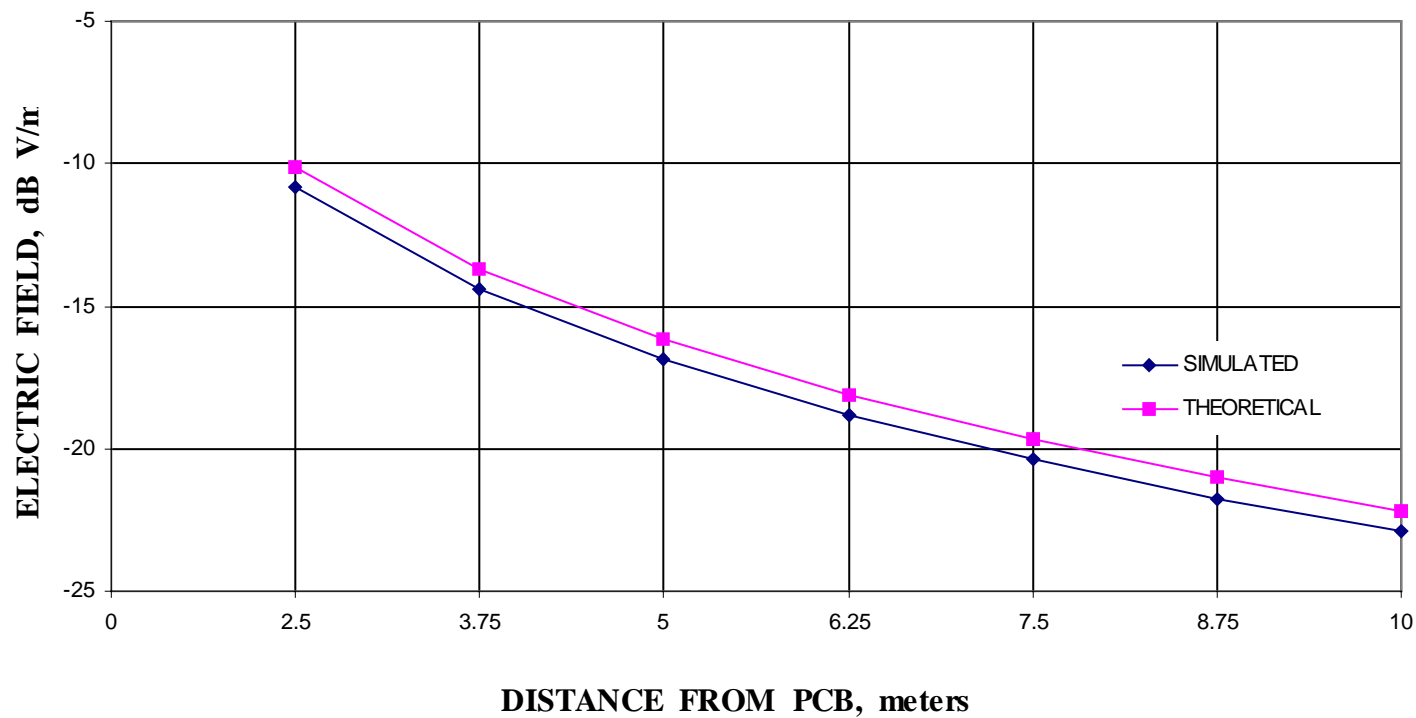
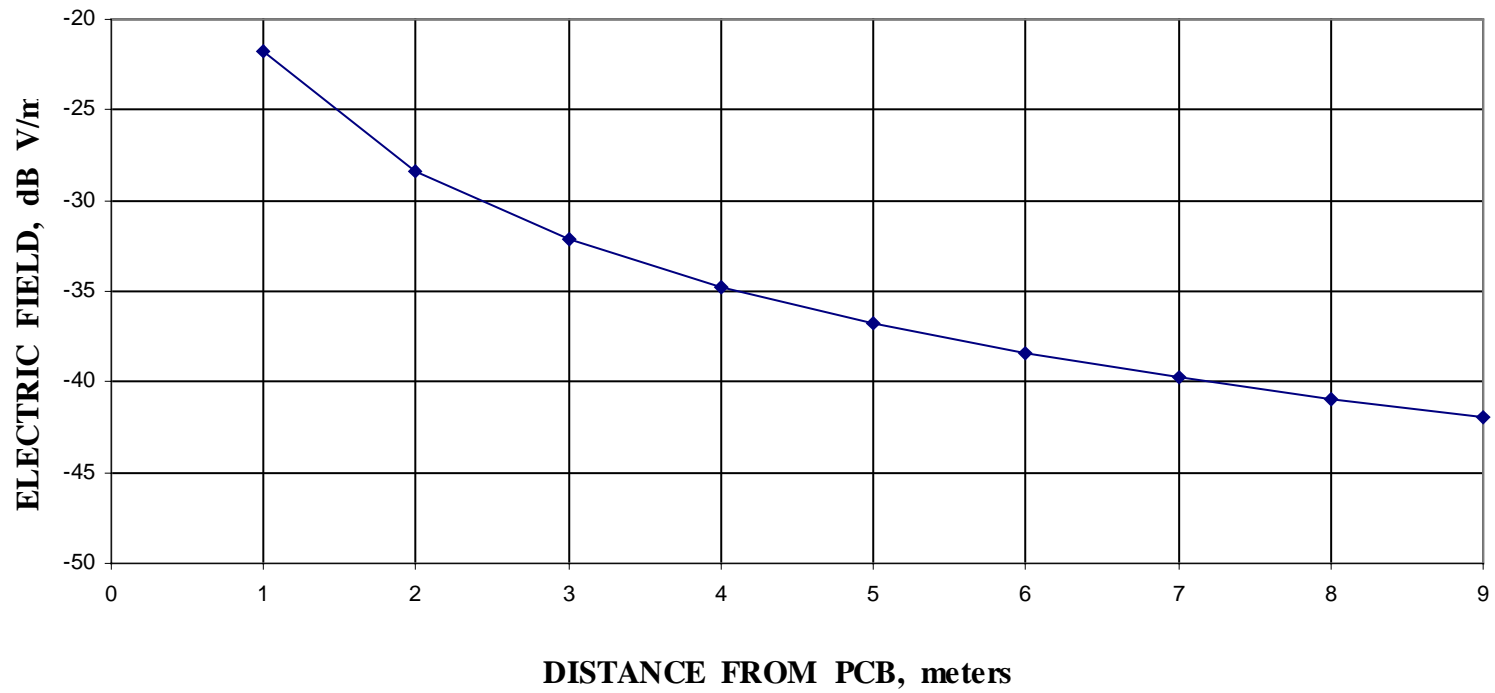


Figure 4.25. Simulated and Theoretical Far Fields at 750 MHz for the Z Trace.

**SIMULATED NEAR FIELDS AT 200 MHz  
RECTANGULAR LOOP**



. Figure 4.26. Simulated Near Fields at 200 MHz for Rectangular Loop

**SIMULATED AND THEORETICAL FAR FIELDS AT 200 MHz  
RECTANGULAR LOOP**

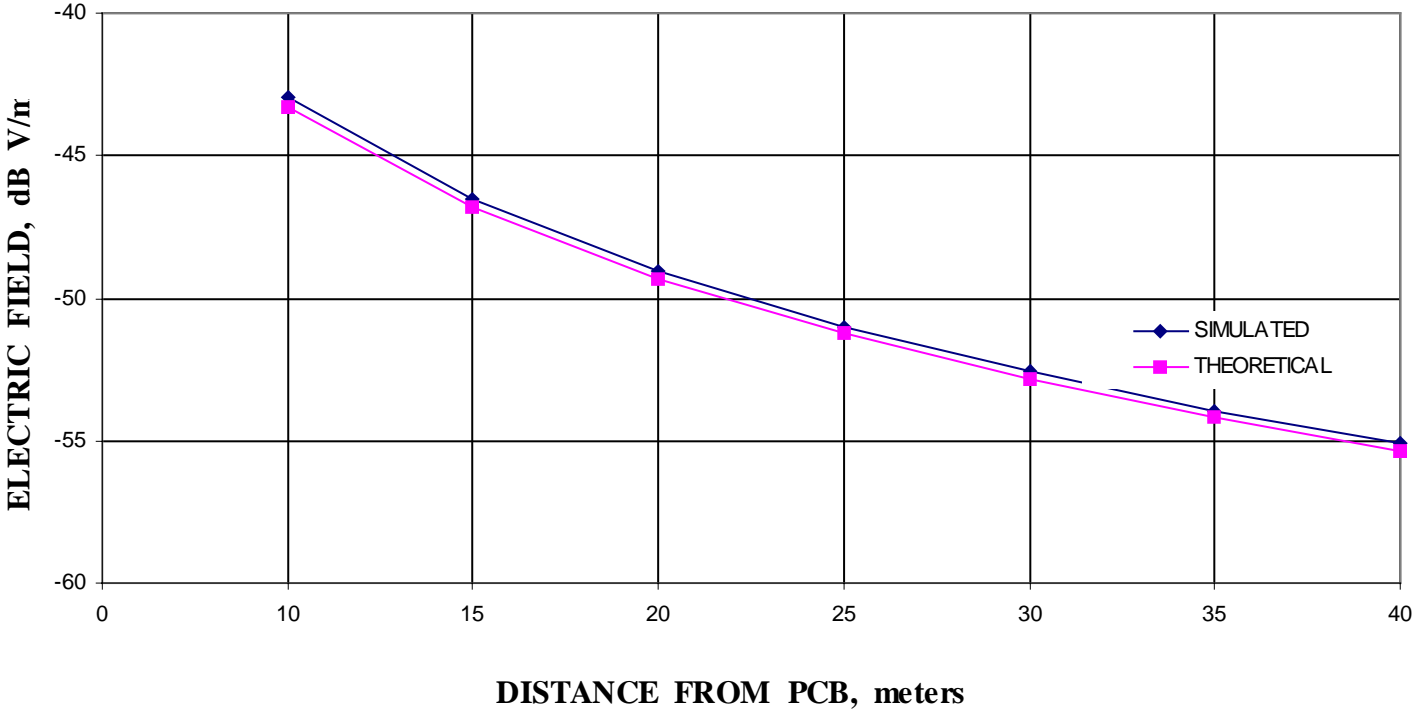


Figure 4.27. Simulated and Theoretical Far Fields at 200 MHz for Rectangular Loop.

**SIMULATED NEAR FIELDS AT 200 MHz  
MAZE TRACE**

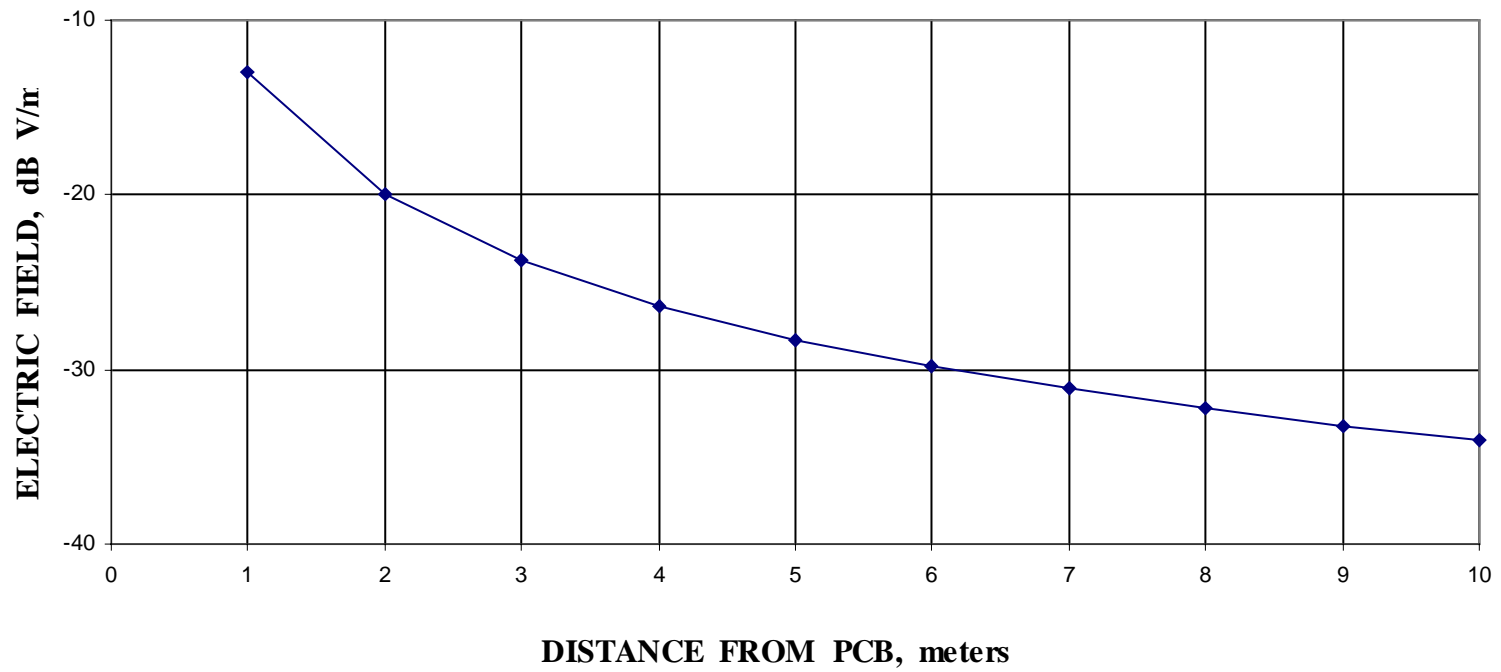


Figure 4.28. Simulated Near Fields at 200 MHz for Maze Trace.

**SIMULATED AND THEORETICAL FAR FIELDS AT 200 MHz  
MAZE TRACE**

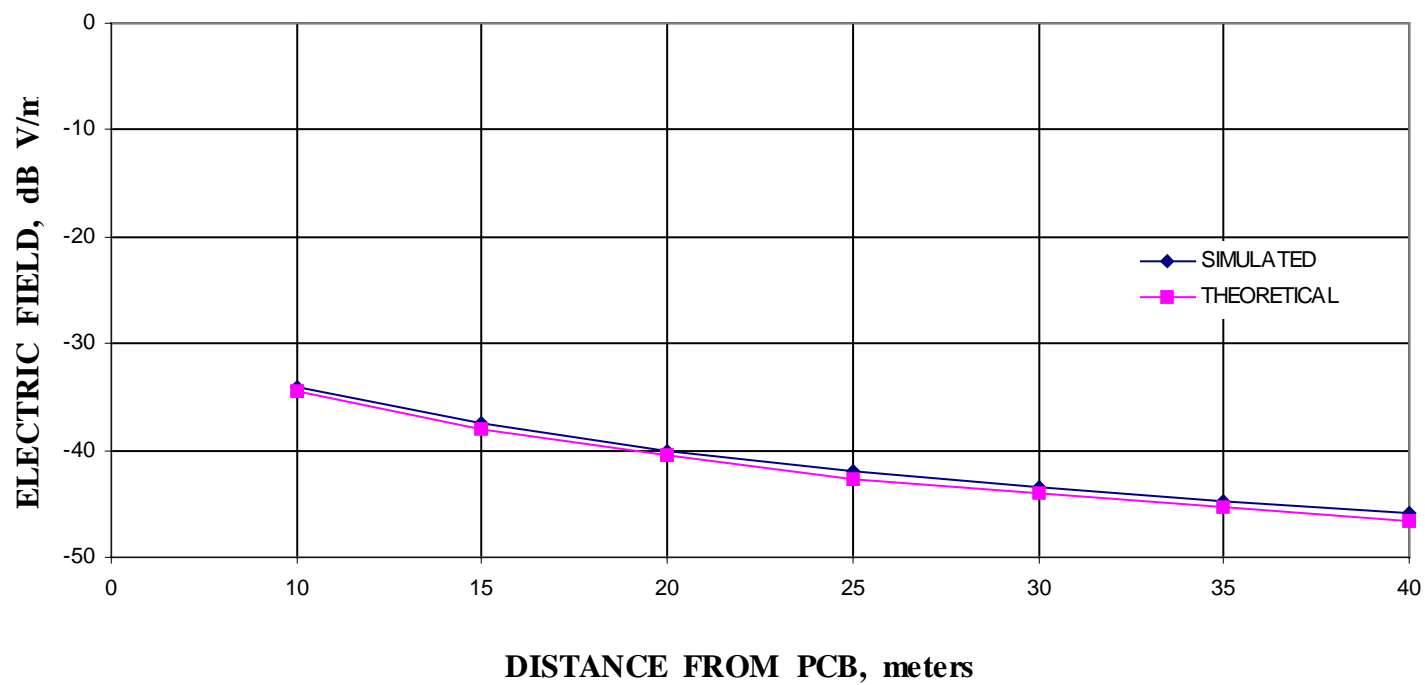


Figure 4.29. Simulated and Theoretical Far Fields at 200 for Maze Trace.

**SIMULATED NEAR FIELDS AT 200 MHz  
CIRCULAR TRACE**

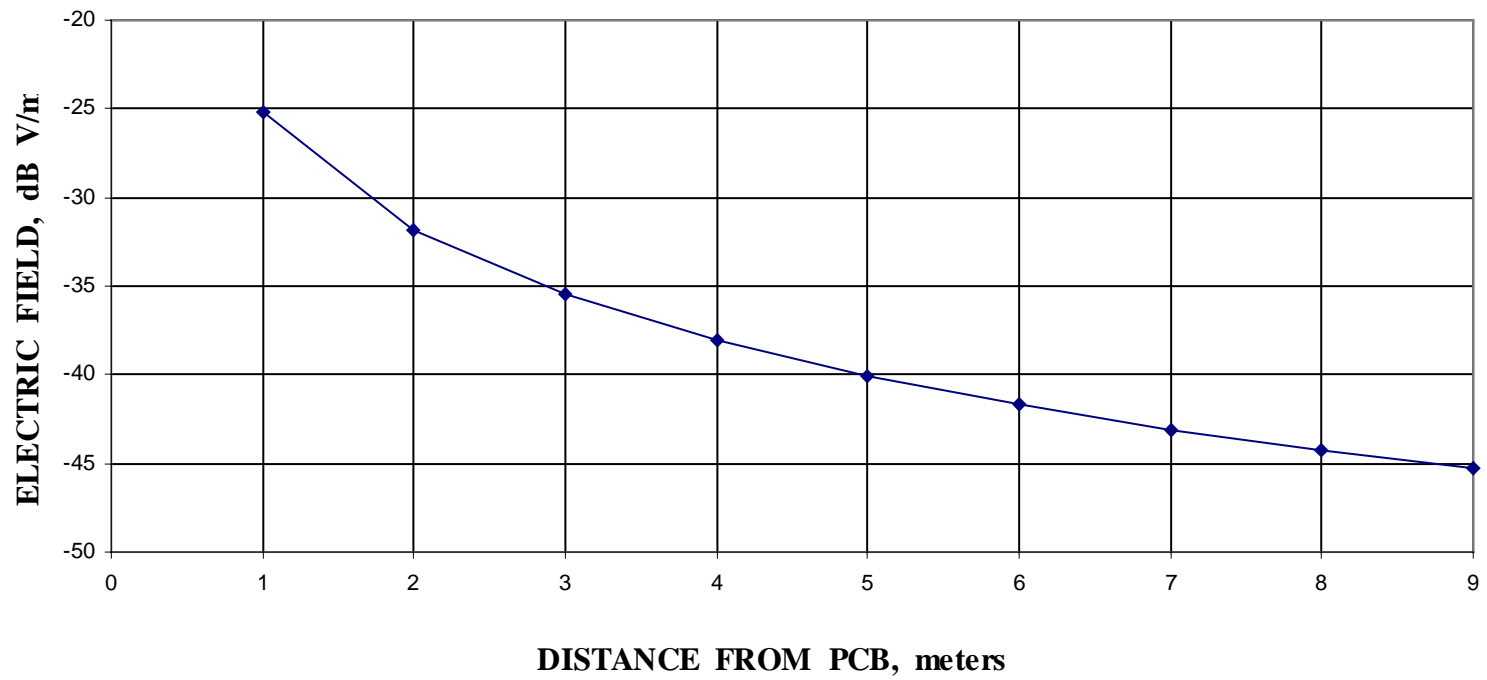


Figure 4.30. Simulated Near Fields at 200 MHz for Circular Loop.

**SIMULATED AND THEORETICAL FAR FIELDS AT 200 MHz  
CIRCULAR TRACE**

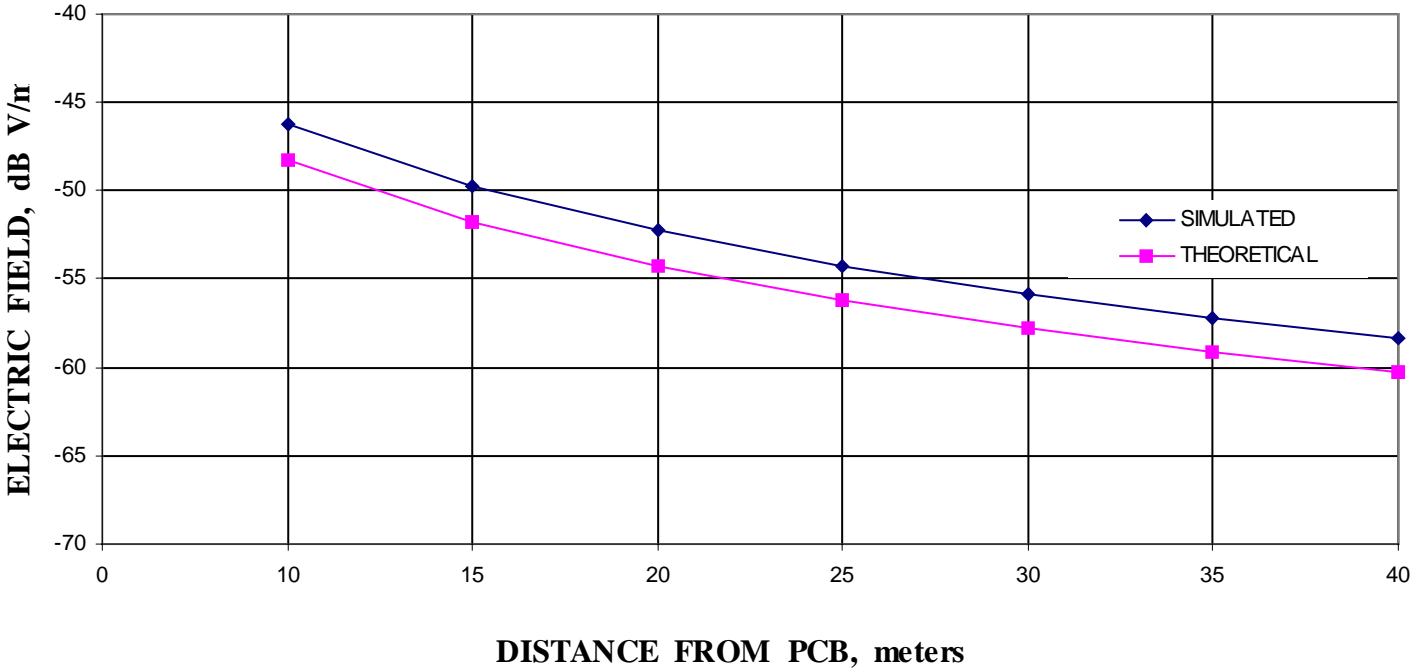


Figure 4.31. Simulated and Theoretical Far Fields at 200 MHz for Circular Loop.

**SIMULATED NEAR FIELDS AT 200 MHz  
CURVED TRACE**

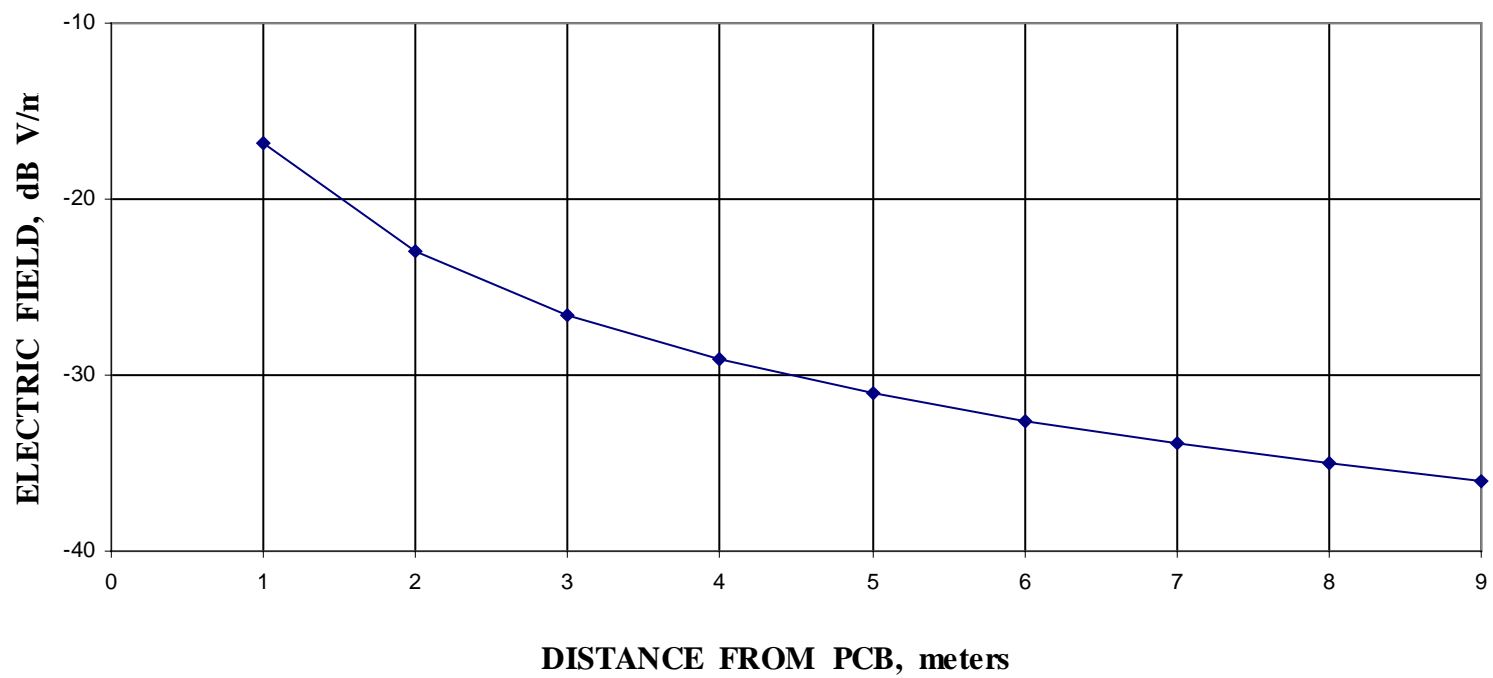


Figure 4.32. Simulated Near Fields at 200 MHz for Curved Trace.

**SIMULATED AND THEORETICAL FAR FIELDS AT 200 MHz  
CURVED TRACE**

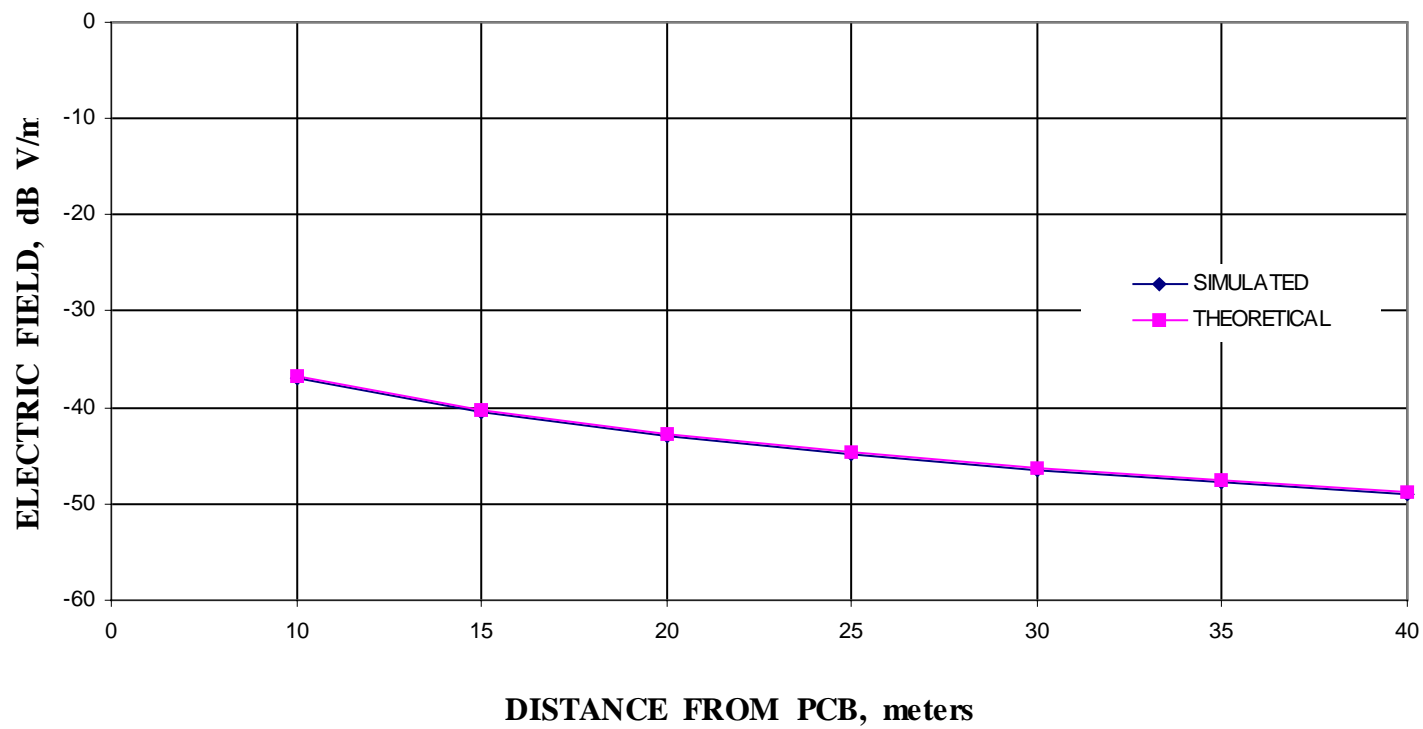


Figure 4.33. Simulated and Theoretical Far Fields at 200 MHz for Curved Trace.

**FREQUENCY SWEEP OF ELECTRIC FIELDS  
Z TRACE & TRACES WITH DISCONTINUITIES  
5 cms FROM THE PCB**

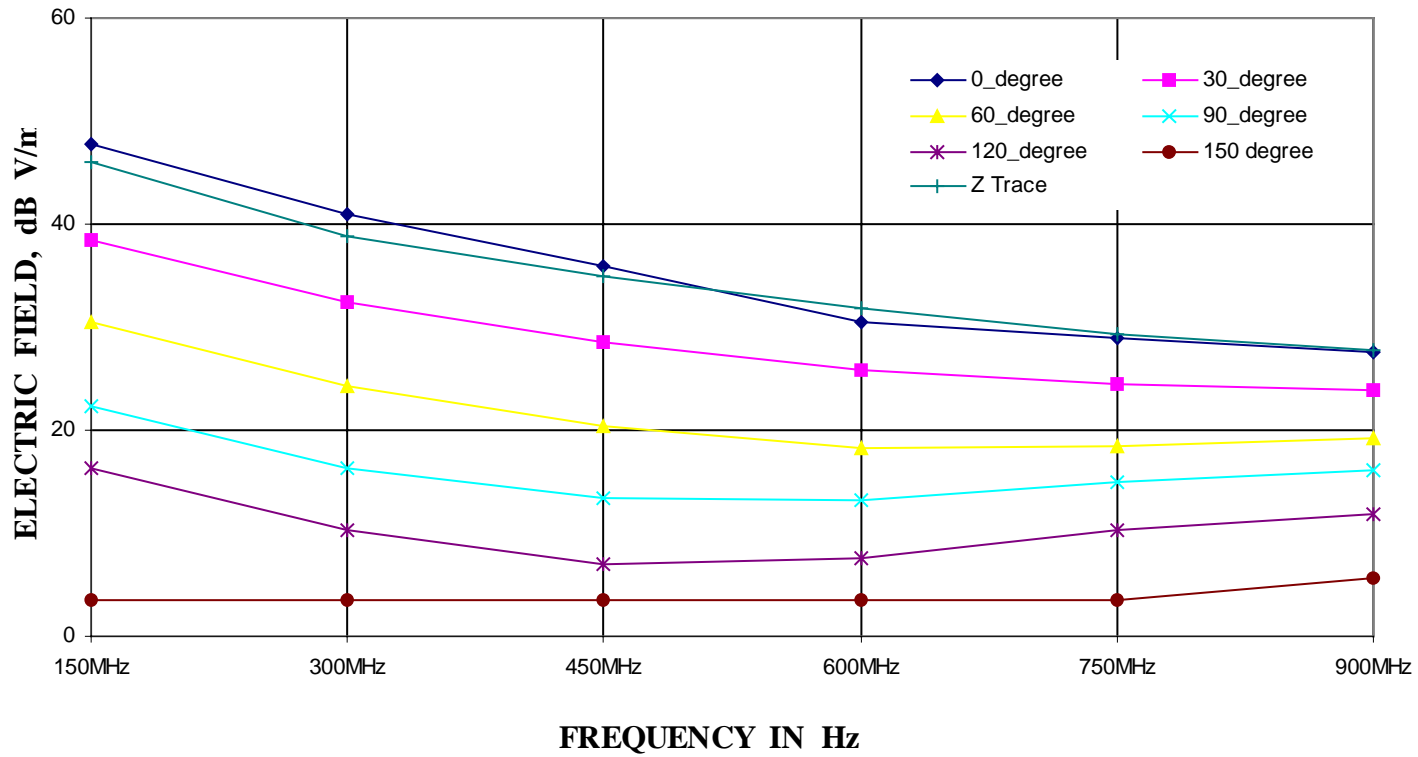


Figure 4.34. Simulated Frequency Sweep at 5 cms for Z Trace and Traces with Discontinuities.

**FREQUENCY SWEEP OF ELECTRIC FIELDS  
Z TRACE & TRACES WITH DISCONTINUITIES  
10 cms FROM THE PCB**

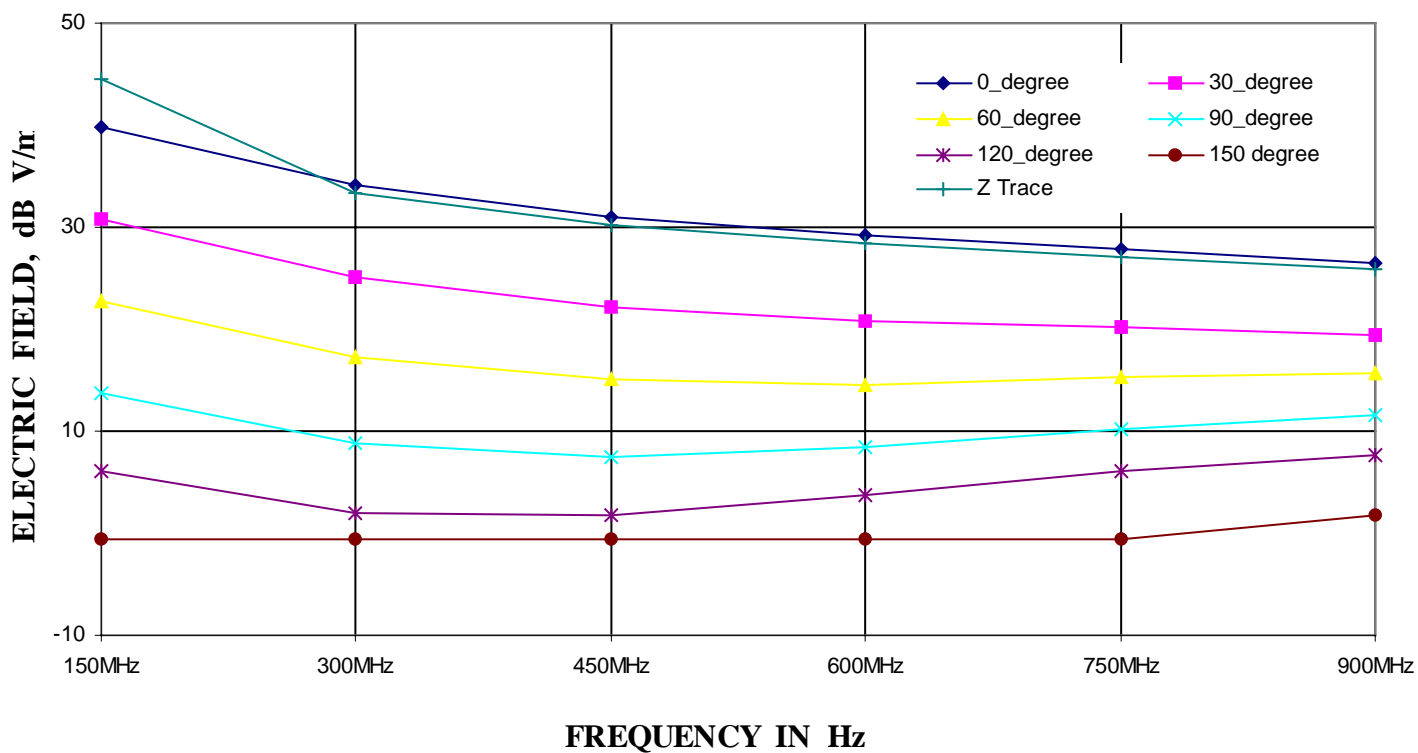


Figure 4.35. Simulated Frequency Sweep at 10 cms for Z Trace and Traces with Discontinuities.

**FREQUENCY SWEEP OF ELECTRIC FIELDS  
Z TRACE & TRACES WITH DISCONTINUITIES  
5 METERS FROM THE PCB**

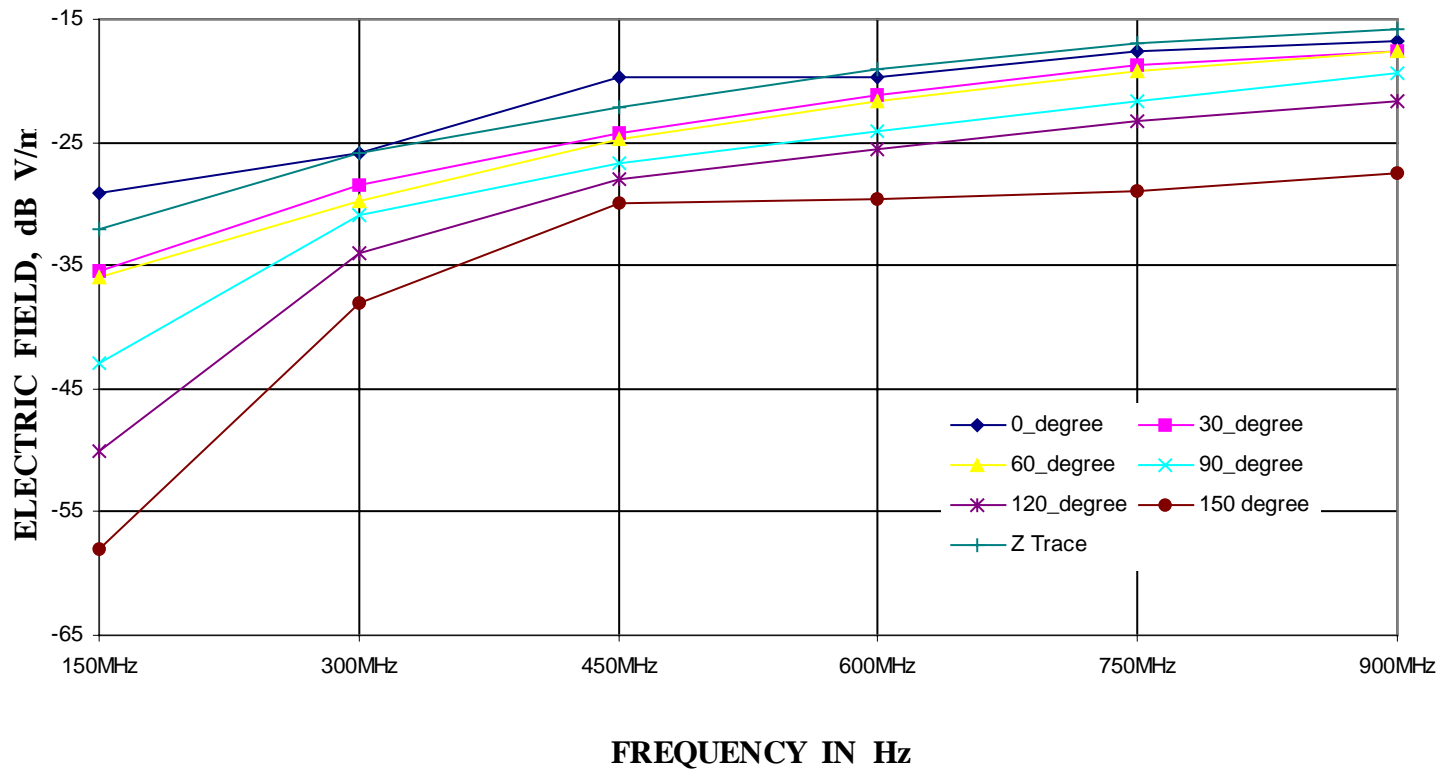


Figure 4.36. Simulated Frequency Sweep at 5 M for Z Trace and Traces with Discontinuities.

**FREQUENCY SWEEP OF ELECTRIC FIELDS  
Z TRACE & TRACES WITH DISCONTINUITIES  
10 METERS FROM THE PCB**

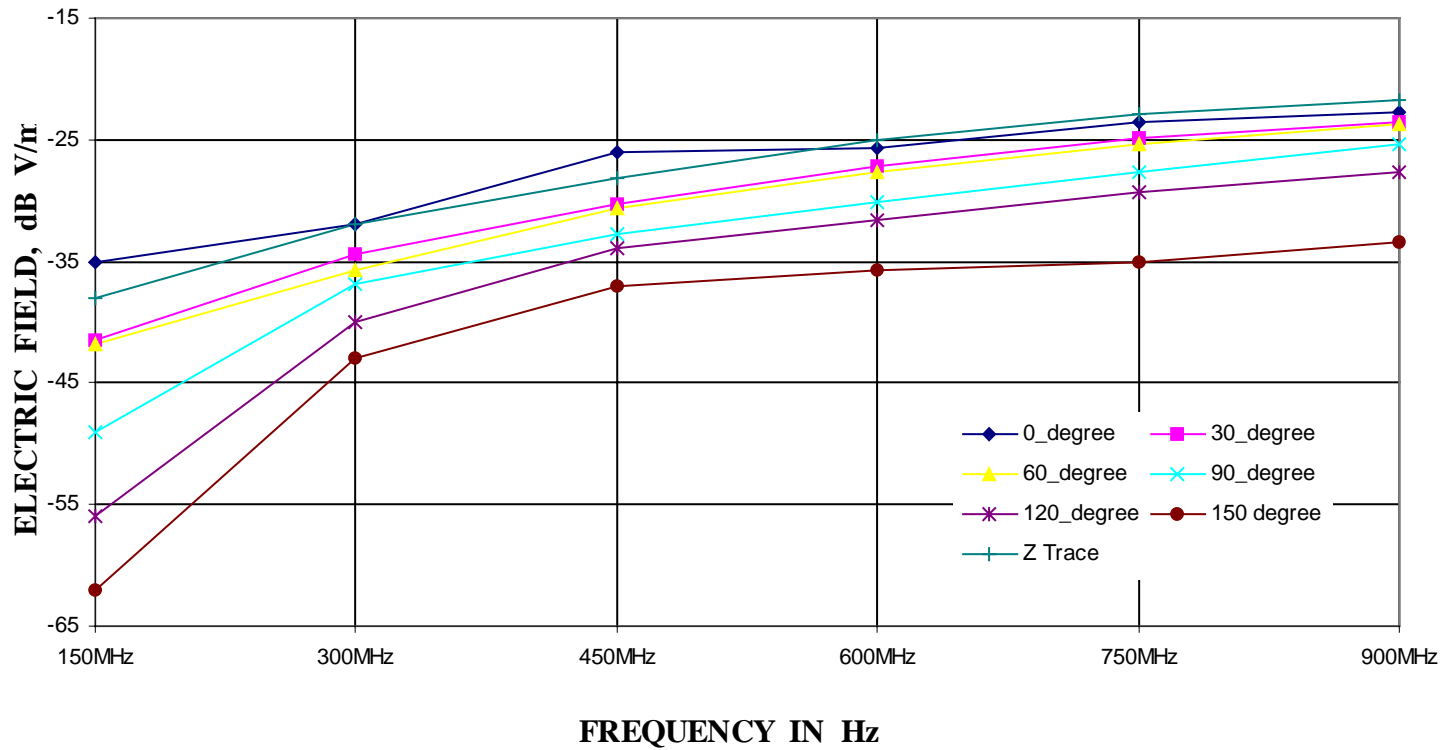


Figure 4.37. Simulated Frequency Sweep at 10 M for Z Trace and Traces with Discontinuities.

**FREQUENCY SWEEP OF ELECTRIC FIELDS  
CURVED, CIRCULAR AND RECTANGULAR  
5 cms FROM THE PCB**

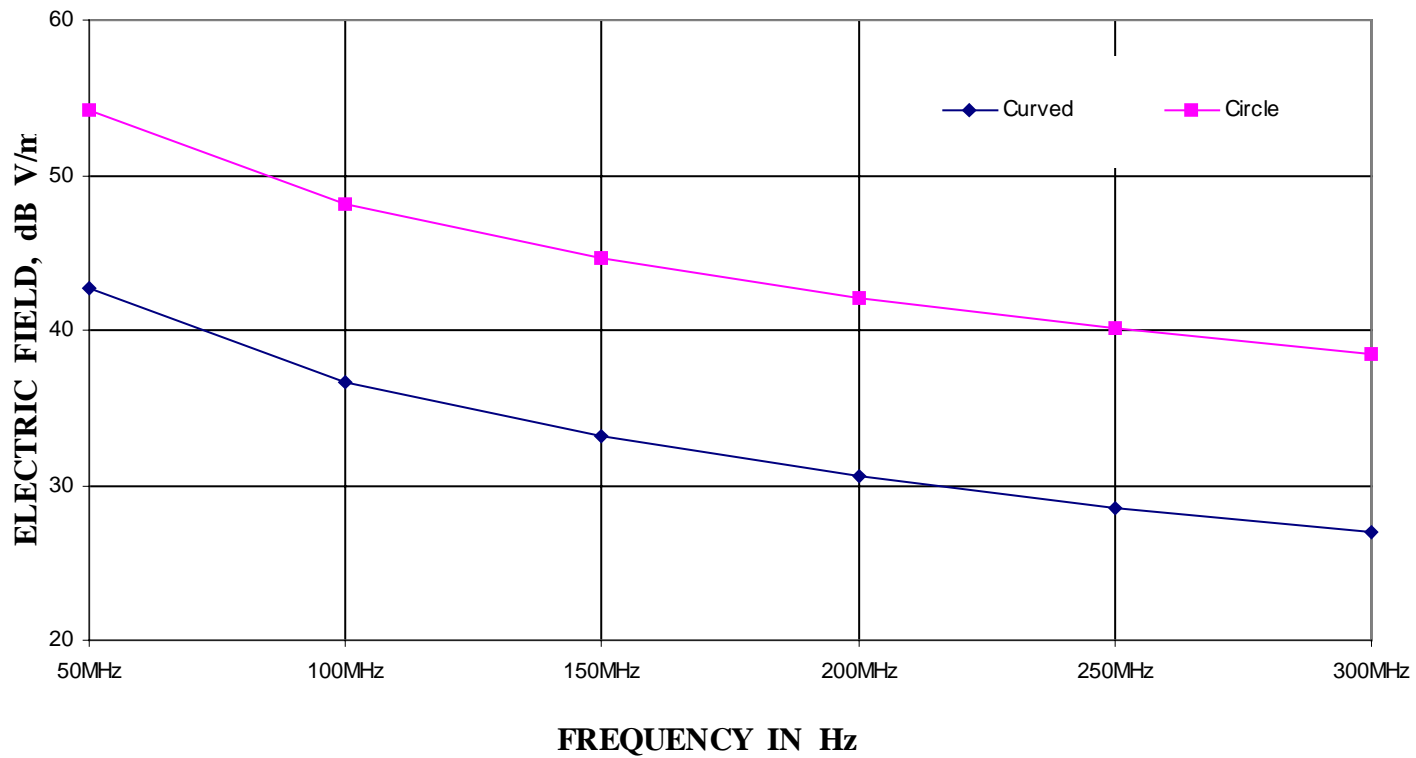


Figure 4.38. Simulated Frequency Sweep at 5 cms for Curved Trace, Circular and Rectangular Loops.

**FREQUENCY SWEEP OF ELECTRIC FIELDS  
CURVED, CIRCULAR AND RECTANGULAR  
10 cms FROM THE PCB**

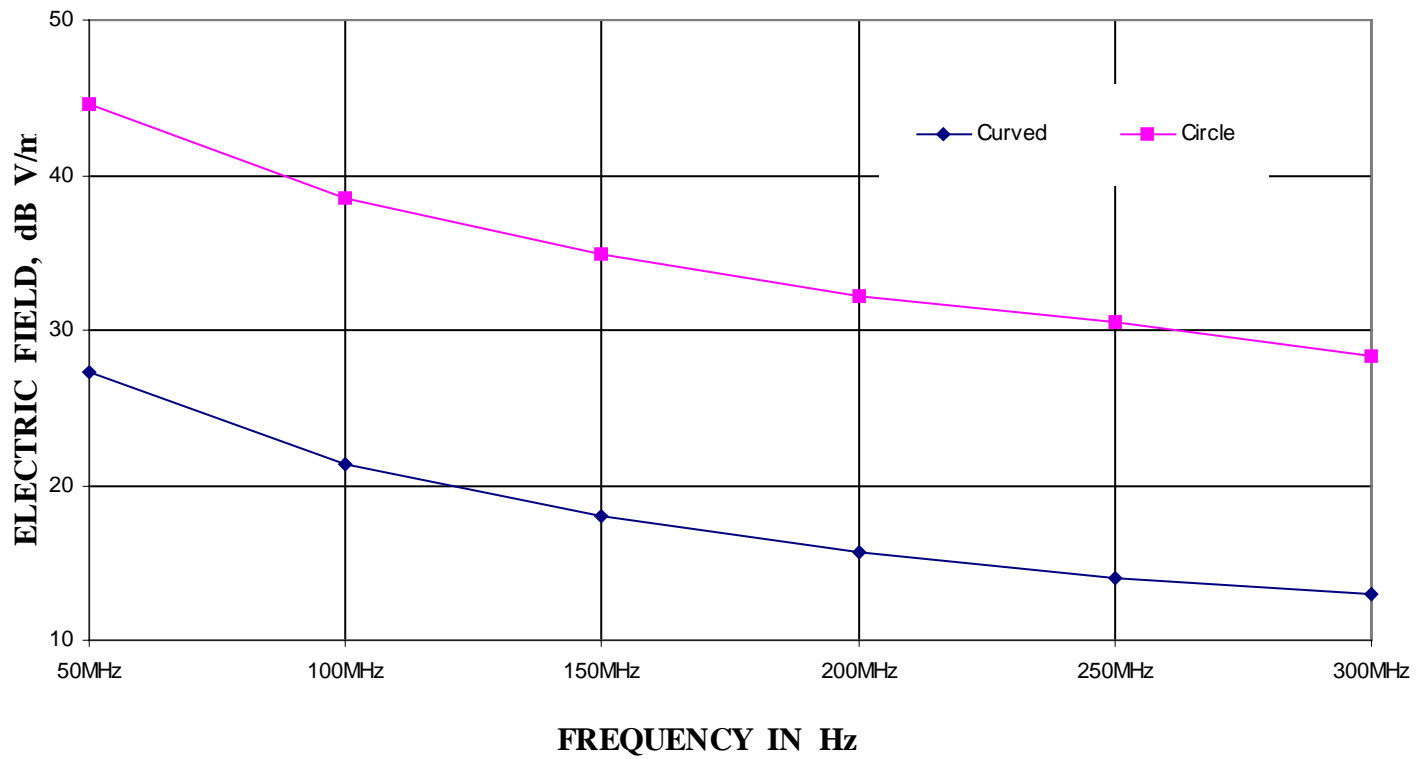


Figure 4.39. Simulated Frequency Sweep at 10 cms for Curved Trace, Circular and Rectangular Loops.

**FREQUENCY SWEEP OF ELECTRIC FIELDS  
CURVED CIRCULAR AND RECTANGULAR  
5 METERS FROM THE PCB**

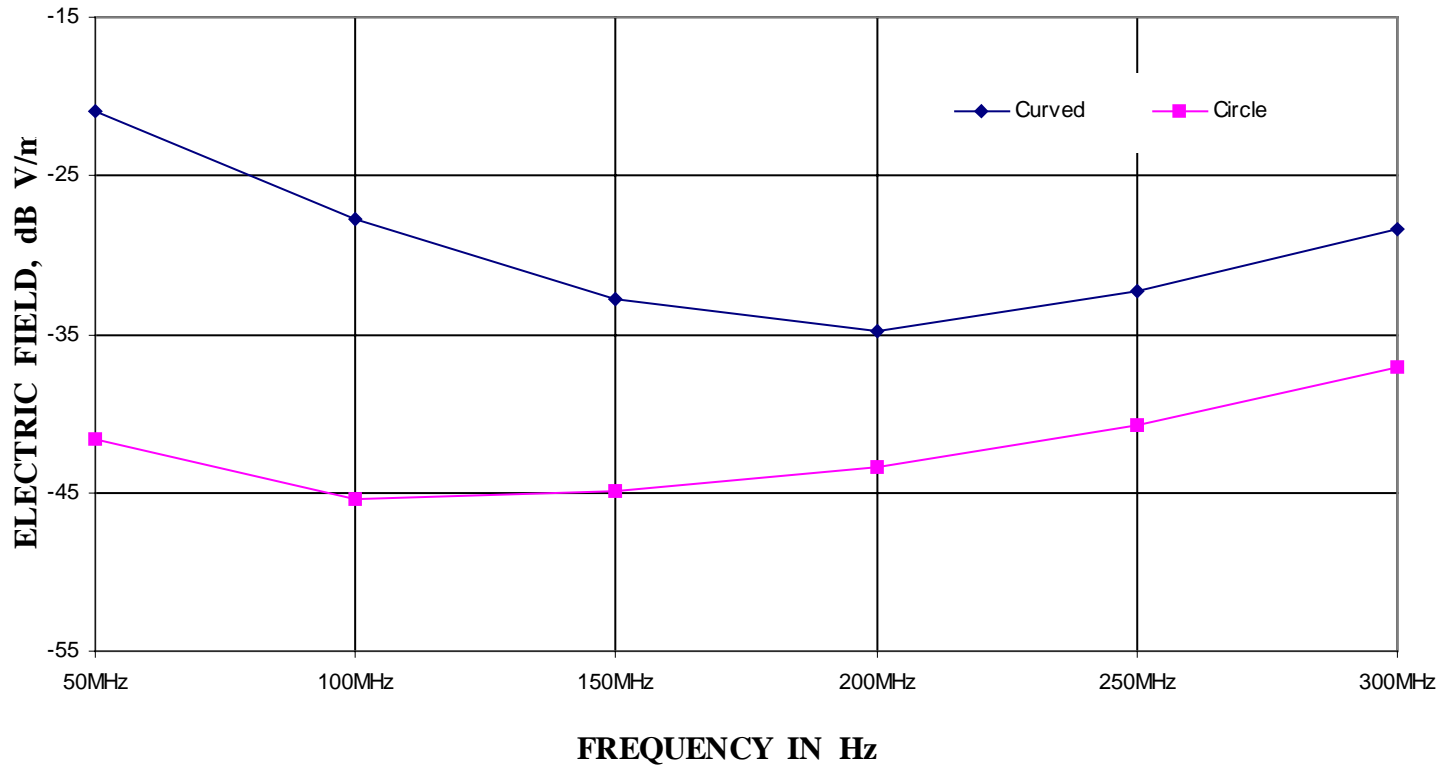


Figure 4.40. Simulated Frequency Sweep at 5 M for Curved Trace, Circular and Rectangular Loops.

**FREQUENCY SWEEP OF ELECTRIC FIELDS  
CURVED CIRCULAR AND RECTANGULAR  
10 METERS FROM THE PCB**

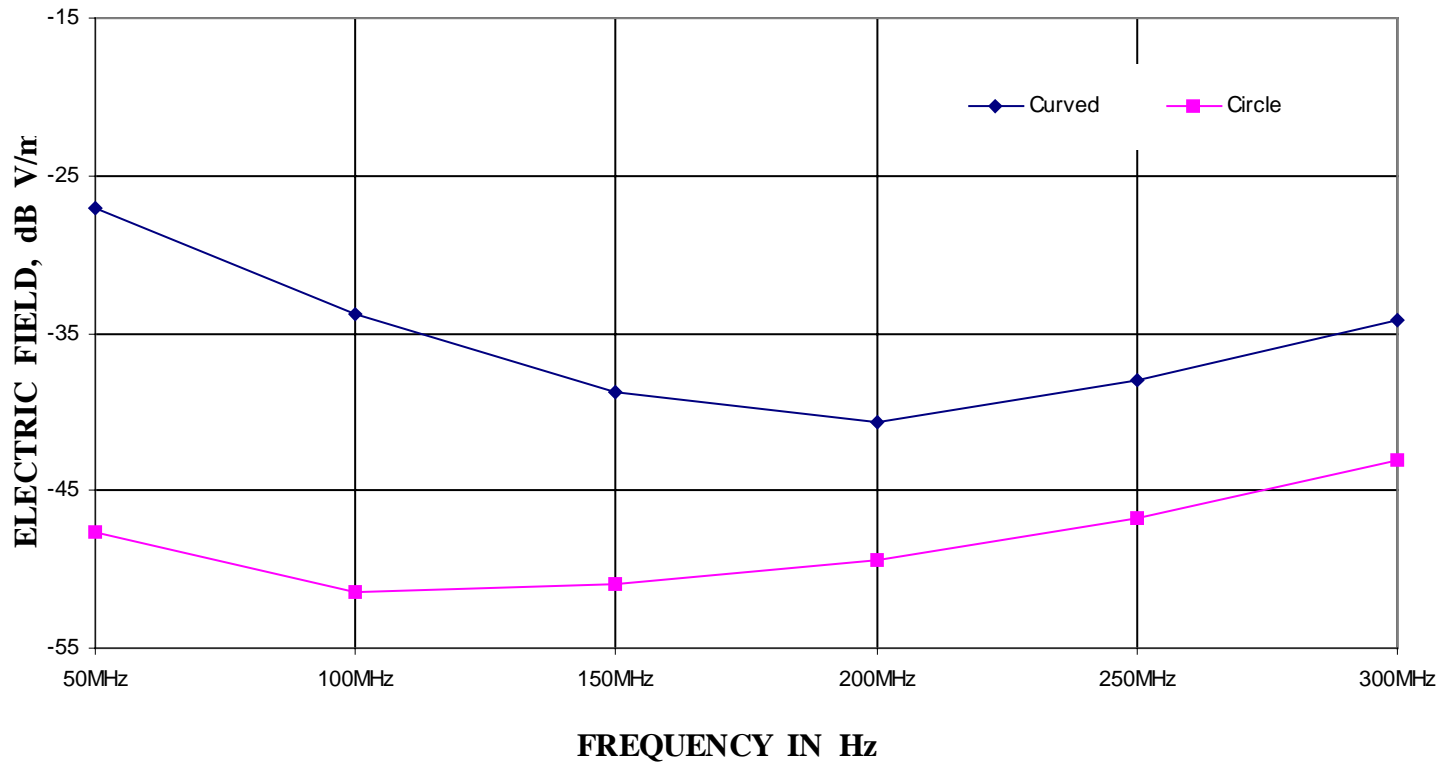


Figure 4.41. Simulated Frequency Sweep at 10 M for Curved Trace, Circular and Rectangular Loops.

## V. INDUCED EMI SIMULATIONS

Consider a printed circuit board with a ground plane and two loops placed on the substrate as shown in Figure 5.1. Let the outer loop have a current  $I_m \sin(\omega t)$  flowing in it. Per Ampere's Law, the current in the outer loop will produce magnetic flux. This magnetic flux will link the

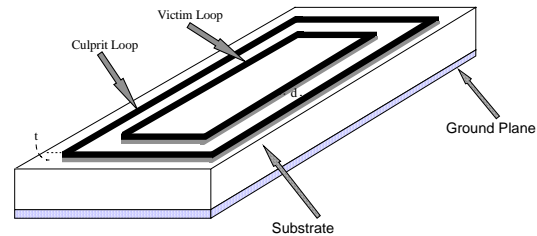
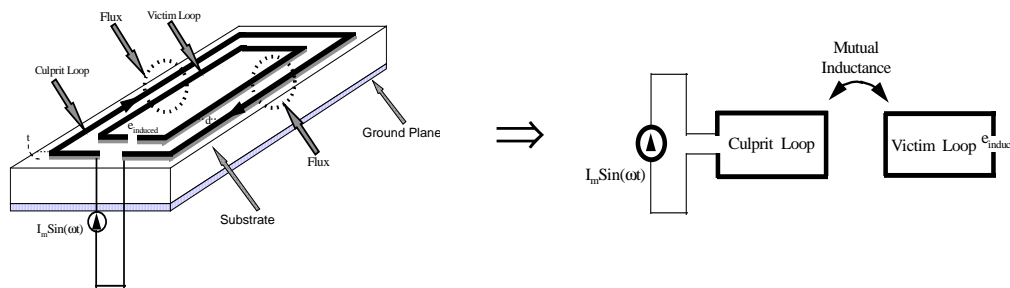


Figure 5.1. Geometry of a Two Loop Card for Induced EMI.

inner loop. Per Faraday's Law, this flux linkage will induce an emf in the inner loop. If the inner loop is open circuited, the emf will appear across the open terminals of the inner loop. This

Figure 5.2. Induced Emf

mechanism of induced  
5.2. If the inner loop is  
mechanism of induced  
Figure 5.3. This



in a Two Loop Card.

emf is shown in Figure  
a closed circuit, then an  
flow in it. The  
current is shown in

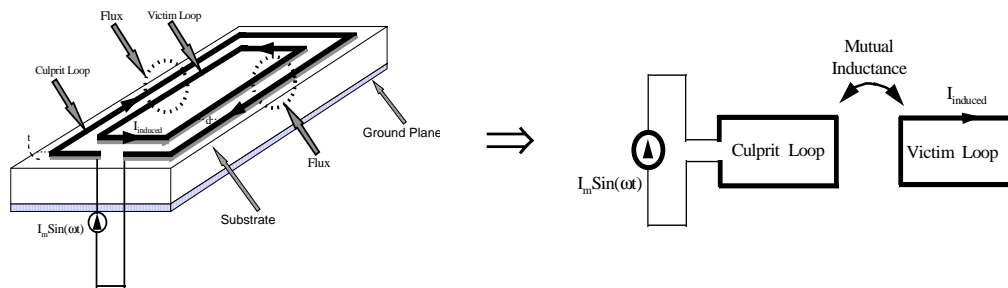


Figure 5.3. Induced Current in Two Loop Card.

induced current in the inner loop is the induced EMI. In effect, the outer loop is the source of the Induced EMI. It is sometimes referred to as the Culprit Loop. The inner loop is the receptor of the Induced EMI. The receptor loop is sometimes referred to as the Victim Loop.

### A. SIMULATION GEOMETRIES

Six geometries with different levels of complexities were selected for Induced EMI simulations. The first objective in the selection of these six geometries was to develop confidence and usage expertise with the commercial software packages. The second objective was to select geometries whose Induced EMI could be theoretically modeled with relative ease. The third objective in the selection of these six geometries was their PEBB relevance. The geometry of the substrate and the ground plane for the Induced EMI simulations is identical to the one used earlier for Crosstalk and Radiated EMIs. The w/h ratio of Figure 3.1 was kept at unity for all Induced EMI simulations. The six geometries are shown in Figure 5.4.

## Induced EMI Geometries

Figure 5.4. The Six Induced EMI

Geometries for Simulations.

### 1. Triangular Loops

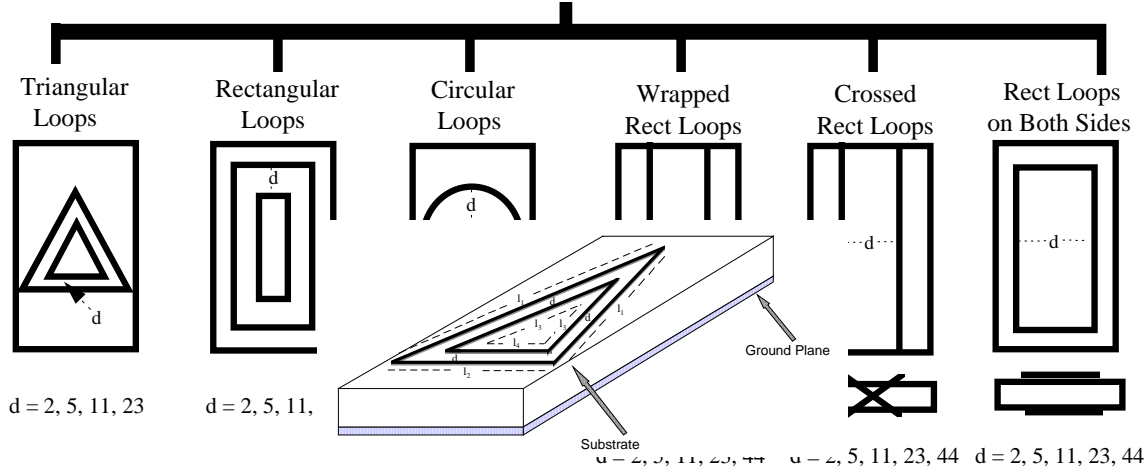


Figure 5.5. Printed Circuit Board Geometry for Triangular Loops.

This geometry comprises of two loops with isosceles triangles. The PEBB is going to have traces which could be approximated to such loops. Thus, this type of geometry would be PEBB relevant. The Printed Circuit Board Geometry of the Triangular Loops is shown in Figure 5.5. The lengths  $l_1$ , and  $l_2$ , of the outer loop are approx. 10 and 8 cms. The lengths  $l_3$  and  $l_4$  of the inner loop are variable depending on the separation distance  $d$  between the outer and the inner loops.

### 2. Rectangular Loops

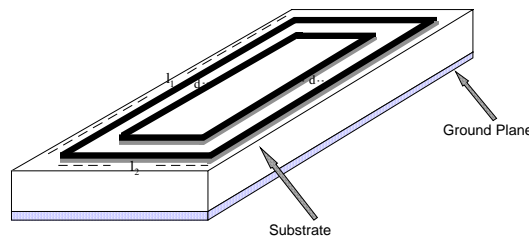


Figure 5.6. Printed Circuit Board Geometry for Rectangular Loops.

This geometry has two rectangular loops placed on the substrate. It is a common geometry and the PEBB is going to have its share of such loops or loops which could be approximated to rectangular loops. Thus, this type of geometry would be PEBB relevant. The Printed Circuit Board Geometry of the Rectangular Loops is shown in Figure 5.6. The lengths  $l_1$ , and  $l_2$ , of the outer loop are approx. 13 and 10 cms. The lengths  $l_3$  and  $l_4$  of the inner loop are variable depending on the separation distance  $d$  between the outer and the inner loops.

### 3. Circular Loops

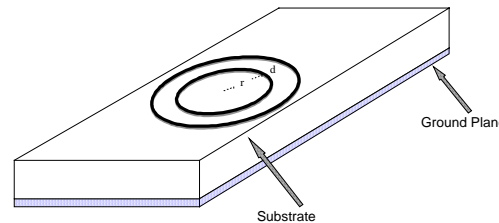


Figure 5.7. Printed Circuit Board Geometry for Circular Loops.

This geometry has two circular loops placed on the substrate. It is another common geometry and the PEBB is going to have its share of such loops or loops which could be approximated to circular loops. The Printed Circuit Board Geometry of the Circular Loops is shown in Figure 5.7. The radius of the outer loop is 5 cms. The radius of the inner the inner loop is variable and will depend on the separation distance between the outer and the inner loops.

### 4. Wrapped Rectangular Loops

This geometry also comprises of two rectangular loops. However, for this geometry the loops instead of being placed on the substrate, are wrapped around the card. The Printed Circuit Board

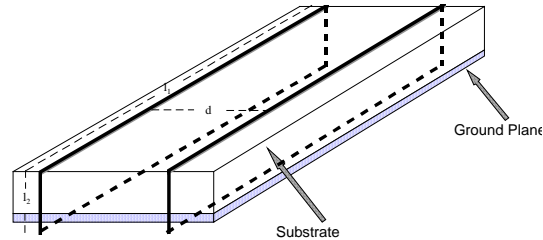


Figure 5.8. Printed Circuit Board Geometry for Wrapped Rectangular Loops.

Geometry of the Wrapped Rectangular Loops is shown in Figure 5.8. The flux linkage for this geometry will be through the substrate of the card. The length  $l_1$  for both loops is approx. 14 cms. The length  $l_2$  for both loops is the height of the card

#### 5. Crossed Rectangular Loops

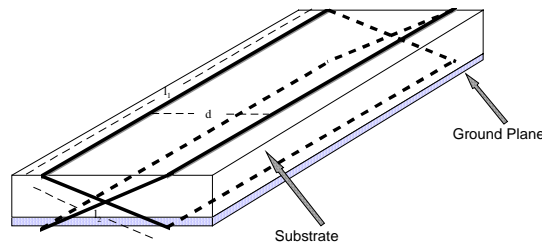


Figure 5.9. Printed Circuit Board Geometry for Crossed Rectangular Loops.

This geometry also has two rectangular loops but placed in a crossed manner. The two loops are crossed across the printed circuit board. The Printed Circuit Board Geometry of the Crossed Rectangular Loops is shown in Figure 5.9. The flux linkage for this geometry will also be through the substrate of the card. The length  $l_1$  for both loops is approx. 14 cms. The length  $l_2$  for both loops is approximate 2.5 cms.

#### 6. Rectangular Loops on Both Sides.

This geometry consists of two identical rectangular loops laid on the upper and lower sides of the printed circuit board. This also is a common geometry and the PEBB is going to have its share of such loops or loops which could be approximated to this situation. This type of geometry would be PEBB relevant. The Printed Circuit Board Geometry of the Rectangular Loops on Both Sides is shown in Figure 5.10. The lengths  $l_1$ , and  $l_2$ , of the outer loop are approx. 13 and 10 cms.

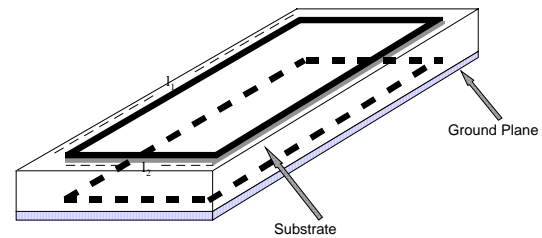


Figure 5.10. Printed Circuit Board Geometry for Rectangular Loops on Both Sides.

The Induced EMI simulations are still in the implementation stage. The models for these geometries are being developed. However, preliminary work has been done to see the feasibility of these simulations. The preliminary work was focused on simple rectangular loops and circular loops of Figures 5.6 and 5.7 respectively. Both models gave predictable and viable results. There is every reason to believe that all six Induced EMI simulations are feasible and will give predictable and viable results. At this juncture, all that is needed is time and effort to implement the six simulations.

## VI. FUTURE PLANS FOR EMI SIMULATIONS

The goals for the next year are:

1. Consummate the Induced EMI simulations. This will be useful in developing EMI Design Criterion for Multiple Cards and Inter-System Compatibility.

2. Consolidate the Radiated EMI simulations. This also will be helpful in developing EMI Design Criterion for Multiple Cards and Inter-System Compatibility.
3. Modify the Induced and Radiated EMI models to predict the susceptibility of PEBB to Radiated and Induced EMIs.
4. Initiate the study of Common Mode EMI. This will be useful in developing models to predict the susceptibility of PEBB to Conducted EMI.
5. Revisit Crosstalk EMI and refine some models to incorporate PEBB relevant design layouts.

The five goals will be pursued simultaneously. The consummation of the Induced EMI simulations will be a major step. The Induced EMI models will enable to determine the electrical signals resulting from incident electromagnetic fields. The Radiated EMI models in conjunction with the Induced EMI models can then be used to predict the susceptibility of PEBB to incident fields. Initiating Common Mode EMI study is also a step in the direction of making the simulations predict the susceptibility of PEBB from external sources. Common Mode EMI models will be used to predict the susceptibility of PEBB via conduction paths. Shifting the focus to a more tangible PEBB relevancy is the broader goal for the next year.

## REFERENCES

Balanis, C.A., 1982, "Antenna Theory: Analysis and Design ". John Wiley & Sons, New York, NY.

Brauer, J. R., 1993, "What Every Engineer Should Know About Finite Element Analysis". Marcel Dekker Inc. New York, NY.

Cerri, G., De Leo, R., and Primiani, V.M., February 1993, "A Rigorous Model for Radiated Emission Prediction in PCB Circuits". IEEE Trans. on EMC, vol. 35, no. 1, pp. 102-109

Chadha, R., Garg, R., and Gupta, K.C., 1981, "Computer Aided Design of Microwave Circuits". Artech House Inc. Dedham, MA.

Chari, M.V.K., and Cendes, Z.J., September 1977, "Finite Element Analysis of the Skin Effect in Current Carrying Conductors". IEEE Trans. Magnetics, Vol. 13, No. 5, pp. 1125-1127.

Cheng, D. K., 1983, "Field and Wave Electromagnetics". Addison Wesley Publishing Co., Inc., MA.

Christopoulos, C., 1995, "Principles and Techniques of Electromagnetic Compatibility". CRC Press Inc., NY.

Costa, M., Sarkar, T.K., Strait, B.J., and Bennet, S., 1981, IEEE EMC Symposium, pp 246-249.

Dixon, D.S., Obara, M.O., and Schade, N., May 1993, "Finite-Element Analysis (FEA) as an EMC Prediction Tool". IEEE Trans. on EMC, vol. 35, no. 2, pp. 241- 248.

Ficci, R. F., 1964, "Electrical Interference". Hayden Book Company, Inc., NY.

Goedbloed, J., 1992, "Electromagnetic Compatibility". Prentice Hall, Inc., NJ.

Gravelle, L.B., and Wilson, P.F., May 1992, "EMI/EMC in Printed Circuit Boards - A Literature Review". IEEE Trans. on EMC, vol. 34, no. 2, pp. 109- 116.

Hubing, T.H., and Kaufman, J.H., February 1989, "Modeling the Electromagnetic Radiation from Electrically Small Table-Top Products". IEEE Trans. on EMC, vol. 31, no. 1, pp. 74- 84.

Keiser, B., 1979, "Principles of Electromagnetic Compatibility". Artech House, Inc., MA.

Kodali, V.P., 1996, "Engineering Electromagnetic Compatibility- Principles Measurements and Technologies". IEEE Press, Inc., NJ.

Laroussi, R., and Costache, G.I., May 1993, "Finite-Element Method Applied to EMC Problems". IEEE Trans. on EMC, vol. 35, no. 2, pp. 178-184.

Lee, J.F., and Cendes, Z.J., April 1987, "Transfinite Elements: A highly Efficient Procedure for Modeling Open Field Problems". J. App Phy., vol. 61, pp. 3913-3916.

Mardiguian, M., 1984, "Interference Control in Computers and Microprocessor-Based Equipment". Interference Control Technologies. Inc., VA.

Mills, J. P., 1993, "Electro-Magnetic Interference Reduction in Electronic Systems". PTR Prentice Hall, Inc., NJ.

Mitra, R., and Ramahi, O., 1990, "Absorbing Boundary Conditions for the Direct Solution of Partial Differential Equation Arising in Electromagnetic Scattering Problems", in Finite Element and Finite Difference Methods in Electromagnetic Scattering. M. Morgan, Editor, vol. II. Elsevier Science, New York, NY.

Montrose, M.I., 1996, "Printed Circuit Board Design Techniques for EMC Compliance". IEEE Press, NJ.

Naishadham, K., and Berry, J.B., May 1989, "A Rigorous Model to Compute the Radiation From Printed Circuit Boards". Proc. IEEE 1989 Nat. EMC Symp. (Denver, CO), pp. 127-130.

Paul, C.R., January 1989, "Modeling Electromagnetic Interference Properties of Printed Circuit Boards". IBM Journal of Research and Development, vol. 33, no.1, pp. 33-50.

Paul, C.R., May 1989, "A Comparison of the Contributions of Common Mode and Differential Mode Currents and Radiated Emissions". IEEE Trans. on EMC vol. 31, no. 2, pp. 189-193.

Paul, C.R., 1992, "Introduction to Electromagnetic Compatibility". John Wiley & Sons, NY.

Ramchandani, R., Narvaez, P., Avalos, T., Mazariego, L., and Ong, C.B., May 1996, "Electromagnetic Interference (EMI) Design Criterion for Power Electronics Building Block (PEBB). Office of Naval Research, Arlington Va.

Raut, R., Steenaart, W.J., and Costache, G.I., February 1988, "A Note on the Optimum Layout of Electronic Circuits to Minimize the Radiated Electromagnetic Field Strength". IEEE Trans. on EMC, vol. 30, no. 1, pp. 88-89.

Shao, K.R., and Zhou, K.D., 1988, "The Iterative Boundary Element Method for Non linear Electromagnetic Field Calculations". IEEE Trans. Mag., vol. MAG-20, pp. 549-552.

Sistino, A.J., March 1989, "Radiation From a Printed Circuit Board: Theory and Application". 8th Intl. Zurich Symp. on Electromagnetic Compatibility, pp. 57-62.

Swainson, A.J.G., 1988, "Radiated Emission and Susceptibility Predictions on Ground Plane Printed Circuit Boards". Proc. Inst. Elect. Radio Eng., EMC Symposium, York, England, pp. 295-301.

Tihanyi, L., 1995, " Electromagnetic Compatibility in Power Electronics". J.K. Eckert & Company, Inc., NJ.

Violette, J.L.N., White, D.R.G., and Violette, M.F., 1987, "Electromagnetic Compatibility Handbook". Van Norstrand Reinhold, New York, NY.

Walker, C.S., 1990, "Capacitance, Inductance and Crosstalk Analysis". Artech House Inc., Dedham, MA.

White, D.R.J., 1982, "EMI Control in the Design of Printed Circuit Boards". Interference Control Technologies, Gainesville, VA.

Yilder, Y. B., Prasad, K. M., and Zheng, D.,1993, "Computer-Aided Design in Electromagnetic Systems: Boundary Element Method and Applications". Control and Dynamic Systems, Vol. 59, pt 2, pp. 167-223, Academic Press Inc.

## APPENDIX: CROSSTALK

Dimensions of Parallel Traces with Discontinuities

| Parallel Traces with Discontinuities |               |           |           |           |           |
|--------------------------------------|---------------|-----------|-----------|-----------|-----------|
| d mms                                | $\alpha$ degr | $l_1$ mms | $l_2$ mms | $l_3$ mms | $l_4$ mms |
| 2                                    | 0             | 140       | 140       |           |           |
| 2                                    | 60            | 70        | 67        | 67        | 61        |
| 2                                    | 90            | 70        | 58        | 65        | 53        |
| 2                                    | 120           | 70        | 67        | 61        | 61        |

Dimensions of Non Parallel Traces

| Non Parallel Traces |               |           |           |
|---------------------|---------------|-----------|-----------|
| d mms               | $\alpha$ degr | $l_1$ mms | $l_2$ mms |
| 2                   | 0             | 140       | 140       |
| 2                   | 30            | 140       | 162       |
| 2                   | 60            | 140       | 108       |
| 2                   | 90            | 140       | 97        |

| Parallel Traces with Discontinuities |               |           |           |           |           |
|--------------------------------------|---------------|-----------|-----------|-----------|-----------|
| d mms                                | $\alpha$ degr | $l_1$ mms | $l_2$ mms | $l_3$ mms | $l_4$ mms |
| 5                                    | 0             | 140       | 140       |           |           |
| 5                                    | 60            | 70        | 68        | 65        | 59        |
| 5                                    | 90            | 70        | 59        | 62        | 51        |
| 5                                    | 120           | 70        | 68        | 59        | 59        |

| Non Parallel Traces |               |           |           |
|---------------------|---------------|-----------|-----------|
| d mms               | $\alpha$ degr | $l_1$ mms | $l_2$ mms |
| 5                   | 0             | 140       | 140       |
| 5                   | 30            | 140       | 162       |
| 5                   | 60            | 140       | 104       |
| 5                   | 90            | 140       | 94        |

| Parallel Traces with Discontinuities |               |           |           |           |           |
|--------------------------------------|---------------|-----------|-----------|-----------|-----------|
| d mms                                | $\alpha$ degr | $l_1$ mms | $l_2$ mms | $l_3$ mms | $l_4$ mms |
| 11                                   | 0             | 140       | 140       |           |           |
| 11                                   | 60            | 70        | 72        | 62        | 56        |
| 11                                   | 90            | 70        | 62        | 56        | 48        |
| 11                                   | 120           | 70        | 72        | 46        | 55        |

| Non Parallel Traces |               |           |           |
|---------------------|---------------|-----------|-----------|
| d mms               | $\alpha$ degr | $l_1$ mms | $l_2$ mms |
| 11                  | 0             | 140       | 140       |
| 11                  | 30            | 140       | 162       |
| 11                  | 60            | 140       | 96        |
| 11                  | 90            | 140       | 88        |

| Parallel Traces with Discontinuities |               |           |           |           |           |
|--------------------------------------|---------------|-----------|-----------|-----------|-----------|
| d mms                                | $\alpha$ degr | $l_1$ mms | $l_2$ mms | $l_3$ mms | $l_4$ mms |
| 23                                   | 0             | 140       | 140       |           |           |
| 23                                   | 60            | 70        | 79        | 55        | 49        |
| 23                                   | 90            | 70        | 68        | 44        | 42        |
| 23                                   | 120           | 70        | 79        | 25        | 51        |

| Non Parallel Traces |               |           |           |
|---------------------|---------------|-----------|-----------|
| d mms               | $\alpha$ degr | $l_1$ mms | $l_2$ mms |
| 23                  | 0             | 140       | 140       |
| 23                  | 30            | 140       | 121       |
| 23                  | 60            | 140       | 84        |
| 23                  | 90            | 140       | 76        |

| Parallel Traces with Discontinuities |               |           |           |           |           |
|--------------------------------------|---------------|-----------|-----------|-----------|-----------|
| d mms                                | $\alpha$ degr | $l_1$ mms | $l_2$ mms | $l_3$ mms | $l_4$ mms |
| 44                                   | 0             | 140       | 140       |           |           |
| 44                                   | 60            | 70        | 91        | 43        | 37        |
| 44                                   | 90            | 70        | 79        | 23        | 32        |

| Non Parallel Traces |               |           |           |
|---------------------|---------------|-----------|-----------|
| d mms               | $\alpha$ degr | $l_1$ mms | $l_2$ mms |
| 44                  | 0             | 140       | 140       |
| 44                  | 30            | 140       | 99        |
| 44                  | 60            | 140       | 59        |

|    |     |  |  |  |  |
|----|-----|--|--|--|--|
| 44 | 120 |  |  |  |  |
|----|-----|--|--|--|--|

|    |    |     |    |
|----|----|-----|----|
| 44 | 90 | 140 | 55 |
|----|----|-----|----|

### Dimensions of Parallel Z Traces

| Parallel Z Traces |                    |                    |                    |                    |                    |                    |
|-------------------|--------------------|--------------------|--------------------|--------------------|--------------------|--------------------|
| d mms             | l <sub>1</sub> mms | l <sub>2</sub> mms | l <sub>3</sub> mms | l <sub>4</sub> mms | l <sub>5</sub> mms | l <sub>6</sub> mms |
| 2                 | 70                 | 10                 | 70                 | 65                 | 10                 | 75                 |
| 5                 | 70                 | 10                 | 70                 | 62                 | 10                 | 78                 |
| 11                | 70                 | 10                 | 70                 | 56                 | 10                 | 84                 |
| 23                | 70                 | 10                 | 70                 | 44                 | 10                 | 96                 |
| 44                | 70                 | 10                 | 70                 | 23                 | 10                 | 117                |

### Dimensions of Z and Straight Traces

| Z And Straight Traces |                    |                    |                    |                    |
|-----------------------|--------------------|--------------------|--------------------|--------------------|
| d mms                 | l <sub>1</sub> mms | l <sub>2</sub> mms | l <sub>3</sub> mms | l <sub>4</sub> mms |
| 2                     | 140                | 70                 | 10                 | 70                 |
| 5                     | 140                | 70                 | 10                 | 70                 |
| 11                    | 140                | 70                 | 10                 | 70                 |
| 23                    | 140                | 70                 | 10                 | 70                 |
| 44                    | 140                | 70                 | 10                 | 70                 |

### Dimensions of Maze Traces

| Maze Traces |                    |                    |                    |                    |                    |
|-------------|--------------------|--------------------|--------------------|--------------------|--------------------|
| d mms       | l <sub>1</sub> mms | l <sub>2</sub> mms | l <sub>3</sub> mms | l <sub>4</sub> mms | l <sub>5</sub> mms |
| 2           | 108                | 136                | 108                | 80                 | 53                 |
| 5           | 108                | 136                | 108                | 80                 | 53                 |

|    |     |     |     |    |    |
|----|-----|-----|-----|----|----|
| 11 | 108 | 136 | 108 | 80 | 53 |
| 23 | 108 | 136 | 108 | 80 | 53 |

Dimensions of Curved Traces

| Curved Traces |                    |                    |                    |                    |                    |                    |
|---------------|--------------------|--------------------|--------------------|--------------------|--------------------|--------------------|
| d mms         | l <sub>1</sub> mms | l <sub>2</sub> mms | l <sub>3</sub> mms | l <sub>4</sub> mms | r <sub>1</sub> mms | r <sub>2</sub> mms |
| 2             | 62                 | 32                 | 62                 | 32                 | 65                 | 69                 |
| 5             | 62                 | 32                 | 62                 | 32                 | 62                 | 69                 |
| 11            | 62                 | 32                 | 62                 | 32                 | 57                 | 69                 |
| 23            | 62                 | 32                 | 62                 | 32                 | 44                 | 69                 |
| 44            | 62                 | 32                 | 62                 | 32                 | 23                 | 69                 |